KTH Industrial Engineering and Management

Techno-economic assessment of CO2 refrigeration systems with geothermal integration, a field measurements and modelling analysis

Fabio Giunta

Master of Science Thesis
KTH School of Industrial Engineering and Management
Energy Technology EGI-2020- TRITA-ITM-EX 2020:3
Division of Applied Thermodynamics and Refrigeration
SE-100 44 STOCKHOLM

KTH Industrial Engineering and Management

Master of Science Thesis EGI 2020: TRITA-ITM-EX 2020:3

Techno-economic assessment of CO2 refrigeration systems with geothermal integration, a field measurements and modelling analysis

Fabio Giunta

Approved	Examiner Samer Sawalha	Supervisor Jörgen Rogstam
	Commissioner	Contact person

Abstract

Several CO2 transcritical booster systems in supermarkets use the potential of integrating geothermal storage, enabling subcooling during warm climate conditions as well as being a heat source during cold climate conditions. First of all, field measurements of one of these systems located in Sweden were analysed with particular focus on the heat-recovery performance. The best theoretical operational strategy was compared to the one really implemented and the differences in the annual energy usage were assessed through modelling. The results show that an alternative to the best theoretical operational strategy exists; heat can be extracted from the ground while low-temperature heat is rejected by the gas cooler. Such an alternative strategy has important technical advantages with a negligible increment of the energy usage. In the second part of this work, the benefits of geothermal subcooling were evaluated. Applying the BIN hours method, it was demonstrated that this system is expected to save on average roughly 5% of the total power consumption, in Stockholm's climate.

The models utilized for the winter and summer season were combined to find the relationship between geothermal storage size and annual energy savings. In this way, it was possible to calculate the present value of the operational savings for the study case. Furthermore, a general methodology for assessing the economic feasibility of this system solution is presented. Finally, several scenarios were investigated to produce parametric curves and to perform a sensitivity analysis. Comparing the results with the typical Swedish prices for boreholes, the cases where this system solution is economically justified were identified. These are supermarkets with a Heat Recovery Ratio (HRR) higher than the average. For examples, supermarkets supplying heat to the neighbouring buildings (considering the Stockholm's climate, systems with an annual average HRR of at least 70%). Relying only on savings from subcooling was found to be not enough to justify a geothermal storage, a not-negligible amount of heat must be extracted in winter. Finally, some interesting concepts and alternatives to a geothermal integration are presented to point out relevant future work.

Keywords: CO2 Refrigeration; Supermarkets; Heat Recovery; Geothermal Storage; Energy Efficiency; Boreholes; Techno-Economic Assessment

Acknowledgement

I would like to thank my academic supervisor, Prof. Samer Sawalha, for his guidance and support. I admire your ability to see the bigger picture and I have constantly tried to improve, learning from you. I think this is an essential quality for both professional and personal development.

I would also like to thank my industrial supervisor Jörgen Rogstam. Your feedback and insights from the industrial world were extremely valuable. Furthermore, working with a leader that truly listen to you and tries to understand what you may need is a privilege more than a pleasure, so thank you for that.

To Simon Bolteau, thanks for your help and patience. Your contagious smile is the most valuable vitamin, during the Swedish winter. To Cajus Grönqvist, thanks for your support and interest in my (often odd) "innovative" ideas. The discussions with you have always been the best way of ending a long working day.

To Juris Pomerancevs, your opinions and advice have been certainly very useful. I have great respect for your diligence and way of reasoning.

A special thanks to my friends and family who have backed me up whenever it was needed in the last two years.

Finally, I would like to dedicate this thesis to my mother. Even though this journey has brought me far away from home, you are and will be always in my heart.

Contents

Figures

Tables

1. Introduction

Supermarkets represent some of the most energy consuming buildings in modern society, with a specific demand varying between 300 kWh/m2 and 600 kWh/m2 (Gullo et al., 2018). Indeed, they are responsible for 3-4% of the annual national electricity consumption in industrialized countries (Karampour et al., 2016). During the last twenty-five years, the utilization of CO2 as a refrigerant has attracted the attention of academics and industrial companies. In 2016, there were roughly 11000 "CO2-only" installations worldwide and 8700 of them were in Europe (Shecco, 2016). Two years later, in 2018, the number of installations worldwide counted for roughly 18000 CO2-based refrigeration systems (Shecco, 2018). The market is expected to grow exponentially reaching 81000 units by 2030 (Shecco, 2016). This is not only due to the low Global Warming Potential (GWP) of CO2 but also to the good performance of this technology when heat is recovered from the refrigeration system (Sawalha, 2008).

Nowadays, the "all-in-one" integrated CO2 trans-critical refrigeration system is considered the best solution to satisfy the heating and cooling demand in supermarkets located in cold climates (Karampour and Sawalha, 2016). Despite this, in warm periods (e.g. summer) the performance dramatically decreases due to high temperatures at the gas cooler outlet. For this reason, the system greatly benefits from sub-cooling the refrigerant (Sawalha, 2012)(Karampour et al., 2018). The integration of geothermal borehole heat exchangers (BHEs) enables the system to sub-cool the refrigerant and, in theory, to provide free-space-cooling to the building.

However, from a techno-economic perspective, the investment cost of the necessary BHE field can exceed the economic gains. The size of the geothermal field, therefore the cost, can be reduced by extracting heat from the ground during winter (Karampour et al., 2018) (Royo, 2017). Moreover, the energy extracted can ensure to fulfil the heating demand of the buildings connected to the refrigeration installation, without the need for additional external heat sources (e.g. district heating). In other words, the boreholes field operates as geothermal seasonal storage.

(Karampour et al., 2018) investigated several scenarios where CO2 trans-critical booster systems were coupled with geothermal boreholes. Through computer-based modelling, the author studied several operational strategies. The outcome of this work was that the heat recovery from the refrigeration cycle should be prioritized, following the control strategy described by (Sawalha, 2012) and described in chapter 5.1, while the heat from the ground should be utilized only for the peaks of heating demand. Furthermore, (Karampour et al., 2018) theoretically demonstrated the profitability of using the geothermal boreholes to provide heat to residential buildings surrounding the installation. The comparison was made assuming that those buildings were previously supplied by a district heating network.

As confirmed by (Gullo et al., 2018) and (Karampour and Sawalha, 2016), there is a shortage of studies dealing with field measurement analysis of CO2 trans-critical booster systems. In particular, such scarcity is more pronounced regarding the integration of geothermal storages. (Royo, 2017) studied ten ground-coupled installations, concluding that not enough measurement points were available for a comprehensive evaluation. In this study, one new system integrated with geothermal boreholes was deeply investigated and the field data were utilized as inputs for a modelling analysis.

1.1. Objective and Scopes

The general aim of this project is to evaluate the performance of one of the state-of-the-art CO2 refrigeration systems based on field measurement data and through modelling to evaluate which parameters affect the profitability of the geothermal integration the most.

The scope of this study can be broken-down in the following objectives:

- Developing a model to elaborate the big amount of data coming from field measurements;
- Analysing the key performance parameter and identify trends to be used as inputs for further modelling;
- Assessing the heat recovery performance (COP) in different working conditions;
- Identifying the main factors influencing the system performance;
- Studying the best theoretical control strategy for heat recovery and evaluate alternatives;
- Comparing the theoretical heat recovery strategies with the current strategy implemented by the system's controller;
- Assessing the economic benefits of the geothermal integration taking into account sub-cooling during summer and heat extraction during winter;
- Assessing the economic benefits and the potential for free space cooling;
- Develop a model for evaluating the economic savings due to the geothermal integration;
- Evaluating the optimal size of the geothermal storage from a techno-economic perspective;
- Identifying the parameters affecting the profitability of a geothermal integration for CO2 refrigeration system installed in supermarket;
- Identifying lessons learned from the operating installation and giving suggestions for the new systems;
- Suggesting relevant future work.

1.2. Limitations

The first limitation of this analysis lays in the fact that every installation is unique. This is not only due to different design choices but also to external constrains such as environmental requirements, availability of resources or magnitude of the demands.

Additionally, some assumptions had to be done due to lack of some measurement points, these are described in section 4.1. Undoubtedly, such an approach leaves room for imprecisions in the results. However, each of the made assumptions is backed-up by a technical explanation and, for this reason, they are thought to not-lead to any relevant error.

The models and the annual energy evaluations were performed utilizing the BIN hours method. Therefore, the thermal and electrical powers utilized are expressed as averages of the outdoor temperature. This leads to a loss of information in terms of peak powers. The effect of peaks on the annual energy use should be minimal. The calculated error between the built models and the measured power consumption is lower than 10%. However, if future work will be carried out an approach using hourly averaged values is advised.

When evaluating the size of a geothermal storage, an hourly demand profile was created using temperatures from a typical year for that location and the average ground load for that temperature. When designing a heating or cooling system, the conditions are usually the worst possible conditions. This is a common problem for energy systems since the design conditions are usually far away from the operational ones. The results presented in the techno-economic analysis do not take into account that the design conditions for the geothermal heat pump (heat injection) are the worst climate conditions under which the system is expected to operate. If this is the requirement an optimization is not possible.

The heat exchanged in the ground and the geothermal storage has been modelled through a software, therefore, once the input parameters (e.g. pipe size, shape etc..) were chosen, they have not been further optimized. This means that the results presented in the techno-economic analysis can be slightly improved. However, this is not thought to modify the final outcome of this work.

Due to time constrains, the free-space-cooling potential could not be fully analysed. Therefore, this has been left for the future work. However, a preliminary analysis shows that free space cooling seems to be unlikely due to the return temperature from the boreholes. A consultation with experts confirmed that the obtained free-space-cooling is almost negligible in these installations.

Another limitation of this work is that, due to time constrains, the geothermal boreholes sizing was not optimized in order to find the best evaporation temperature at the load evaporator for the winter functioning. Values have been taken from literature (Karampour et al., 2018) (Royo, 2017) and the studied case uses the heat extraction for very few hours per year. For these reasons, this limitation does not lead to a relevant error for the studied case. However, this limitation impacts the scenarios generated in the sensitivity analysis. This means that the results shown for those scenarios are conservative and that there is room for improvements. Despite the mentioned limitations, the outcomes of this work are found to be representative of the general trends in this type of installations.

2. Geothermal Boreholes Integration in CO2 trans-critical booster systems

The general concept of integrating a geothermal storage into a refrigeration system is the improvement of the thermodynamic boundaries. The efficiency of a refrigeration/heat pump cycle is mainly determined by the temperature of the heat sink and heat source. The smaller the difference between them, the higher the efficiency. This means that the efficiency of a heat pump improves, extracting heat from a source that is warmer than the outdoor temperature. While a refrigerator benefits from rejecting heat into a sink that is colder than the outdoor temperature. Since the ground is colder than the outdoor temperature in summer and warmer in winter, it represents a better heat sink or source compared to the outdoor temperature.

Due to the high amount of heat that needs to be rejected, in summer the geothermal storage does not exchange energy with the condenser. Instead, it is used to provide subcooling. When a refrigerant expands after having reject heat to the ambient, it becomes a mixture of liquid and vapour. The vapour part is usually referred as flash gas. This portion of the fluid is almost useless for cooling purposes since it is already evaporated. The amount of flash gas grows with the temperature of the refrigerant at the inlet of the high-pressure expansion valve. Therefore, during summer, is the moment when flash gas is produced the most. Subcooling offers the advantage of reducing the amount of flash gas. This means that less mass flow is elaborated by the compressors. In other words, less power is required for the same cooling capacity.

During winter, the main difference between a stand-alone CO2 refrigeration system and one with a geothermal integration lays in the control strategy. In other words, the heat recovery potential of a stand-alone system is limited by the cooling demand, once the maximum mass flow of refrigerant is circulating in the installation it is not possible to recover additional heat. The geothermal integration means that additional mass flow can be circulated in the high-pressure branch since an additional cooling load (the ground) is available. How and when to use such load evaporator is determined by the control strategy.

Dumping heat into the ground in summer and extracting it when needed makes the ground a thermal storage. However, differently from the other type of storages, the main function of the ground is to improve the thermodynamic boundaries of the system, as explained above. The effect of the energy injected into or extracted from the ground is to warm up or cool down the storage. This means that the energy exchanged impacts the temperature of the ground, thus, it impacts the efficiency of the system. In other words, if a refrigeration system injects a lot of heat in summer, during winter the ground will be warmer than what it would have normally been. On the other hand, the energy extracted in winter will cool down the ground for the next summer.

However, if the energy extracted, in the cold months, is very little compared to what has been injected in the previous season, the ground will start warming up. This means that during the years, the subcooling capacity will be reduced, as well as, the efficiency of the refrigeration system.

These are the reasons why the combination of the needed mean fluid temperature in the boreholes and the heat injected/extracted is determining the size of the storage. The interconnection between the heat exchanged with the ground, its impact on the efficiency of the refrigeration system and the necessary size of the geothermal storage is the key to understand the techno-economics of this system solution.

Regarding the geothermal storage, nowadays, the most common configuration consists of vertical or inclined ground heat exchangers (GHEs) connected in parallel. These are usually referred as boreholes. A borehole field is made up of single or multiple drills, with a diameter ranging from 0.075 to 0.180 m and with a depth between 40 and 200 m. The most spread types of heat exchanger are single and double U-shape plastic pipes. Finally, in Sweden, the heat carrier fluid is usually (70-75% of the heat pumps) an aqueous solution of 20-25 wt-% ethyl alcohol, with -15°C freezing point (Monzó, 2018).

3. Methodology

The methodology is organized in two main parts, one dealing with the data analysis and computational tools utilized, the other explaining the equations through which the systems was analysed.

3.1. Data Analysis tools and methodology

Overall, the data handling method can be summarised as a four steps process. The first consists of synchronizing the time series of the measurements. Secondly, the thermal powers are calculated through the thermal properties of the refrigerant. Then, a filtering algorithm corrects those measurements errors which could strongly affect the results. Finally, a data visualization procedure is necessary in order to extrapolate the key information and draw reasoned conclusions.

3.1.1. Synchronization

The investigated plant is monitored through an online platform, connected to a columnar database which can be used to download the field measurements. In the following section, the methodology used to extract key performance parameters from the raw data will be described.

The installed sensors send a measurement reading each minute. However, to save memory in the database the readings are saved only when a change in the value happens. This means that the time series generated when extracting the data are not synchronized.

For this reason, the first step is to synchronize the measurements with a time interval of one minute. Regardless, the tool utilized the general methodology consists of four main steps. The first is to generate an array (m x n) with an empty space in the position where a measurement is missing, this array will have n columns and m rows, n is the number of variables to be synchronized and m is the total amount of moments of time. Secondly, it is important to fill in the empty spaces with the last available recorded value preceding the empty cell. The third step consists of generating a new array (m x 1) containing 1 column with a time series, divided into intervals of the wanted resolution (e.g. 5 minutes), from the first to the last day of the considered period. Finally, the two arrays are merged using a logical test.

Then, to reduce the required computational time, the time interval is downsampled. Downsampling can be done in two different ways. The simplest option is to capture the value at the desired moment of time (e.g. ten minutes). While a more accurate method is to average the value taking into account half of the interval before and after the desired moment of time. For instance, when downsampling from a one-minute to ten-minutes interval, one should take the average of the values starting from five minutes before until five minutes after the specific moment of time. Giving a more specific example, the value at 00:10 AM would be the average of the ten values starting from 00:05 AM until 00:15 AM.

3.1.2. Transformation

From the synchronized data the thermodynamic properties of CO2 can be calculated as first output. Then, these are translated into thermal and electrical powers to be used to assess the performance. Equation are described in the next sub-chapter.

3.1.3. Filtering

Only after that the COPs have been calculated one can proceed with data filtering. When filtering there are two possibilities either the value is imposed to a specific number (e.g. 0) or is "marked" as unknown. The effect is different and also the case in which one or the other should be applied. For example, it is possible that the raw data shows a "negative" power exchanged in the desuperheater, gas cooler or sub-cooler. A null or very small power exchanged is the main possible reason for this error. This is why, in this case, the value of exchanged power should be imposed equal to 0. On the other hand, when a COP is outside a reasonable range the whole dataset in that instant should be "marked" as unknown (erased). This is due to the fact that the COP is a factor which takes into account multiple effects and the error could be everywhere in the dataset.

The difference between these two conditions comes when averaging the data. If the value is imposed to zero the average will be affected by it while, if the value is marked as unknown (empty cell) it will not be taken into account when calculating the average.

3.1.4. Visualization

The field data analysis model is organized into excel workbooks, one for each month. Then, through several queries the filter's outputs are compiled and gathered in one matrix. The filter output does not only contain powers and COPs but also key parameters such as discharge pressure, gas cooler inlet temperature, ambient temperature. Thus, the matrix is composed of an array (m x n) where m is the number of instants considered (e.g. time series of 1 year with values each 5 minutes, m = 8760*12) and n is the number of parameters.

Such a matrix represents the input for Microsoft Power Tools (e.g. Power Pivot or Power BI). These can build one-to-many-relationships and averaging the data using as a base one of the parameters contained in the matrix (e.g. outdoor temperature or Heat Recovery Ratio). Using these tools, it is possible to create "advanced" aggregations using the DAX language. For instance, it is possible to easily extrapolate from such a matrix the COP heat recovery averaged over the outdoor temperature but considering only the moments when parallel compressors are active.

3.1.5. Computational Tools

The computational tools utilized for the data analysis were Microsoft Power Tools as described. A Visual Basic (VBA) Code connected to the software REFPROP is used for calculating the thermodynamic properties and also for the built models. Finally, the software Energy Earth Designer (EED) was used for simulating the geothermal boreholes.

3.2. System Description

The supermarket refrigeration system described in this session is installed in south of Sweden, in the climate zone III and started operating in May 2018. The plant scheme is displayed in Figure 3.1. This CO_2 trans-critical booster system provides cooling at two temperature levels, corresponding to cabinets and freezers. The heat is recovered from the refrigeration cycle to provide space heating during winter and tap water heating during the whole year.

The geothermal storage consists of 16 boreholes heat exchangers of 200-meter depth; these are used to satisfy the peaks of heating demand extracting heat from the ground. Additionally, the boreholes enable the sub-cooling of refrigerant during warm periods. This makes such a solution very promising in terms of cost-effectiveness. Summarizing, the only energy carrier bought externally is the electricity needed for compressors, pumps, ventilation, auxiliaries and lighting.

Four medium temperature (MT) compressors represent the heart of the system, recirculating refrigerant from the cabinets evaporator to the gas cooler. Additionally, four parallel compressors were implemented to take care of the flash gas generated at the outlet of the high pressure expansion valve. These machines are also used to extract heat from the ground and to provide air conditioning. Finally, three low temperature (LT) compressors bring the refrigerant from the freezers evaporator to the suction line of MT compressors.

The heat recovery is done in two stages according to the different temperature levels of the heating demand, respectively tap water and space heating. Such a strategy increases the heat that can be recovered from the cycle since the temperature profiles of the secondary fluid in the heat exchangers can be adjusted to fit the CO_2 temperature profile (Rogstam et al., 2013). Then, the refrigerant goes through a gas cooler installed on the rooftop which, depending on the operational conditions, can also act as a condenser. Finally, a geothermal sub-cooler was implemented to dump excess of heat into the ground during warm seasons.

Four internal heat exchangers (IHXs) were installed, these are mainly used to provide further sub-cooling of the refrigerant before entering cabinets and freezers (Kauko et al., 2016). The evaporator which is used to extract heat from the ground and to provide air conditioning works at an intermediate pressure between the liquid receiver and the medium temperature level. Obviously, this is the same suction pressure of the parallel compressors. In case the amount of flash gas does not reach the minimum mass flow elaborated by the parallel compressors, the flash gas is by-passed on the suction line of the MT compressors. The expansion valves on the different temperature levels are regulate to control the internal superheat in the evaporators. An essential component is the by-pass valve before the gas cooler which enables the regulation of the heat recovery, as will be discussed in chapter 5.

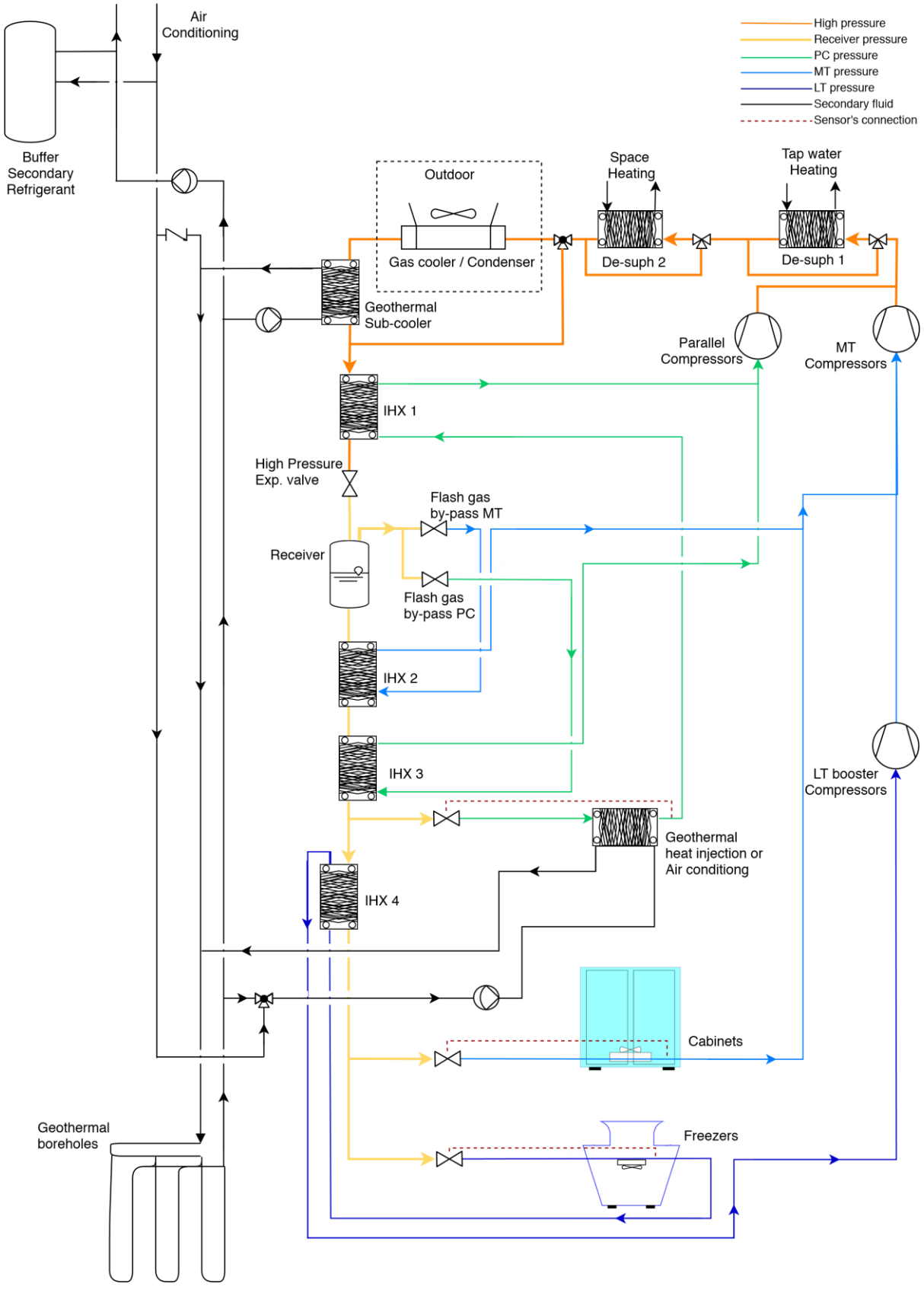

Figure 3.1 Scheme of the CO2 trans-critical booster system integrated with heat recovery, air-conditioning and geothermal boreholes.

3.3. Mathematical model

The mathematical model utilized to calculate the cooling capacities, heating demand and electricity consumption of the installation is described in the following section. The model is explained analysing the different components separately.

3.3.1. Compressors

Regarding the compressors, the two key parameters which had to be calculated were the refrigerant mass flow and electricity consumption. In this case, compressors are analysed as a black box. The mass flow elaborated by a compressor is calculated as follow:

$$\dot{m} = \eta_v(\beta) * V * \alpha * \rho_{suc}(T_{suc}; p_{suc}) \tag{3.1}$$

Where the volumetric efficiency $\eta_v(\beta)$ is a function of the compression ratio β and was calculated from the manufacturer data. V is the swept volume, α is the running capacity of the compressors and $\rho_{suc}(T_{suc}, p_{suc})$ is the density of the fluid in the suction line. The Electricity consumed is then calculated as:

$$\dot{E} = \frac{\dot{m} * (h_{dis} - h_{suc})}{(1 - \dot{Q}_{loss})} \tag{3.2}$$

Where $\dot{Q}_{loss}$ is the heat dispersion from the compressors' shell, estimated to be 7% (Berglöf, 2018). $(h_{dis} - h_{suc})$ is the difference of specific enthalpy between discharge and suction line. The discharge enthalpy was calculated from the compressors data sheet, using the total efficiency $\eta_{tot}(\beta)$ defined as follow:

$$\eta_{tot}(\beta) = \frac{\dot{m} * (h_{dis_{is}} - h_{suc})}{\dot{E}} \tag{3.3}$$

The term $h_{dis_{is}}$ represents the discharge enthalpy of an isentropic compression performed considering the same boundaries (β *and* h_{suc}) of the real compression. The efficiency $\eta_{tot}(\beta)$ not only takes into account the isentropic losses but also transmission (mechanical) and electrical losses.

3.3.2. Desuperheaters , Gas cooler and Sub-cooler

The necessary parameter to be obtained for the heat exchangers was the thermal power exchanged between the fluids. The heat exchanged in these components was calculated as:

$$\dot{Q} = \dot{m} * (h_{out} - h_{in}) \tag{3.4}$$

Where $(h_{out} - h_{in})$ is the difference between the inlet and outlet of the heat exchangers. In the whole high pressure branch, the conditions at the outlet of one heat exchanger were assumed to be the same as the one at the inlet of the following.

3.3.3. Liquid receiver

For this component, the crucial values to be calculated are the outlet mass flows of liquid and vapour. These depend on the thermodynamic conditions at the inlet of the expansion valve. Figure 3.2 shows the simplified schematic of the inlet and outlet flows in the liquid receiver.

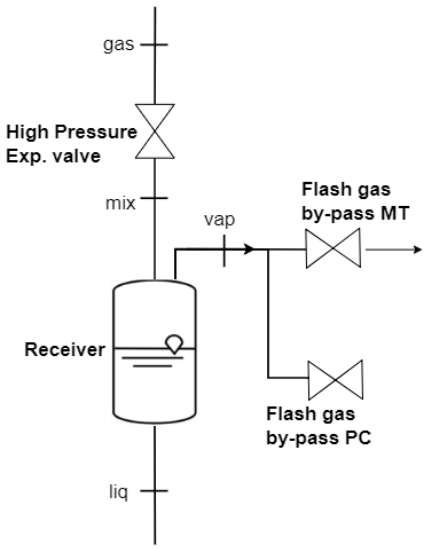

Figure 3.2 Simplified scheme of the liquid receiver.

The process through an expansion valve is assumed to be an isenthalpic expansion, for this reason the enthalpy at the receiver inlet is:

$$h_{mix} = h_{gas}(T_{gas}, P_{gas}) \tag{3.5}$$

Considering that the plant was analysed assuming steady-state operations, the mass flows of vapour and liquid are respectively:

$$\dot{m}_{vap} = \dot{m}_{gas} * \chi_{mix}(h_{mix}, P_{rec}) \tag{3.6}$$

$$\dot{m}_{liq} = \dot{m}_{gas} * \left(1 - \chi_{mix}(h_{mix}, P_{rec})\right) \tag{3.7}$$

Where $\chi_{mix}(h_{mix}, p_{rec})$ is the quality of the fluid considering the enthalpy at the outlet of the expansion valve and the receiver pressure. The title χ_{mix} can also be calculated as the ratio shown in Eq. 3.8

$$\chi_{mix} = \frac{h_{gas} - h_{liq}}{\Delta h_{vap,rec}} \tag{3.8}$$

$\Delta h_{vap,rec}$ refers to the enthalpy of vaporization at the receiver pressure, while h_{liq} is the enthalpy of the saturated liquid for the same pressure. Eq 3.8 will be used in chapter 8, for modelling the savings reduction resulting from a heat injection reduction.

3.3.4. Internal Heat Exchangers

Four internal heat exchangers (IHXs) are implemented in this installation. The effect of this type of integrations was studied by (Karampour and Sawalha, 2014). The efficiency of this heat exchangers ε varies between 35 and 50%. It is worth to mention that their influence was found to be marginal on the overall performance of these systems (Karampour and Sawalha, 2014). However, such an efficiency was found to be necessary to calculate the properties of the refrigerant in points were measurements were missing. This will be further discussed in the following sections. Figure 3.3 gives a graphical representation of one of this IHXs, highlighting the difference between cold and hot side.

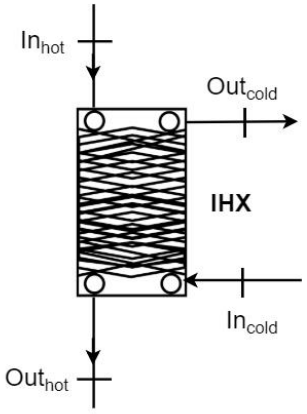

Figure 3.3 Scheme of an Internal Heat Exchanger (IHX), highlighting cold and hot side.

The heat exchanged is equal to:

$$\dot{Q}_{IHX} = (\dot{m} * c_p)_{cold} * (T_{out_{cold}} - T_{in_{cold}}) = (\dot{m} * c_p)_{hot} * (T_{in_{hot}} - T_{out_{hot}}) \quad (3.9)$$

Taking into account Eq. (3.9) the efficiency of an IHX can be calculated as:

$$\varepsilon = \frac{\dot{Q}_{IHX}}{\dot{Q}_{IHX\,max}} = \frac{(\dot{m} * c_p)_{cold} * (T_{out_{cold}} - T_{in_{cold}})}{(\dot{m} * c_p)_{min} * (T_{in_{hot}} - T_{in_{cold}})} = \frac{(\dot{m} * c_p)_{hot} * (T_{in_{hot}} - T_{out_{hot}})}{(\dot{m} * c_p)_{min} * (T_{in_{hot}} - T_{in_{cold}})} \quad (3.10)$$

In these applications, the minimum heat capacity rate $(\dot{m} * c_p)_{min}$ is always the one of the cold fluid, $(\dot{m} * c_p)_{cold}$.

3.3.5. Cabinets, Freezers and geothermal evaporator.

The primary function of a refrigeration system in a supermarket is to satisfy the cooling loads in the cabinets and freezers. A symbolic representation of these components is given in Figure 3.4. The device controlling the electronic expansion valves functions targeting a temperature set-point. To be more precise, the set-point is calculated chasing a constant degree of superheat at the cabinets outlet. In Figure 3.4, the control signal is represented by the red dashed line.

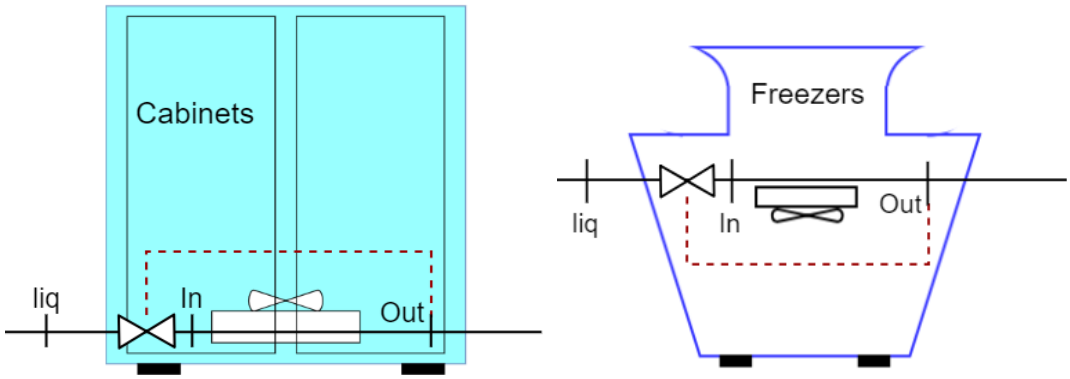

Figure 3.4 Scheme representing cabinets and freezers.

The cooling capacity in the evaporators is calculated as:

$$\dot{Q}_{cool} = \dot{m}_{liq}(h_{out} - h_{in}) \quad (3.11)$$

In this model, the mass flow of refrigerant is aggregated for all the cabinets as well as for all the freezers. This is equivalent to assume to have only one big cabinet and one big freezer. The specific enthalpies h_{in} and h_{out} are calculated as follow:

$$h_{in} = \mathrm{h_{liq}} \quad (3.12)$$

$$h_{out} = h(P_{ev}; T_{ev} + T_{suph}) \quad (3.13)$$

Where the specific enthalpy of the liquid refrigerant ($\mathrm{h_{liq}}$) is calculated assuming that the fluid is at the same conditions as the output of the last internal heat exchanger, IHX_4 in Figure 3.1. While, the term $h(P_{ev}; T_{ev} + T_{suph})$ is the specific enthalpy of CO_2 at the evaporation pressure and at the evaporation temperature, increased of a constant degree of superheat. The latter was obtained analysing the field measurements which will be discussed in section 4.1 . The same methodology was applied to the geothermal heat extractor.

3.3.6. External Superheating.

The heat absorbed through external superheating was also considered in this analysis. The heat absorbed was calculated as:

$$\dot{Q}_{xsh} = \dot{m}_{liq}(h_{suc} - h_{out}) \quad (3.14)$$

Where h_{suc} is the enthalpy at the suction point of the compressor and h_{out} is the outlet enthalpy from the evaporators.

3.3.7. Missing data and Iterative processes

Due to the lack of measuring devices, the inlet temperature at the expansion valve had to be calculated through an iterative process. This was based on the assumption of having an internal heat exchanger (IHX1) with an efficiency ε_{IHX_1} of 45% (Karampour and Sawalha, 2016). The numbering utilized in this sub-chapter refer to the scheme displayed in

Figure 3.5.

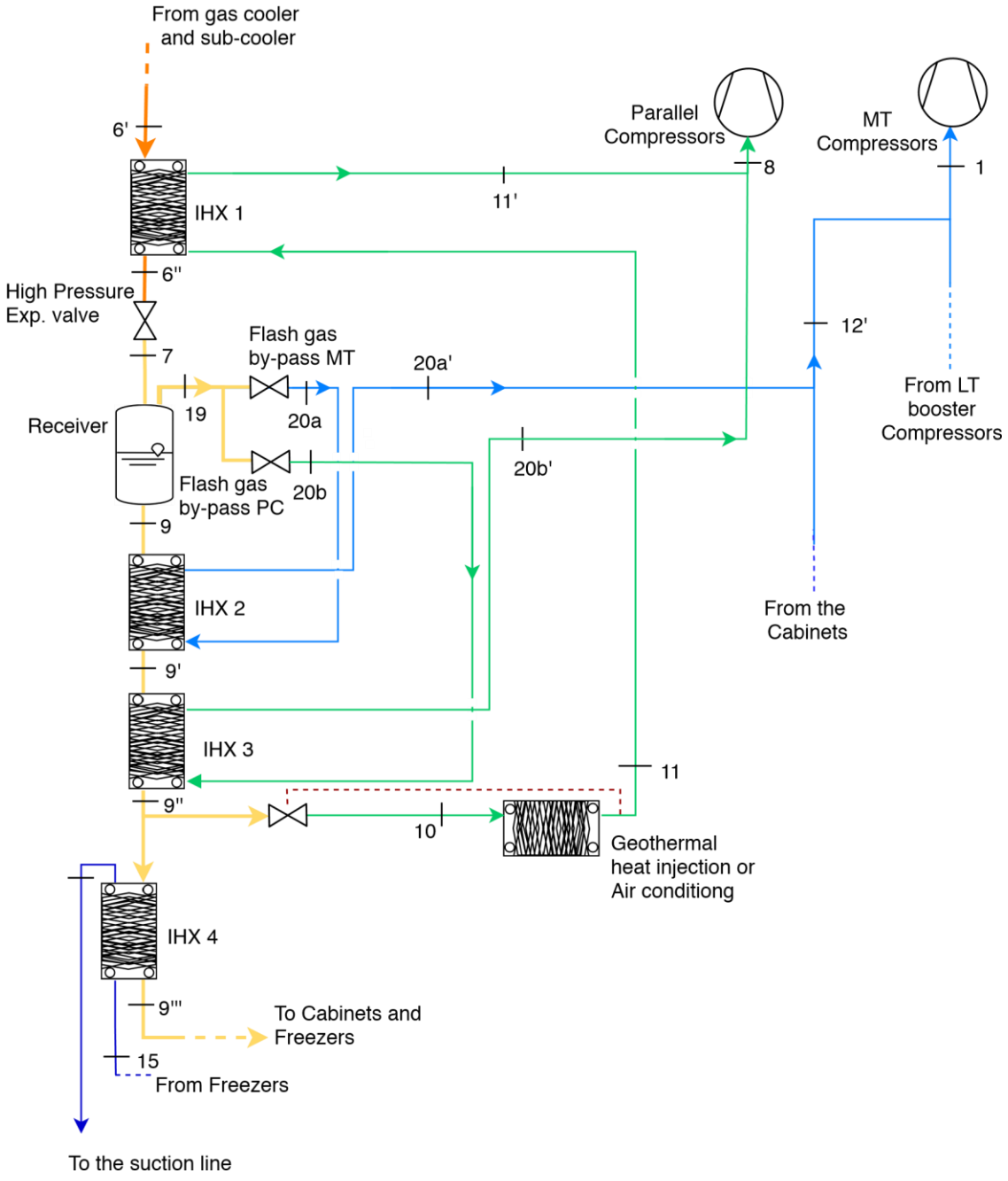

Figure 3.5 Scheme of the installation section where an iterative process was performed.

The iteration process is shown in Figure 3.6.

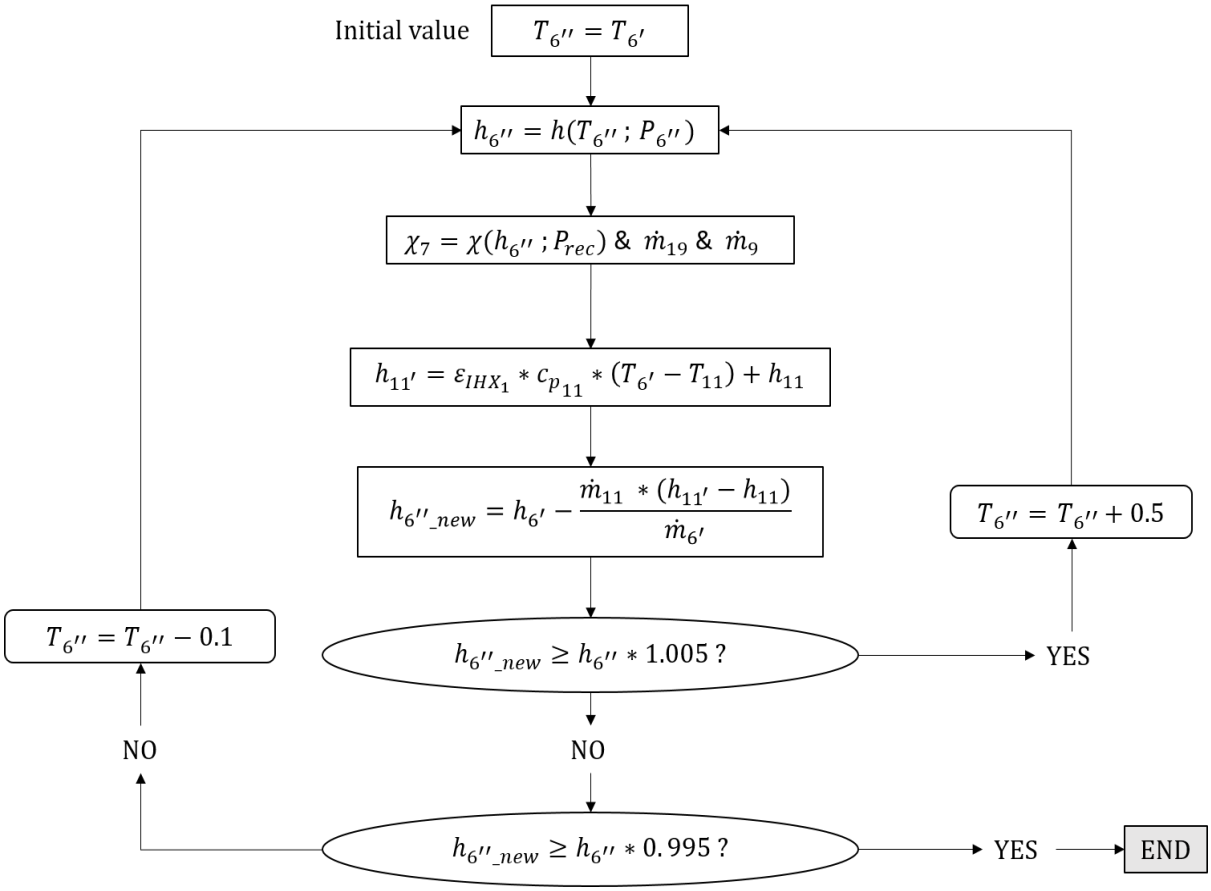

Figure 3.6 Iterative procedure used to calculate the expansion valve inlet temperature.

Once the mass balance on the receiver is solved, the outlet enthalpies from the internal heat exchangers on the liquid line (IHX 2-4) can be calculated. These are derived using Eq. 3.8. and Eq. 3.9

3.3.8. Heat Recovery Ratio

In this document, the heating demand is often expressed in terms of heat recovery ratio (HRR), which is defined as the total heat available at suction of the medium-temperature compressors and the total heat recovered. The mathematical formula is expressed in equation 3.15.

$$HRR = \frac{\dot{Q}_{SH} + \dot{Q}_{TW}}{\dot{Q}_{MT} + \dot{Q}_{LT} + \dot{E}_{LT_{Shaft}} + \dot{Q}_{MT_{xsh}} + \dot{Q}_{LT_{xsh}}} \tag{3.15}$$

3.3.9. Coefficients of Performance

Once calculated the refrigerant mass flows, enthalpies and heat exchanged, it is possible to calculate the Coefficients of Performance (COPs). These formulas were taken from (Karampour and Sawalha, 2016), adding pump consumption for the secondary fluid in the geothermal loop where necessary. The total COP of the system takes into account both cooling and heating loads.

$$COP_{TOT} = \frac{\dot{Q}_{MT} + \dot{Q}_{LT} + \dot{Q}_{AC} + \dot{Q}_{SH} + \dot{Q}_{TW}}{\dot{E}_{MT} + \dot{E}_{LT} + \dot{E}_{PC} + \dot{E}_{fan} + \dot{E}_{geo_{pump}}} \tag{3.16}$$

If one evaluates only the cooling loads the COP cooling can be defined as:

$$COP_{cool} = \frac{\dot{Q}_{MT} + \dot{Q}_{LT} + \dot{Q}_{AC}}{\dot{E}_{MT} + \dot{E}_{LT} + \dot{E}_{PC} + \dot{E}_{fan} + \dot{E}_{geo_{pump}}} \tag{3.17}$$

Where $\dot{Q}_{MT}$, $\dot{E}_{MT}$, $\dot{Q}_{LT}$ and $\dot{E}_{LT}$ are respectively cooling capacity and compressor's power consumption of medium and lower temperature level (cabinets and freezers). $\dot{Q}_{AC}$ refers to the cooling load of the air conditioning while $\dot{Q}_{SH}$ and $\dot{Q}_{TW}$ are the heating demand for space heating and tap water. $\dot{E}_{PC}$ is the power consumption of the parallel compressors, finally, $\dot{E}_{fan}$ and $\dot{E}_{geo_{pump}}$ represent the power consumption of gas cooler fan and pumps of geothermal loop. The coefficient of performance for the medium temperature level was calculated as:

$$COP_{MT} = \frac{\dot{Q}_{MT} + \dot{Q}_{LT} + \dot{E}_{LT_{Shaft}} + \dot{Q}_{MT_{xsh}} + \dot{Q}_{LT_{xsh}}}{\dot{E}_{MT} + \dot{E}_{fan}} * \frac{\dot{Q}_{MT}}{\dot{Q}_{MT} + \dot{Q}_{MT_{xsh}}} \tag{3.18}$$

The terms $\dot{Q}_{MT_{xsh}}$ and $\dot{Q}_{LT_{xsh}}$ refer to the heat absorbed through external superheat. $\dot{E}_{LT_{Shaft}}$ is the power directly transmitted to the fluid. This does not take into account the heat dispersion from the compressors. Moving forward, the COP for the low temperature level was calculated as:

$$COP_{LT} = \frac{\dot{Q}_{LT}}{\dot{E}_{LT} + \left(\dot{E}_{MT} + \dot{E}_{fan}\right) * \left(\frac{\dot{Q}_{LT} + \dot{Q}_{LT_{xsh}} + \dot{E}_{LT_{Shaft}}}{\dot{Q}_{MT} + \dot{Q}_{LT} + \dot{E}_{LT_{Shaft}} + \dot{Q}_{MT_{xsh}} + \dot{Q}_{LT_{xsh}}}\right)} \tag{3.19}$$

In order to compare the efficiency of the heat recovery from the refrigeration plant to the one of a stand-alone heating system, a COP heat recovery is utilized. This is defined as:

$$COP_{HR} = \frac{\dot{Q}_{SH} + \dot{Q}_{TW}}{\dot{E}_{TOT} - \dot{E}_{FC_{MODE}}} \tag{3.20}$$

In Eq 3.20 the value $\dot{E}_{TOT}$ represents the total power consumption, while, $\dot{E}_{FC_{MODE}}$ is the power the system would consume in floating condensing mode (FC).

One of the demands satisfied by all-in-one CO_2 trans-critical installations is space cooling. The COP defined in Eq. 3.21 can be used to compare the efficiency of supplying space cooling with the COP of a classic air conditioning device. In this case, the air conditioning evaporator was connected to the parallel compressors, therefore, the energy spent for this function will be equal to the power consumed by the parallel compressors minus the power absorbed for re-compressing the flash gas.

$$COP_{AC} = \frac{Q_{AC}}{\dot{E}_{pc,AC} - \dot{E}_{pc_{fg}}} \tag{3.21}$$

Where $\dot{E}_{pc,AC}$ is the energy spent by the parallel compressors to extract heat from the AC loop and $\dot{E}_{pc_{fg}}$ is the energy spent for re-compressing the flash-vapour generated after the expansion valve and only due to the liquid mass flow of cabinets and freezers. Finally, a COP for the geothermal heat extraction is proposed (Eq. 3.22) in order to assess the efficiency of the geothermal heat pump function.

$$COP_{hex} = \frac{(\dot{Q}_{SH} + \dot{Q}_{TW})_{TOT} - (\dot{Q}_{SH} + \dot{Q}_{TW})_{from\,MT}}{E_{TOT} - E_{no_{hex}}} \tag{3.22}$$

In Eq. 3.22, the term $(\dot{Q}_{SH} + \dot{Q}_{TW})_{from\,MT}$ represents the heat recovered taking into account only the mass flow coming from the MT compressors. In other words, the mass flow of refrigerant evaporated in cabinets and freezers.

$E_{no_{hex}}$ is the total power consumption without taking into account the power absorbed by parallel compressors and by the pumps for the secondary refrigerant in the geothermal loop. It is worth to mention that when the geothermal heat extraction is active, the amount of flash gas generated is negligible. Therefore, this was not subtracted from the total mass flow elaborated by the parallel compressors.

3.3.10. Floating condensing mode

A system is said in floating condensing mode (FC mode), if the medium temperature compressors are controlled to discharge the CO_2 at the minimum pressure as possible, according to the outdoor temperature. During winter, the floating condensing mode is used as reference scenario for calculating the COP heat recovery. For these reasons, the assumption on which the winter FC mode is based are crucial for the COP. The assumptions for the floating condensing mode when the heat recovery is active were taken from field data. The condensing temperature was assumed to be 7 K higher than the outdoor temperature with 12°C as minimum, even in subcritical operations, 3K of subcooling were estimated inside the condenser. The minimum outlet temperature from the gas cooler was assumed to be 10 °C.

4. Field Measurements Analysis

4.1. Assumptions due to lack of data

Due to the lack of measurement points several assumptions were necessary. The main ones are described in the following paragraphs.

4.1.1. Internal Super heat

In the studied installation there are no measurement sensors on the common return line from cabinets (MT) and freezers (LT). However, measurements are available at the outlet of each unit. Figure 4.1 depicts the monitoring device utilized for regulating the refrigerant mass flow across the evaporators. The temperature signal S2 and the pressure signal P are utilized to chase a specific degree of internal superheat at the evaporator's outlet.

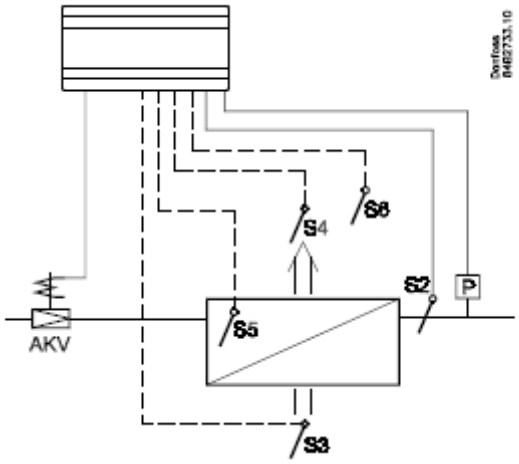

Figure 4.1 Field Measurements: Scheme of Danfoss' monitoring device AK-CC 550A for a typical supermarket cabinet source: (Danfoss, n.d.).

In order to evaluate the total cooling demand, it was necessary to assume a fixed value of internal superheat or a fixed cabinets outlet temperature (S2). This assumption leads to a negligible error due to the cabinets control system which, as previously mentioned, chases a specific degree of internal superheat. Moreover, due to the legal constraints on temperature variation inside cabinets and freezers, not only the degree of internal superheat is strictly controlled but also the cabinets outlet temperature (S2).

To identify a general value for the S2 temperature (which will be utilized to calculate the cooling demand), field measurements of all the cabinets were studied for three days in three different periods of the year: July 15th; January 15th; September 15th. Figure 4.2 depicts the trend of the average outlet temperature (S2) from all the freezers on July 15th. The visible peaks are due to the defrosting (periodic melting of the ice formed on the cooling coils through electric resistances).

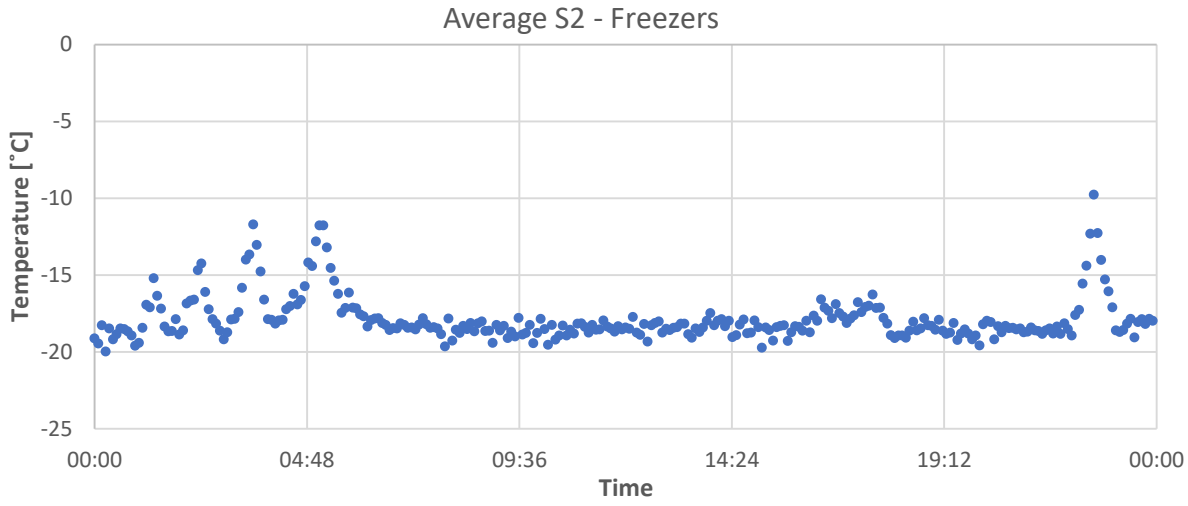

Figure 4.2 Field Measurements: Average Freezers' coils outlet-temperature on July 15th.

Then, the measurements were averaged on an hourly basis and a comparison between the three days was made. This is displayed in Figure 4.3.

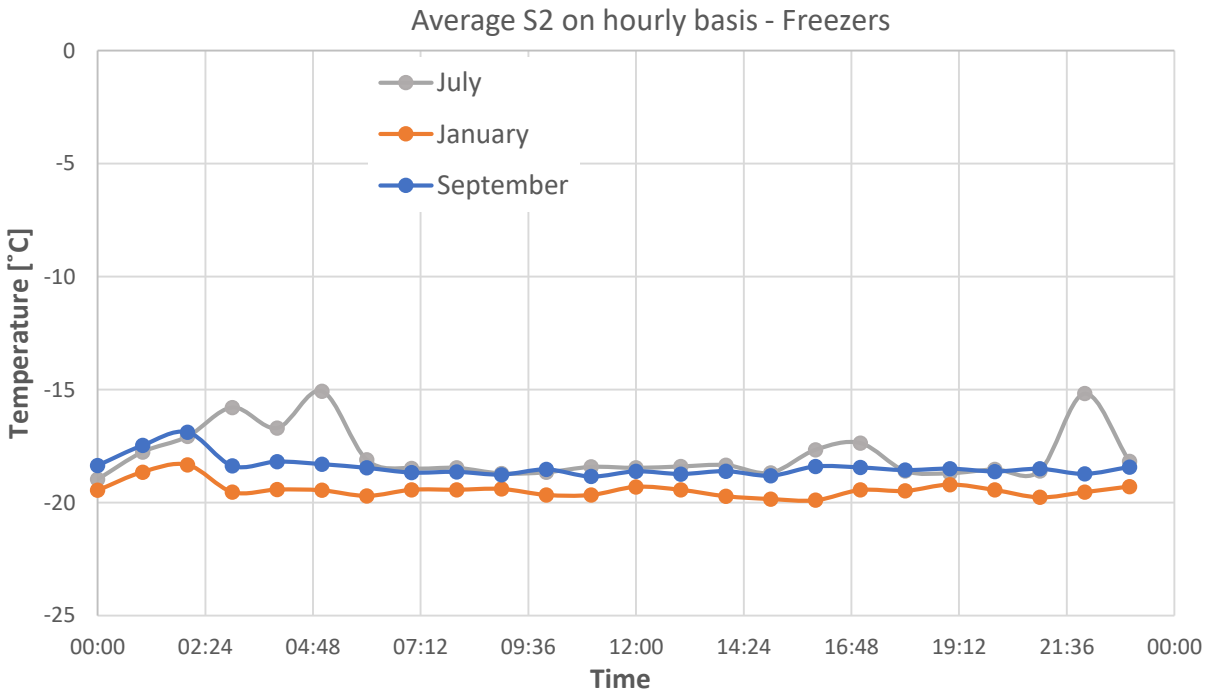

Figure 4.3 Field Measurements: Comparison between Freezers' coils outlet temperature for different months.

The same plots are presented for the freezers in Figure 4.2 and Figure 4.3 are proposed for the cabinets in Figure 4.4 and Figure 4.5.

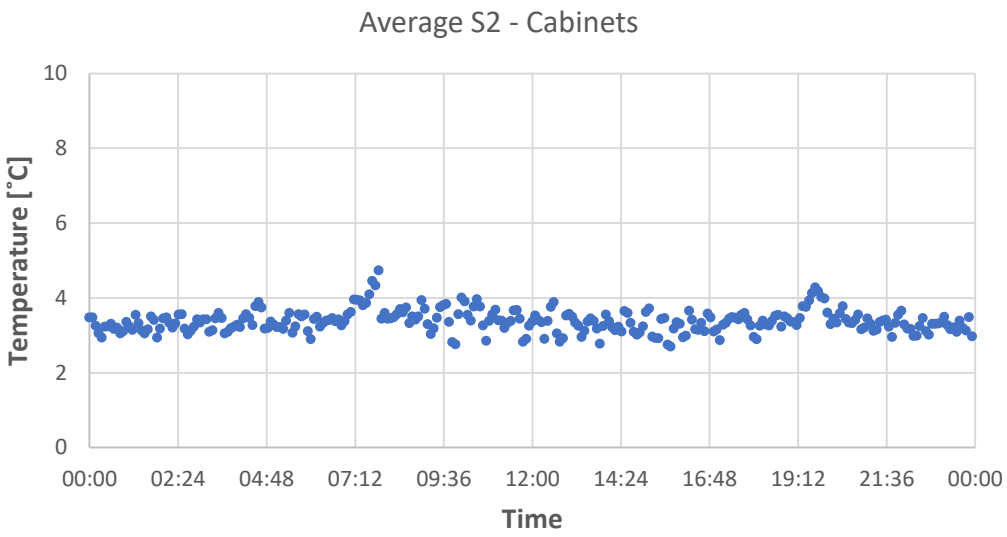

Figure 4.4 Field Measurements: Average Cabinets' coils outlet temperature on July 15th

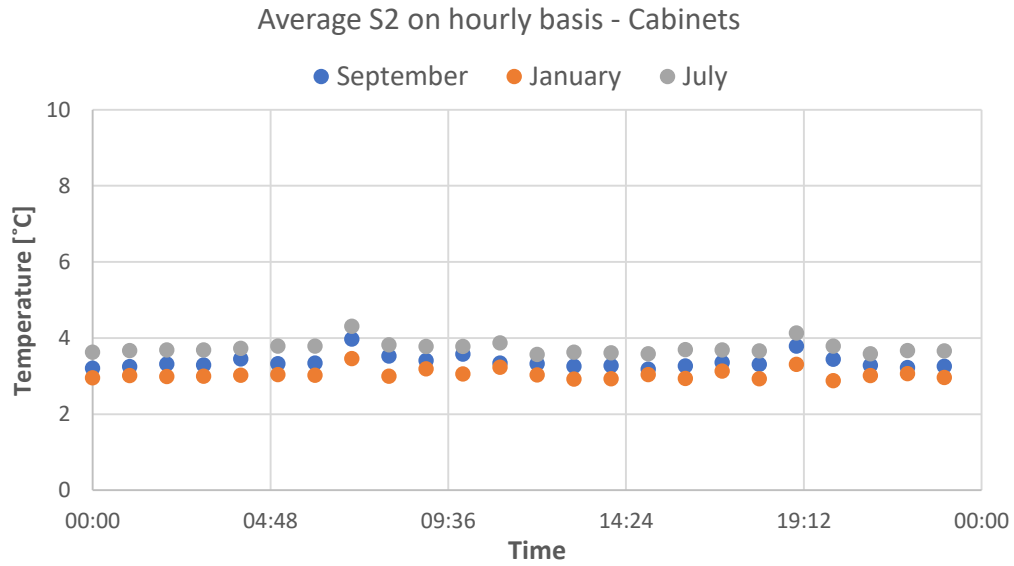

Figure 4.5 Field Measurements: Comparison between Cabinets' coils outlet temperature for different months.

A slight increase in the S2 temperature is visible during the warmer months, however, for the scope of the analysis, such a variation has a negligible effect on the final result. The S2 temperature stability in this supermarket can be attributed to the installed glass doors which not only lead to a reduced energy consumption (Mainar Toledo and Garcìa Peraire, 2016) but also to a more stable temperature variation. To summarize, the average S2 temperature used to calculate the outlet cabinet's enthalpy is 3.5°C while -18.5°C was used for the freezers.

4.1.2. Specific enthalpy at compressors' outlet

The specific enthalpy at the discharge of the compressors is strongly dependent on the temperature measurement in that point. The measured discharge temperature is accurate enough for calculating the heat recovered from the first de-superheater but it cannot be used for the compressors' power consumption (Eq 3.2). This is due to heat losses through the compressors' jacket, heat removed by the lubricant and heat losses between the discharge valve and the sensor. Moreover, the compression is made through several

compressors installed in parallel and they are never working simultaneously, leaving additional room for imprecisions.

For these reasons, when evaluating the power absorbed for compressing the refrigerant, it is not possible to calculate the discharge enthalpy utilizing field temperature measurements. Therefore, the specific discharge enthalpy was obtained using the total efficiency (Eq. 3.3) extrapolated from the manufacturer data. The total efficiency for MT compressors obtained in this way is shown in Figure 4.6. As depicted, the efficiency's equations differ from transcritical to subcritical operations, this was taken into account.

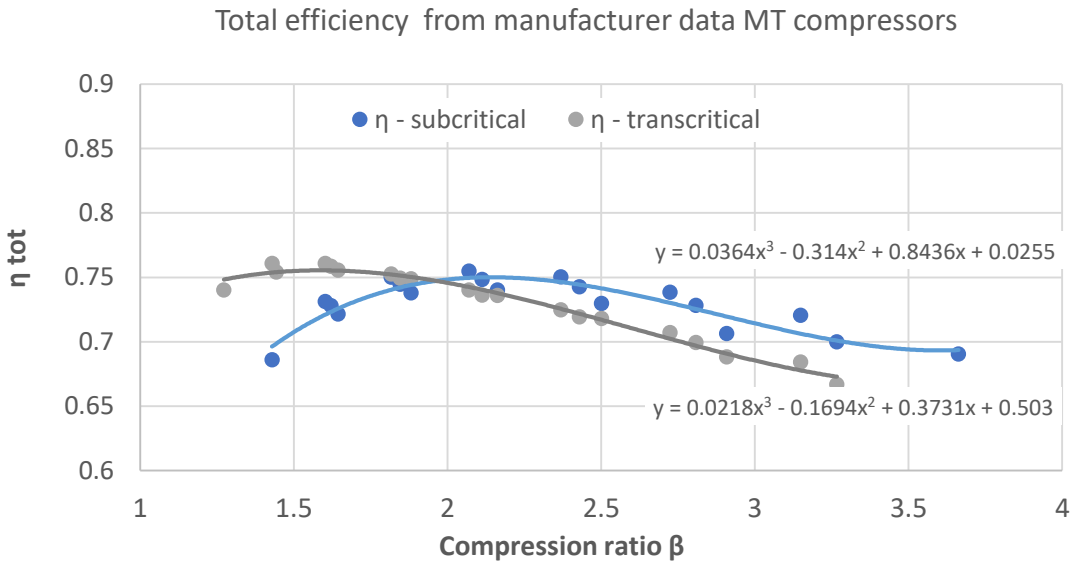

Figure 4.6 Total efficiency from manufacturer data - MT compressors.

4.1.3. Suction conditions parallel compressors in winter

In this case, the parallel compressors were found to be extremely over-dimensioned for the heat extraction mode (winter operations). Such an over-sizing lead to a highly discontinue (frequent start and stop) functioning of the parallel compressors. Moreover, this type of operation gives rise to unstable conditions at the suction point of these devices. For this reason, when modelling the functioning of the parallel compressors for simulating floating condensing mode and the operational strategies during winter, the suction pressure was assumed to be respectively 35 bar. This data was obtained by analysing the field measurements and filtering all the points of discontinue operation.

4.1.4. Load evaporator's outlet temperature

The outlet temperature of the load evaporator is not measured in the installation. This is an essential value to estimate the AC load and the heat extracted from the ground. In order to cope with this issue, a fixed value of internal superheat equal to 3.5 K was utilized. While in cooling coils (e.g cabinets and freezers) the internal superheat is in the order of tens degrees Kelvin in plate heat exchangers (HEXs) this value is way lower. This is due to the evaporation front which, in the case of plate HEXs, is relatively closer to the liquid injection points, therefore, easier to control.

4.2. Key Parameters

In this section, the key parameters are introduced with the scope of describing the general functioning of the system. The trends and functions identified from the field measurements have been used to generate the inputs for the models described in this thesis.

4.2.1. High-pressure branch

The high pressure-branch key parameters are the discharge pressure from the MT and parallel compressors, the gas cooler outlet-temperature, the gas cooler fans's power and the expansion valve inlet-temperature. The latter is presented in chapter 6 , were the subcooling analysis is discussed. Figure 4.7 displays the trend of three key parameters averaged on the ambient temperature.

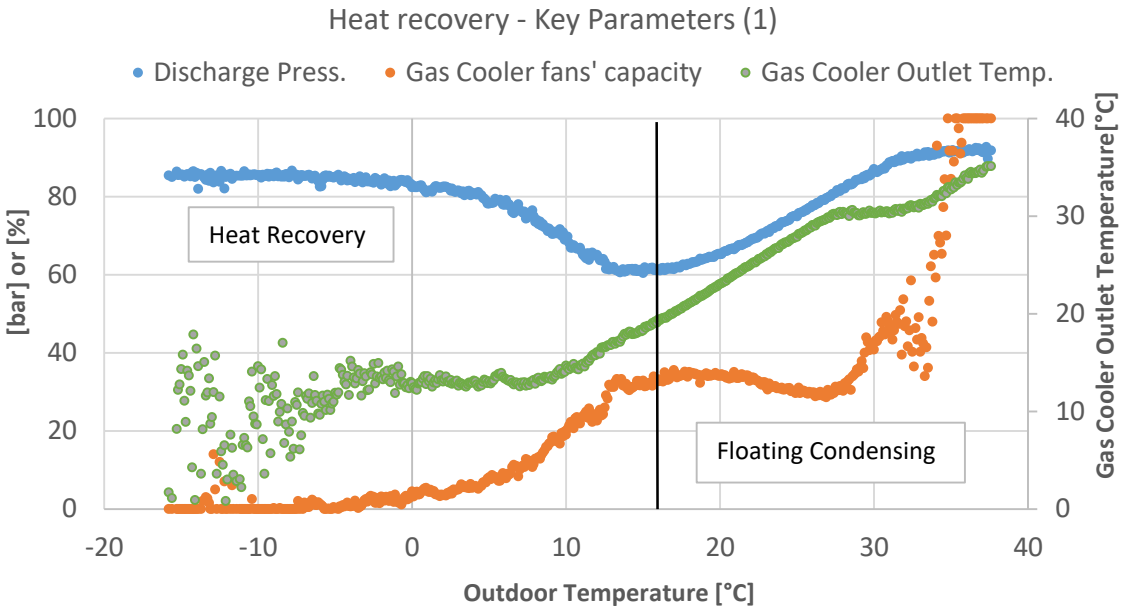

Figure 4.7 Field Measurements: Discharge Pressure (primary axis); Gas Cooler fans capacity (primary axis) and Gas Cooler inlet temperature (secondary axis), plotted as a function of the ambient temperature.

In floating condensing mode, the discharge pressure (blue points) depends on the ambient temperature. The equivalent condensing temperature is on average 7K higher than the ambient temperature. The gas cooler outlet temperature (green points) is roughly 3.5K higher than the outdoor temperature, when the CO2 temperature is lower than the critical temperature. This means that during subcritical operations, at the outlet from the gas cooler the refrigerant has 3.5K of subcooling. For a conservative estimation when modelling, a subcooling of 3K was considered. At around 25°C (outdoor temperature) the discharge pressure overcome the critical point. When this happens, the discharge pressure is controlled following the Eq 4.1

$$P_{dis_{fc}} = 2 * T.amb.\ [^{\circ}C] + 26\ [bar] \tag{4.1}$$

For very warm outdoor conditions (>29°C), a change in the behaviour of the gas cooler outlet temperature can be noticed. This is the point where the outlet temperature from the gas cooler exceeds the critical temperature. In this conditions the approach temperature become 2K.

The gas cooler in this installation was found to be over-dimensioned (750 kW cooling capacity) for the application. Indeed, for the vast majority of the time the system works around 30% of its capacity. This is probably the reason why there is sub-cooling in sub-critical conditions. Only when the outdoor temperature achieves incredibly high values (for the Swedish climate) the system tries to compensate and it steeply increases the fans power from 30 to 100%.

During heat recovery mode, the gas cooler outlet temperature decreases until it reaches its minimum that in this case is set at roughly 10 °C. The gas cooler fan capacity is inversely proportional to the discharge pressure. When the latter arrive at its designed value (85 bar), the gas cooler fan is switched-off and the CO2 is cooled for natural convection as it continues to flow through the gas cooler. When this happens, the system is not able to control the gas cooler outlet temperature anymore, as it can be seen in Figure 4.7 (green points). In this system a malfunctioning of the gas cooler by-pass valve does not allow the refrigerant to by-pass the gas cooler when necessary. The effects of such a malfunctioning on the heat recovery control strategy are discussed more in details in chapter 5

During the heating period (outdoor temperature < 13°C), the discharge pressure is increased in order to satisfy the space heating demand which, in this case, is the controller's priority among the two heating demands. The average heating demand grows linearly with the decrease of outdoor temperature as it can be seen in Figure 4.12 . The discharge pressure gradually raises bringing the cycle from sub-critical to trans-critical until the pressure reaches its maximum value (without considering troubleshooting). At this point, if more heat is necessary, the controller activate the heat extraction from the ground evaporating part of the refrigerant in a load evaporator connected to the boreholes. Regulation is done through a temperature signal from a sensor positioned on the space heating supply line. As previously mentioned, the gas cooler is never by-passed. The heat recovery control strategy will be discussed more in details in chapter 5.

4.2.2. Suction lines

Part of the key parameters of the suction lines have been already discussed in the assumptions. These parameters are usually quite stable since the conditions in cabinets and freezers have to be maintained very stable. The stability is further increased considering that this is a newly-built system which started operating in 2018. To begin with, the evaporation temperature at the MT level was found to be roughly -4˚C, in winter, and -5˚C in summer when the load is higher due to higher humidity. The evaporation temperatures at the LT level are -30 ˚C and -32 ˚C, respectively in winter and summer. Air Conditioning is supplied with an evaporation temperature of 2.6˚C, obviously, this value presents slightly more fluctuations than cabinets and freezers but still very stable. Regarding the suction temperatures, only the freezers presented a quite stable temperature of -4 ˚C. The suction temperature for the MT and parallel compressors are presented in Figure 4.8. The decrease of the suction temperatures during the warm period is due to a gradual increase of the refrigerant mass flow.

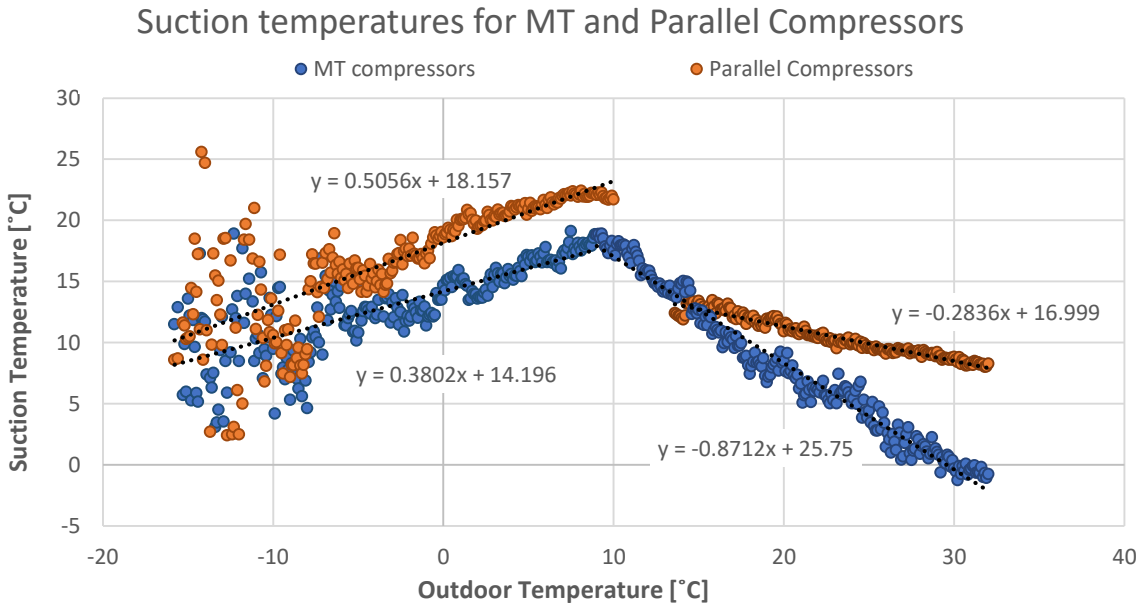

Figure 4.8 Field Measurements: Suction temperature for MT and parallel compressors.

4.2.3. Space Heating - Supply and Return Temperatures

The heating system regulates both the temperature difference (ΔT) between supply and return and the water mass flow. Figure 4.9 shows both space-heating supply and return temperature. For relatively warm temperatures (5˚C ≤ Outdoor Temperature ≤ 13˚C) the ΔT is increased until roughly 11 K, then the water mass flow is regulated in order to extract more heat from the refrigeration system. At around -10˚C (Outdoor Temperature), the system start increasing the ΔT again. This is a very efficient way of regulating the heat recovery since avoid reaching pinch points inside the heat exchanger.

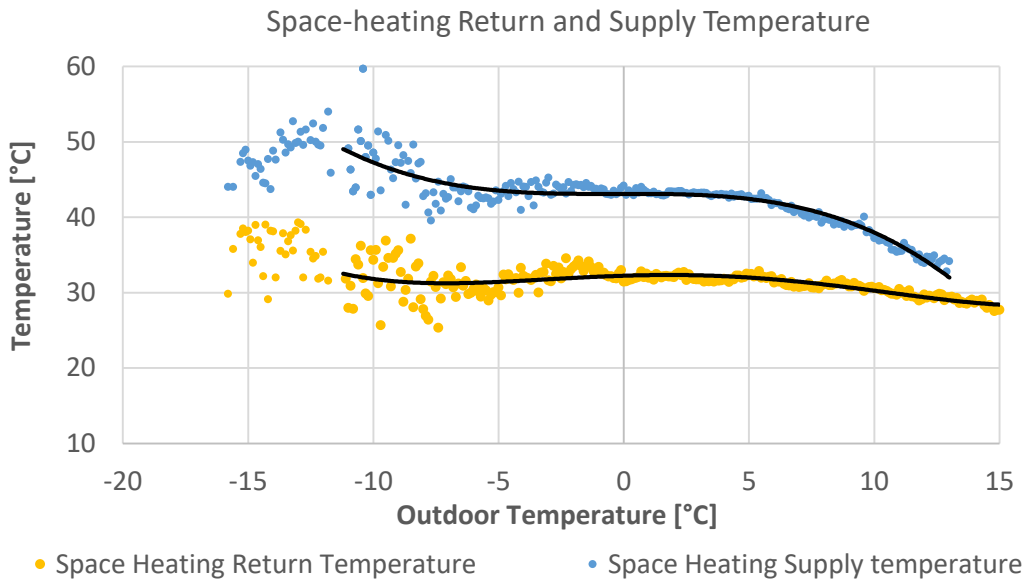

Figure 4.9 Field Measurements: Space heating return and supply temperature.

4.3. Analysis of the Demand

The examined CO2 transcritical booster system satisfies five different demands: medium temperature (MT) and low temperature (LT) refrigeration, high-temperature heating for tap water (TW), space heating (SH) and space cooling (AC). The information presented in this subchapter have been obtained averaging on an hourly basis the values resulting from the field measurements analysis.

4.3.1. In relation to the ambient temperature

Medium and Low temperature refrigeration

The refrigeration load is strictly dependent on the type of cabinets (with or without doors) and the outdoor absolute humidity. The latter varies proportionally with outdoor temperature, the warmer the weather, the higher the absolute humidity. As the outdoor air flow is not dehumidified, a high outdoor absolute humidity is translated into high indoor relative humidity which, in turn, results in a higher frost formation rate inside the cabinets (Sawalha, 2012). When doors are installed a small difference can be seen between day and night demand and the effect of outdoor humidity is reduced. The examined installation is connected to cabinets and freezers equipped with doors. This explains the stable trend of the freezers cooling demand, displayed in Figure 4.10.

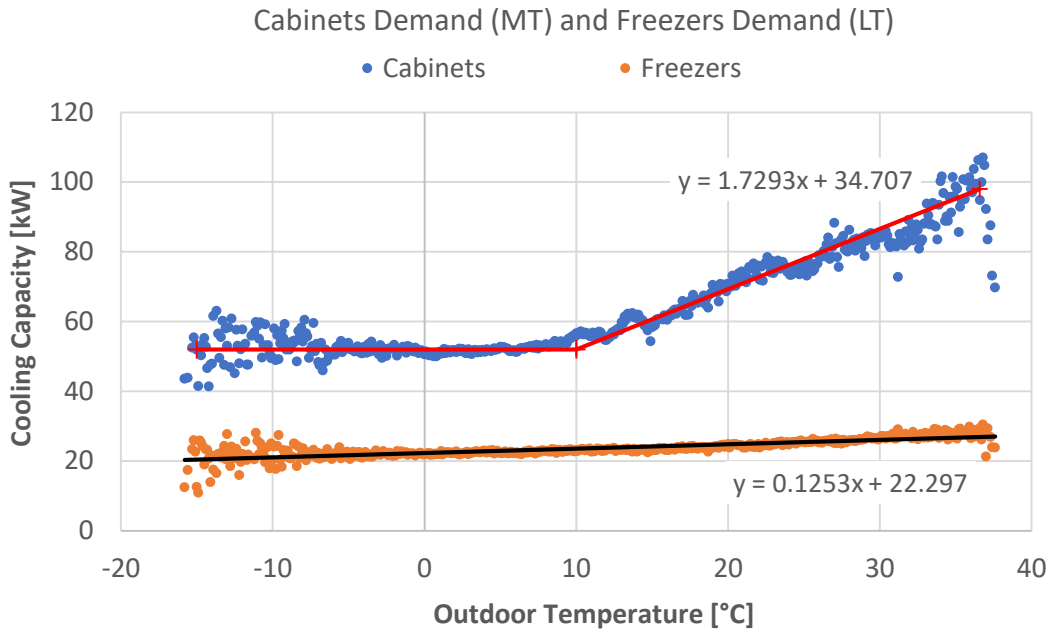

Figure 4.10 Field Measurements: Cooling demand for cabinets and freezers as a function of ambient temperature.

As can be seen, the MT demand (cabinets) is stable during the heating period (when the outdoor temperature is lower than 12°C) while it increases proportionally to the ambient temperature when the indoor is not heated.

High temperature heating for tap water

The heat recovered for the tap water production follows the discharge pressure (shown in Figure 4.7). This is due to the fact that the system controls the discharge pressure to satisfy the space heating demand, recovering the available high temperature heat for tap water as a B-product. An additional electric heater is usually utilized to satisfy the small amount of extra – energy needed for tap water. Figure 4.11 depicts the heat supplied in the first de-superheater. The scattered pattern at the edges is due to scarce amount of data for very low or very high outdoor temperatures.

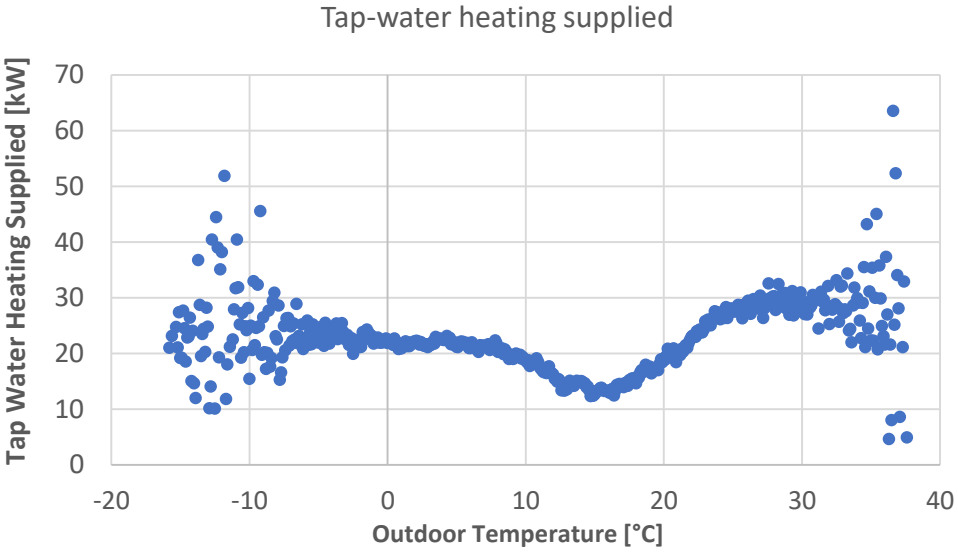

Figure 4.11 Field Measurements: Heat supplied to the tap-water loop.

Space heating

Being that the supermarket is self-sufficient in terms of heating, the heat supplied is representative of the space heating demand of the building (no external heat sources), which is shown in Figure 4.12.

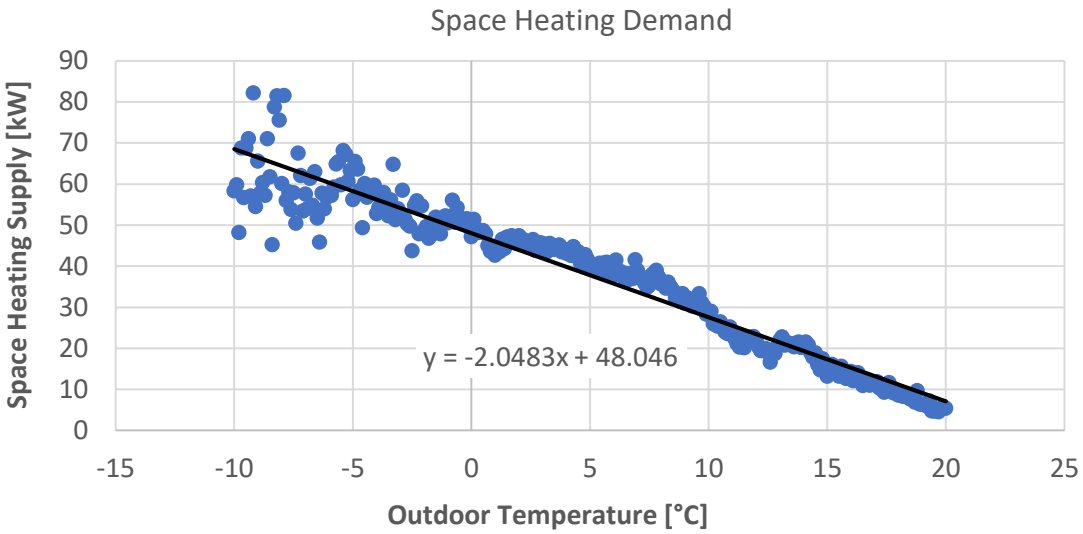

Figure 4.12 Field Measurements: Space Heating Demand.

For an outdoor temperature between 13°C and 20°C, the heat is recovered as "waste heat" while for temperatures lower than 13°C the control system increases the refrigerant discharge pressure in order to satisfy the heating demand. The detailed explanation of the control strategy will be discussed in the chapter 5 . It must be said that the heating demand not only varies with the outdoore temperature but also with the activities inside the supermarket.

Air Conditioning

The Supply of cooling for the building is done through the same evaporator used to extract heat from the ground. A valve signal on the secondary refrigerant loop was used to filter the field measurements in order to differentiate from where the heat exchanger was extracting heat. Figure 4.13 shows the air conditioning supply curve, clearly, the activation set point is at 13°C outdoor temperature.

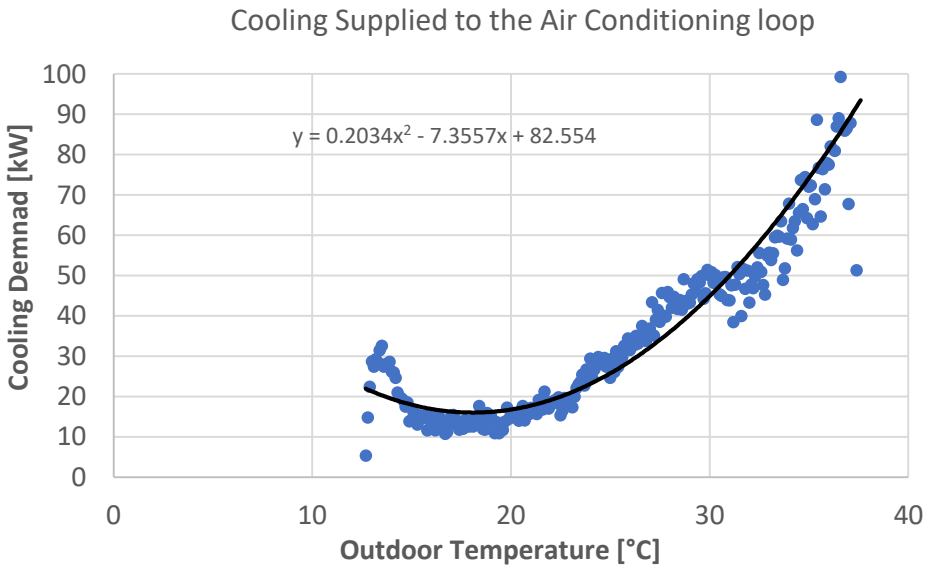

Figure 4.13 Field Measurements: Air Conditioning Demand.

4.3.2. Power Consumption

In the installation studied during this project two power meters were installed, one aggregating the MT compressors, the LT compressors and their auxiliaries, while another aggregating the parallel compressors (PC) and its auxiliaries. For this reasons, the individual compressors' powers were calculated from the manufacturer data using the thermodynamic properties at the discharge and suction point of the compressors. Then, the total calculated electricity consumption (in kWh) was validated comparing it with the total measured consumption (in kWh). Such a comparison is shown in Table 4-1.

Table 4-1 Validation of the Power Consumption.

Month	Total Power Consumption (Calculated) [MWh]	Total Power Consumption (Measured) [MWh]	Error
Jan	35.2	35.7	1.4%
Feb	32.6	33.4	2.5%
Mar	32.0	32.4	1.4%
Apr	33.8	32.6	-3.5%
May	32.6	30.3	-7.4%
Sep	33.6	33.4	-0.6%
Oct	32.0	31.5	-1.6%
Nov	29.3	29.6	0.9%
Dec	30.5	31.4	3.0%
TOT	32.4	32.3	-0.3%

The breakdown of the calculated power consumption is shown in Figure 4.14 .

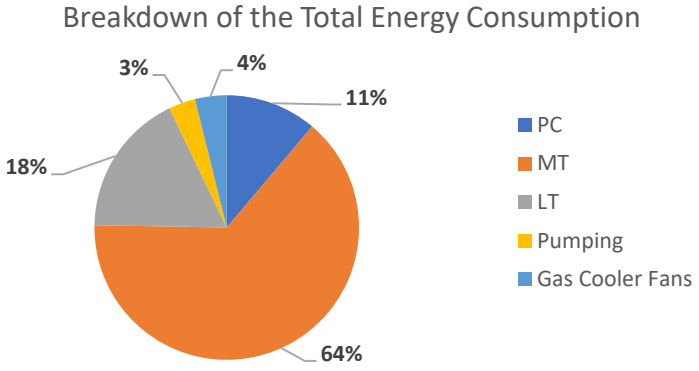

Figure 4.14 Breakdown of the Total Energy Consumption.

The electricity metering started only in September, therefore, it was not possible to compare the consumption of the first three months of operation: June, July and August. The error concerning the MT and LT compressors varies between -7.5% and 3%. When parallel compressors (PC) are operate in stable operations, the difference between their consumption and the energy metered falls into the same range.

On the other hand, during the winter months, PC compressors are used only for very high peaks of the heating demand which means that their operation is very unsteady. Under these conditions the methodology applied is not accurate as the frequent start and stops greatly modify the predicted consumption which is based on the thermodynamic conditions between suction and discharge. Moreover,

the PC power meter records a consumption of 1 kW as base load even when the PC are not active. This is probably due to some of the auxiliaries. For all these reasons, the winter consumption of the parallel compressors cannot be validated. However, their winter consumption is so limited that it does not affect the overall result, as it can be seen from Table 4-1.

The power absorbed by the system, averaged on the outdoor temperature, is shown in Figure 4.15 . The small step visible when passing from heat recovery mode to floating condensing is due to the activation of the air conditioning, which is connected to the load evaporator.

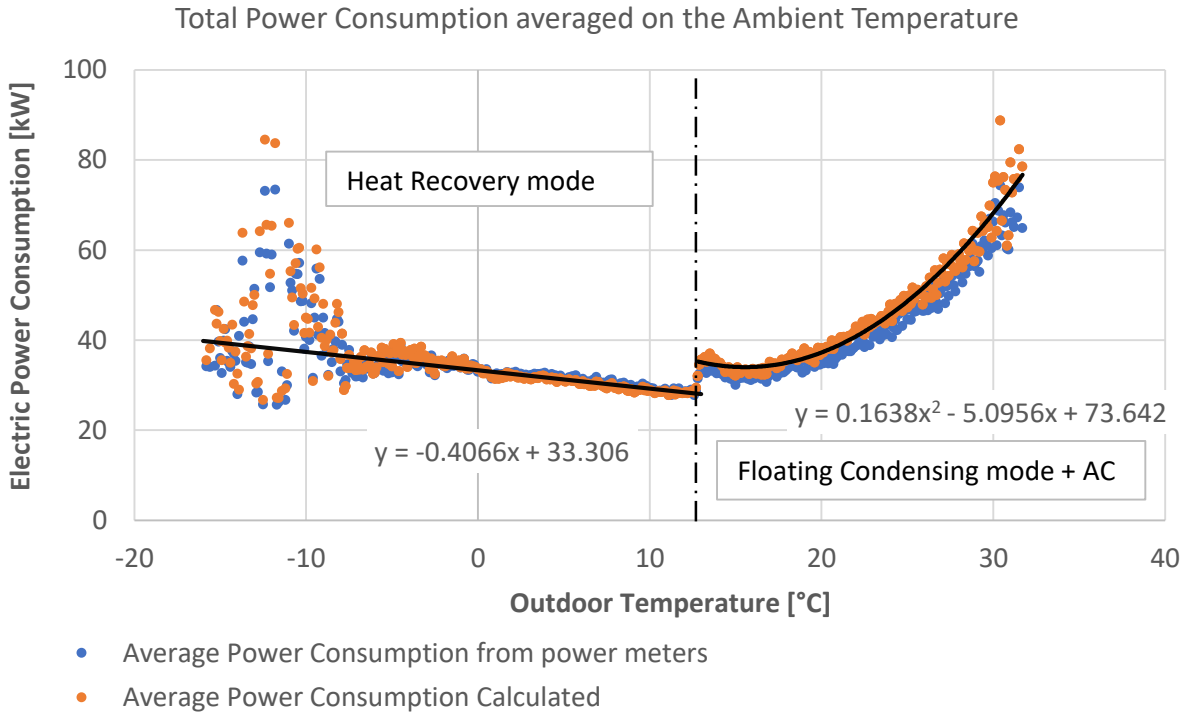

Figure 4.15 Comparison between measured and calculated power consumption.

Finally, evaluating the energy consumption right before the start-up of the heat recovery mode, it was possible to validate the floating condensing consumption used for the COP calculation. The power reading used for the validation is the one recorded at 00:30 of the 31-01-2019 is 14.6 kW. The value estimated for the floating condensing mode is 7% higher (15.6 kW). It is worth to mention that the estimated fan power consumption at that moment was 1.6 kW. It is unknown whether the power meters were measuring also the fan power or not. In case that the fan power was not included the estimated floating condensing consumption would be lower than 5% compared to measured value.

4.3.3. In relation to the daily activities

The several energy needs satisfied by this installation are not only dependent on the outdoor conditions but also on the daily activities. The daily demand profile was studied taking into account the months of January and July, respectively, the coldest and the warmest. Figure 4.16 and Figure 4.17 display monthly averages on an hourly basis of the cooling and heating demands with the addition of the heat rejected from the gas cooler and the heat exchanged with the ground (injection or extraction). The negative powers represent the cooling loads, while the heat rejected/recovered is positive. Additionally, a key parameter is plotted for each month, the gas cooler inlet-temperature for January and the outdoor temperature for July. The difference between the cooling loads and the sum of all the recovered and rejected heat is the compressors' power consumption and the heat losses.

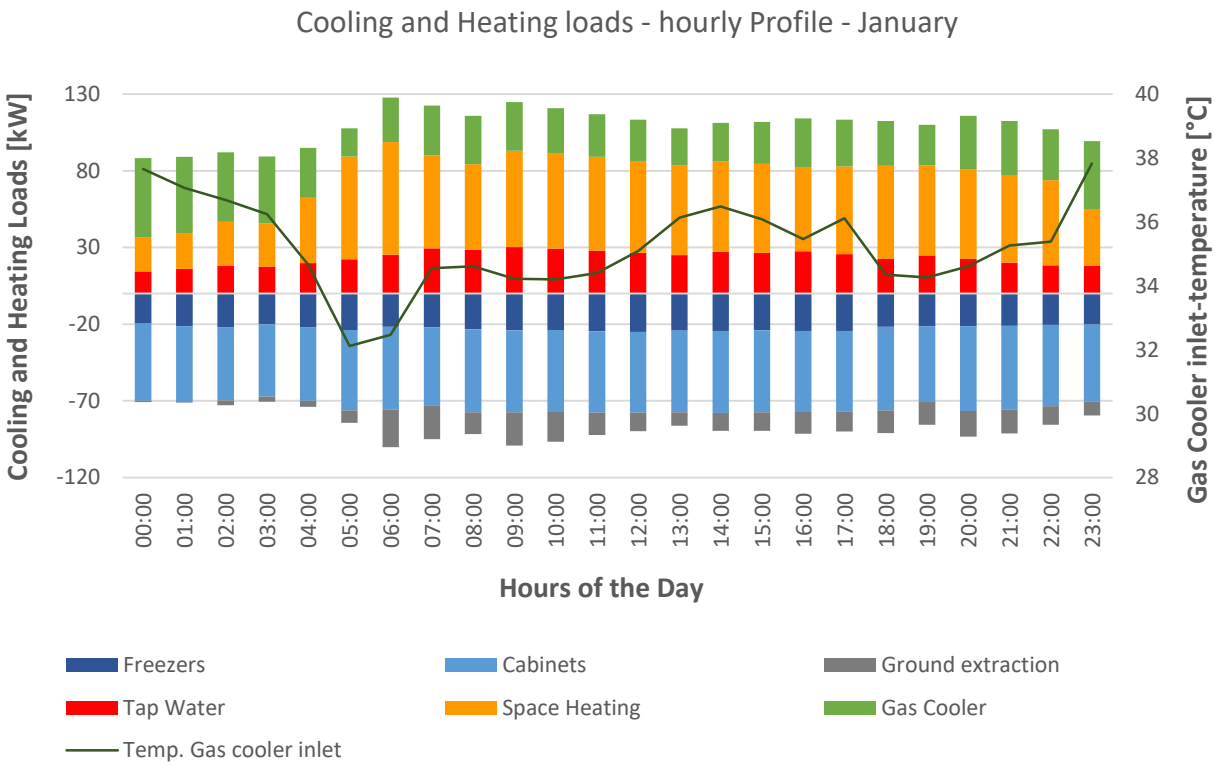

Figure 4.16 Average cooling and heating loads during the day in January.

To begin with January, the cooling demand for cabinets and freezers is quite steady during the day, as well as, the tap water demand. On the other hand, the energy required for space heating changes a lot along the day. When the heat available from cabinets and freezers is not enough the system start extracting heat from the ground.

The contemporary heat extraction from the ground and heat rejection through the gas cooler is due to a malfunctioning of the gas cooler by-pass valve. However, theoretically, such a malfunctioning leads to a negligible amount of extra compressor's power consumption.

The visible drop in temperature around 05:00 AM is due to a preheating of the outdoor air, used to ventilate the kitchen immediately after that the first and biggest portion of bakery products has been prepared. This causes a drop in the return temperature from the space heating system and subsequently a decrease of the gas cooler inlet temperature. It is worth to notice how the ratio between the heat rejected from the gas cooler and the heat recovered for space heating varies proportionally to the gas cooler inlet temperature. Indeed, a drop in this temperature means that the system is recovering more heat for the same electric power consumption.

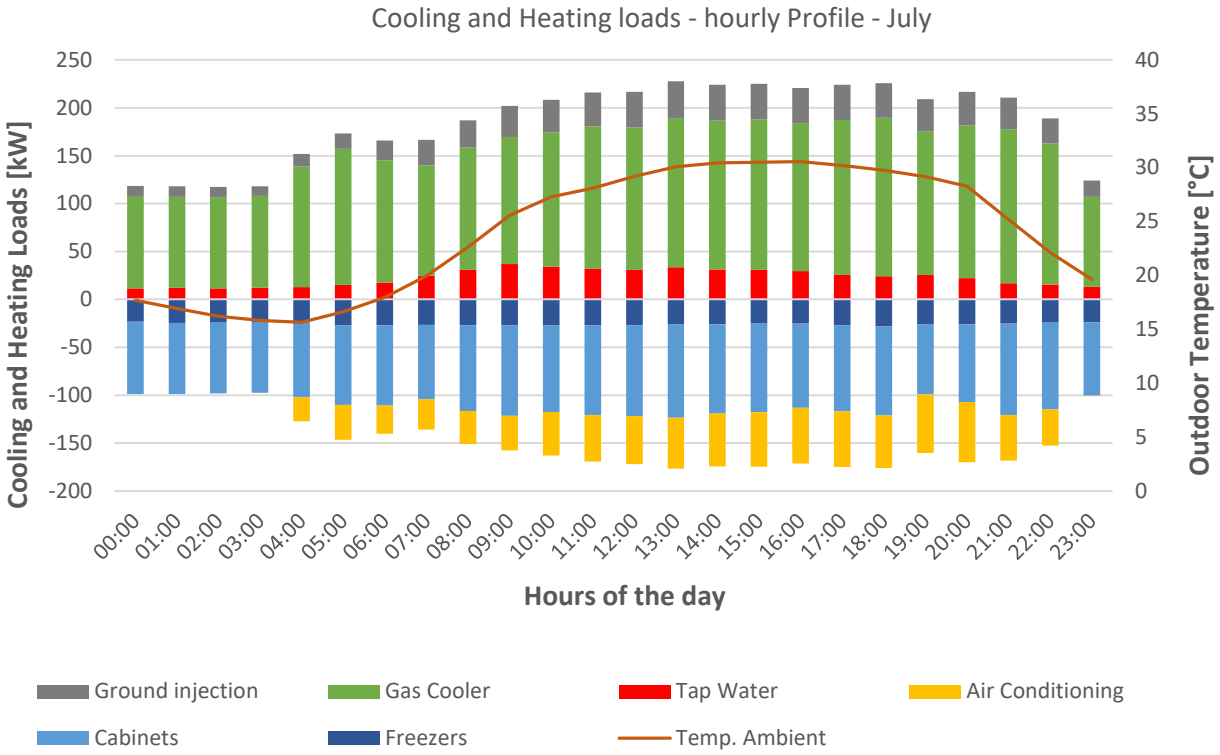

Figure 4.17 Average cooling and heating loads during the day in July.

Differently from the winter case, in July, the cabinets' cooling load fluctuates visibly more. During business hours, the opening and closing of cabinets' doors lead to a higher load. This is more evident in summer than winter due to the highest outdoor absolute humidity, in fact, supermarkets usually do not dehumidify the inlet air (Sawalha, 2012). With the increase of the outdoor temperature not only the cooling loads are higher, especially due to the air conditioning, but also the ability to reject heat from the gas cooler is reduced. For this reason, part of the heat is injected into the ground in order to subcool the CO2 as much as possible.

5. Heat Recovery

First of all, an important best practice in transcritical CO2 refrigeration systems is to recover heat through at least two desuperheaters (Thanasoulas, 2018) and (Rogstam et al., 2013). Doing so, it is possible to optimize the flow of the heat recovery fluid (water or a mixture of water-glycol) matching the CO2 temperature profile in the heat exchangers and avoiding technical issues due to the pinch point (Thanasoulas, 2018). In this way, the heat will be available at two temperature levels for the supply of hot tap water and space heating.

5.1. Control Strategies

5.1.1. Theory – Control strategy of a stand-alone system

Concerning the control strategy, the theoretically best for a stand-alone installation (no additional systems e.g. boreholes or heat pumps) is described by (Sawalha, 2012). The best theoretical control strategy consists of three main steps which can be summarized as follow:

Step 1) The system is working in floating condensing mode with the lowest possible condensing pressure. As soon as the heating demand increases, the condensing pressure is raised.

Step 2) When the pressure brings the refrigerant in its supercritical region, the pressure should be gradually increased until it reaches the optimal value which is described in equation 5.1 (Sawalha, 2012).

$$P_{dis} = 2.7 * T_{desuperheater\ exit}[°C] - 6\ [bar] \tag{5.1}$$

$T_{desuperheater\ exit}$ is the outlet temperature from the last desuperheater. In case that the system is operating in transcritical mode but no heat is recovered (e.g. warm summer day), the value to be utilize should be the gas cooler outlet temperature.

Step 3) Once the pressure reaches the optimal value in the supercritical region, it is kept constant and the gas cooler fans' power starts to be regulated. When fans are switched off, CO2 continues to be circulated through the gas cooler which works in natural convection.

The effect of step 3 is to increase the high-pressure expansion valve inlet-temperature. This leads to an increase of generated flash gas and subsequently to an increase of mass flow elaborated by the MT compressors. Indeed, they are controlled to satisfy to cooling loads (for the same amount of liquid refrigerant the total mass flow increases proportionally to the quality).

Step 4) The last step is to fully by-pass the gas cooler. In this case the high-pressure expansion valve inlet temperature would be very close to the desuperheater outlet. This is the condition where the system reaches the maximum Heat Recovery Ratio (Eq. 3.15).

Step 5) A further growth in the heating demand could be satisfied by the system only increasing the pressure to the maximum allowed. However, this step should be avoided since the extra-heat available would be extremely low while the increase in compressor's power very high.

One can encounter a potential limitation of this methodology if the heat recovery system is very efficient and the desuperheater outlet temperature is very low (< 30°C). The resulting optimal pressure could be too low, in some cases, even lower than the critical pressure. Without considering the technical implications, If

the pressure is too low (e.g subcritical, but not only) the discharge temperature risks to be lower than tap water supply temperature.

This limitation does not really apply to supermarkets. These systems are usually controlled to satisfy the space heating demand, in case that (a small amount of) additional heat is needed to increase the supply temperature of tap water some electric resistances back-up the heat recovery system.

On the other hand, such a limitation is definitely relevant for other applications such as ice rinks, where the high temperature demand is considerably higher than the other demands. Moreover, the outlet temperature in the last desuperheater can be as low as 10°C. However, this application is out of the scopes in this study.

5.1.2. Theory – Control strategy with geothermal integration

When geothermal boreholes are installed, some modification to the control strategy has to be made as they represent an additional heat source. The latter is different from cabinets and freezers as it does not represent a cooling load that must be guaranteed.

As demonstrated by (Karampour et al., 2018), step 1 and 2 described in the previous section should be followed also when the refrigeration system is coupled with the ground. The heat recovery efficiency during step 1 and 2 is hardly comparable to any other heating apparatus since the system takes advantages from the cooling loads of cabinets and freezers.

The real question is whether the heat extraction from the ground should be activated before or after by-passing the gas cooler. For this reason, it is possible to distinguish two different control strategies referred as "*Gas cooler capacity regulation*" and "*Geothermal capacity regulation*".

"*Gas Cooler capacity regulation*" (control strategy A) follows the same steps as the stand-alone system. The difference is in the last step of the control strategy. In this case, after that the gas cooler is by-passed (Step 4), the last step (Step 5A) consists of extracting the necessary extra-heat from the ground through the load evaporator.

"Geothermal capacity regulation" (control strategy B) follows the first two steps but, once that the optimal pressure is reached (Step 2), the parallel compressors connected to the boreholes are activated while the gas cooler is controlled to reach the minimum outlet temperature (Step 3B). If the maximum amount of heat that can be recovered is reached, then, the system proceeds with the gas cooler capacity regulation (previously described as step 3) and its eventual by-pass (previously described as step 4).

Theoretically, (Karampour et al., 2018) demonstrated that the ground should be activated after that the gas cooler is by-passed. In case the ground was activated before by-passing the gas cooler, part of the heat extracted from the ground would be necessarily rejected through the gas cooler.

However, from a thermodynamic perspective, there is no difference in terms of COP_{TOT} (Eq. 3.16) between the two cycles. Indeed, both the heat rejected in the gas cooler and the heat extracted from the ground are considered not useful. What matters is the power consumption of the compressors. This does not change if the fluid is cooled in the gas cooler and then evaporated through the load evaporator or if it is expanded at "higher temperatures", producing flash gas, and then by-passed to the suction line of the parallel compressor.

To summarize, the only theoretical difference between control strategy A and B is the power spent for pumping the secondary refrigerant through the geothermal loop. It is clear that the control strategy A is the most efficient, however, option B has some important co-benefits.

First of all, it helps to discharge the ground which is extremely unbalanced as explained in Chapter 8. Theoretically, this could be beneficial for the summer operations, increasing the subcooling potential. The magnitude of this benefit is discussed in section 8.5 where a quantitative analysis is presented.

The second indirect advantage is related to technicalities. Control strategy A is more difficult to be implemented since regulating smoothly the high-pressure expansion valve inlet-temperature and the partial mass flow in the gas cooler is more challenging than regulating the capacity of the parallel compressors.

5.1.3. Practice – Implemented heat recovery control strategy

Going from the theory to the practice presents always some challenges and, as usual, not everything that is recommended by theoretical modelling is implemented in the real word. Analysing the field measurements, the real control strategy and its effectiveness can be assessed.

The control device utilized is the Danfoss product AK-PC782A. The latter device converts a signal coming from a thermometer (Shr4 in Figure 5.1) on the supply line of the second desuperheater (Space heating supply) in a 0-10V output. Figure 5.1 shows a general scheme of this branch to better visualize which are the monitored parameters.

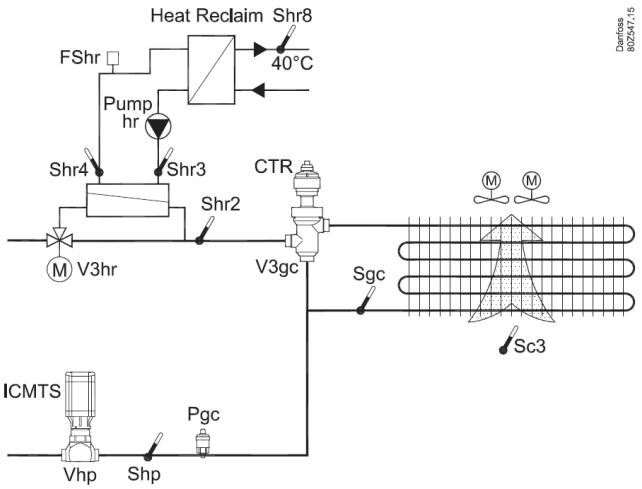

Figure 5.1 Measuring system for discharge pressure control Source: (Danfoss, 2019).

As soon as the heat recovery system is activated (V3hr coupled up), the control increases the pressure to the minimum heat recovery value. Then, the 0 – 10V output is translated into a 0-100% "heat requested" which is the basis for the pressure, pump and gas cooler by-pass valve (V3gc) regulation. Figure 5.2 shows the principal of such a regulation. The "heat request" signal is shown on the x-axis. On the secondary fluid side, a variable speed pump is used to keep the temperature Shr4 close to the reference value while. On the CO2 side, the pressure is regulated according to the "heat request" signal linked to the reference value (Shr4).

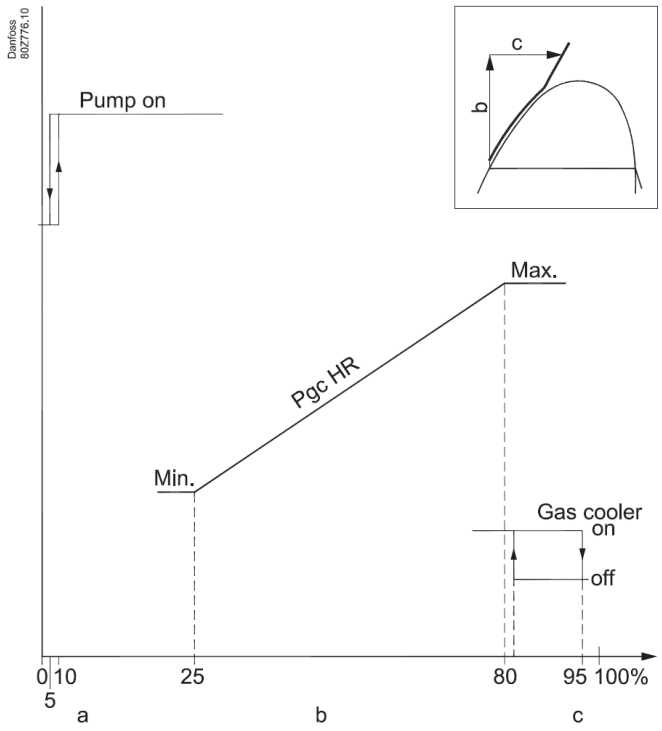

Figure 5.2 Discharge pressure regulation Danfoss controller Source: (Danfoss, 2019).

The set points and the corresponding minimum and maximum pressure can be adjusted in order to match the demand of the building.

In order to identify the set points shown in Figure 5.2 ,the trend of discharge pressure (Pdis) and the space heating supply temperature (Shr4) were studied. Figure 5.3 displays the trends of these two parameters averaged on the outdoor temperature.

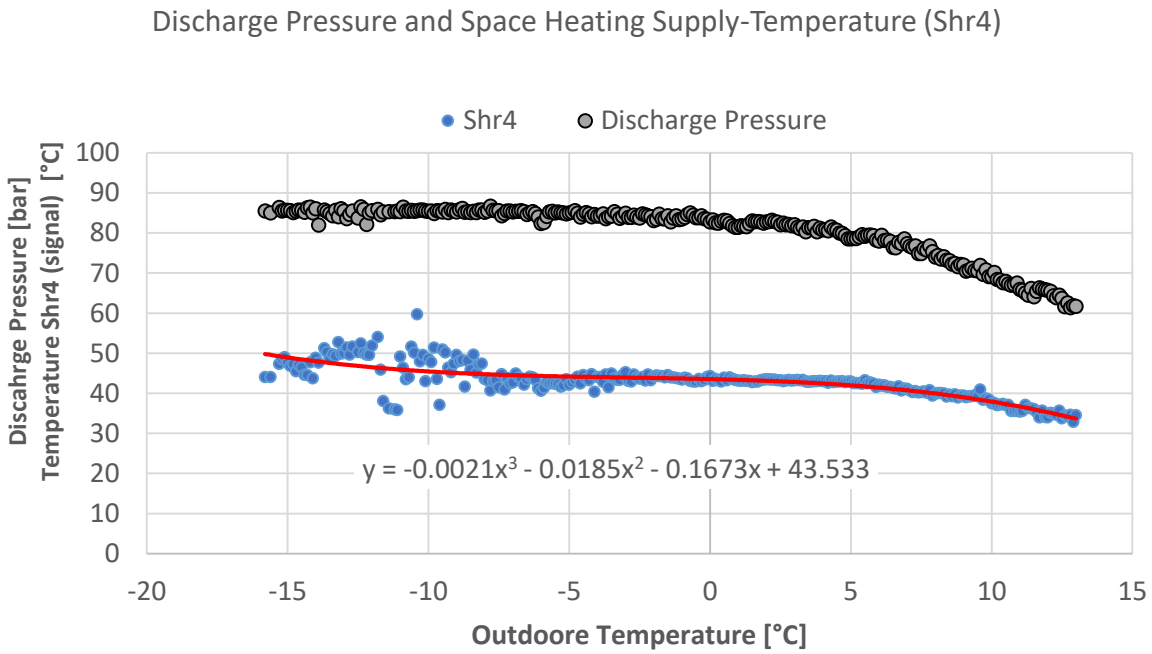

Figure 5.3 Field data: Discharge pressure and supply temperature for space-heating demand.

The concept at the basis of this process is that the supply temperature of the heating system should be regulated according to the outdoor temperature, the colder, the higher the supply temperature. This is why the trend of the supply temperature was studied. Following, the discharge pressure was plotted as a function of the Shr4 trend line (red) visible in Figure 5.3. In this way, it was possible to express the discharge pressure as a function of the space heating supply-temperature (Shr4).

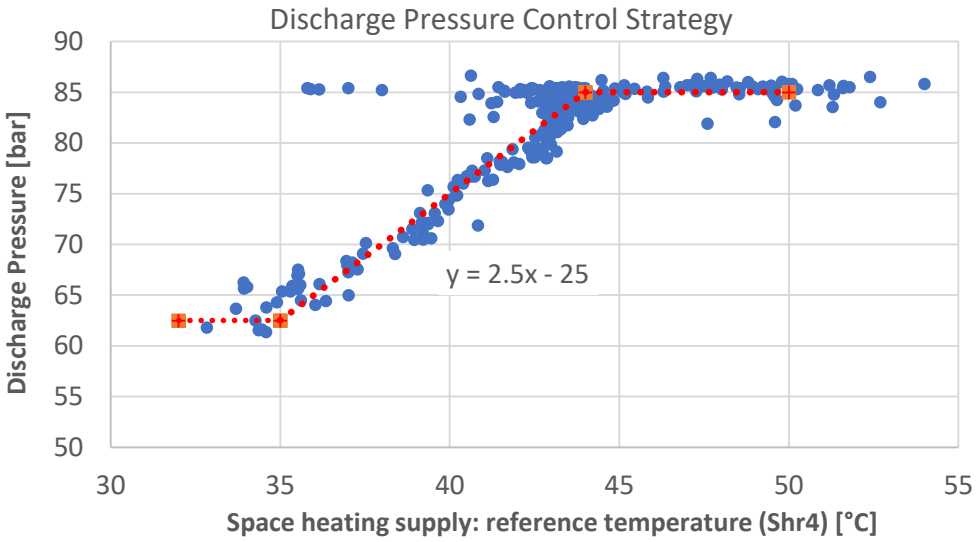

Figure 5.4 Field data: Discharge pressure as a function of space heating supply temperature (Shr4).

It is visible the similarity between the function displayed in Figure 5.4 and the one shown in Figure 5.2. It is possible now to express the discharge pressure as a function of a function of the outdoor temperature, $P_{dis} = f\big(g(T_{amb})\big)$, being the space heating supply temperature $Shr4 = g(T_{amb})$.

The obtained functions are:

$$Shr4\,(T_{amb}) = \; -0.0021 * \; T_{amb}^{3} - \; 0.0185 * \; T_{amb}^{2} - \; 0.1673 * T_{amb} \; + \; 43.533$$

$$\begin{cases} if\ Shr4(T_{amb}) > 44; & Pdis = 85 \\ if\ 35 \leq Shr4(T_{amb}) \leq 44; & Pdis = 2.5 * Shr4 - 25 \\ if\ Shr4(T_{amb}) < 35; & Pdis = 62.5 \end{cases}$$

The recalculated discharge pressure is shown in Figure 5.5 (yellow line).

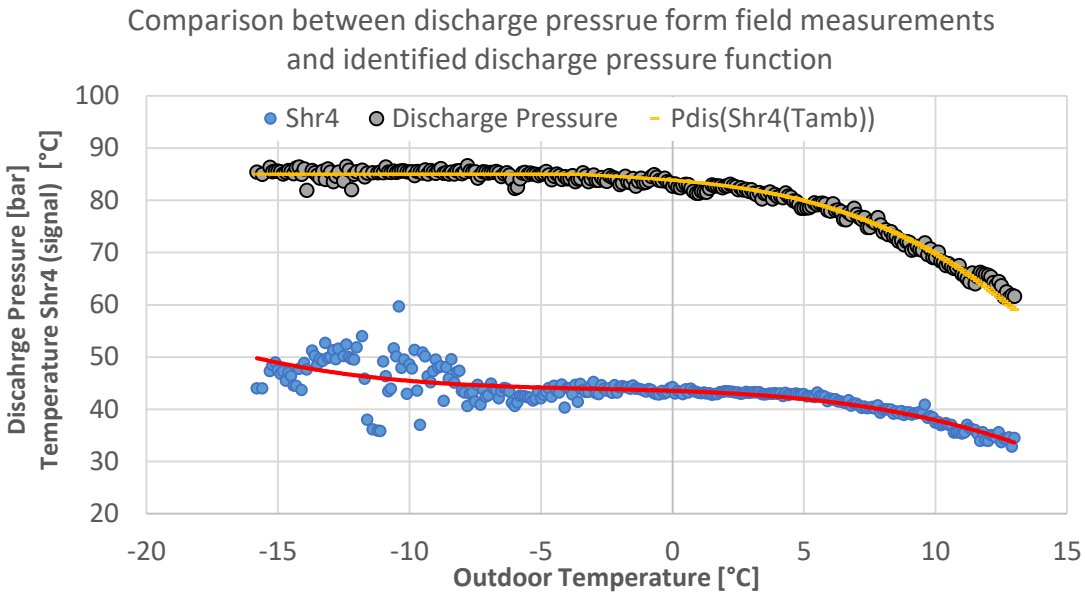

Figure 5.5 Comparison between discharge pressure from field measurements and identified function.

The identified discharge pressure function was used for the models presented in sections 5.3 and 8.

5.2. COP Heat recovery

The efficiency of the heat recovery function strongly depends on the floating condensing (FC) conditions used as a reference, this can be easily deduced from Eq. 3.20. Figure 5.6 displays the COP heat recovery averaged on the ambient temperature for the whole heating period (Ambient Temperature < 13°C). As expected, the COP is incredibly high for very low temperatures where a lot of waste heat is available from cabinets and freezers. At around 7.5 °C ambient temperature, the pressure exceeds the critical point and this why the loss of efficiency is less steep until -5°C where the maximum pressure is reached (on average). At this pressure level the system takes advantage of all the available heat. For a further increase in the supplied heat, the only option is to increase the mass flow. This can be done either by-passing the gas cooler or activating the parallel compressors, as explained in the previous sections. In this system the parallel compressors are activated and the heat is extracted from the ground.

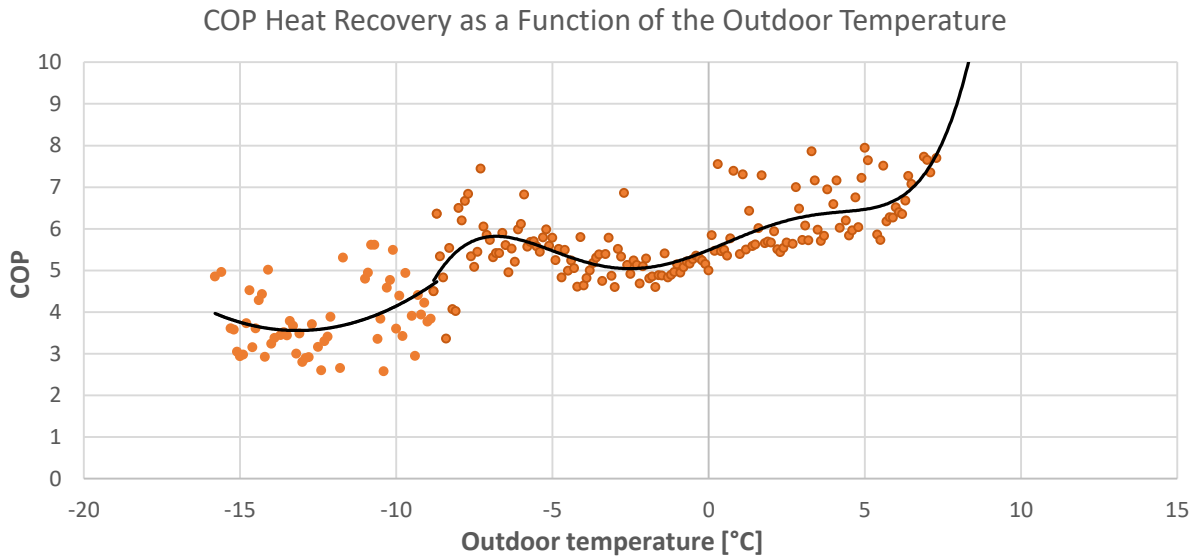

Figure 5.6 Field measurements analysis: COP Heat Recovery.

It is worth to notice the influence of the return temperature from the space heating circuit on the COP heat recovery.

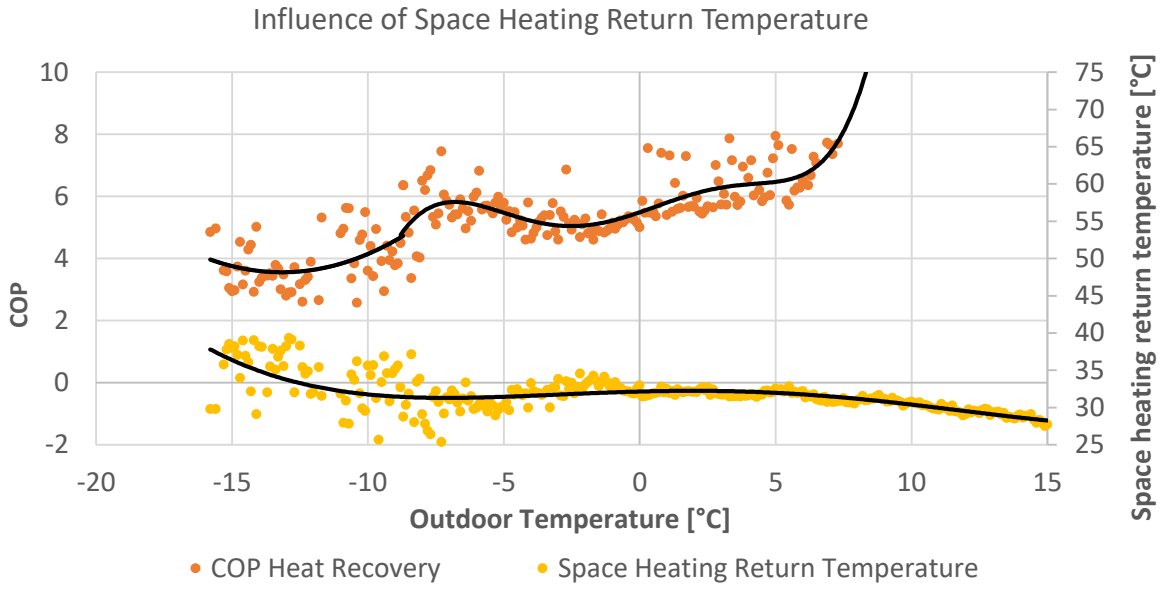

Figure 5.7 Influence of space heating return temperature on heat recovery.

Even if field measurements for such low temperatures are limited, from Figure 5.7, it is clear that the high space heating return temperature is connected to an efficiency loss.

The heat extracted from the ground, averaged on the ambient temperature, is shown in Figure 5.8. For outdoor temperatures lower than -7.5°C, the average thermal power extracted from the ground increases steeply. The power extracted at outdoor temperatures higher than -7.5°C is due to sporadic peaks of heating demand. The average values are low as they take into account also the moments when the power extracted is equal to zero.

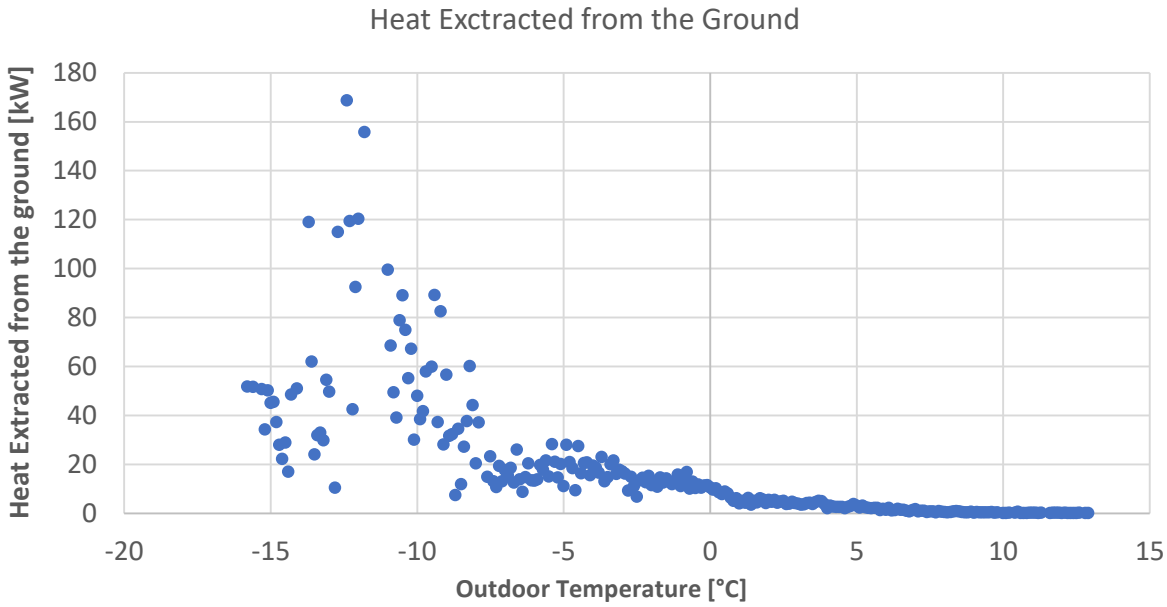

Figure 5.8 Heat Extracted from the ground averaged on the outdoor temperature.

Furthermore, an analysis of the efficiency of the heat extraction was performed, as shown in Figure 5.9. The blue points represent the COP heat extraction calculated according to Eq. 3.22. As it can be seen, the

average COP heating for the geothermal function varies between 3 and 4, making the system competitive with modern heat pumps.

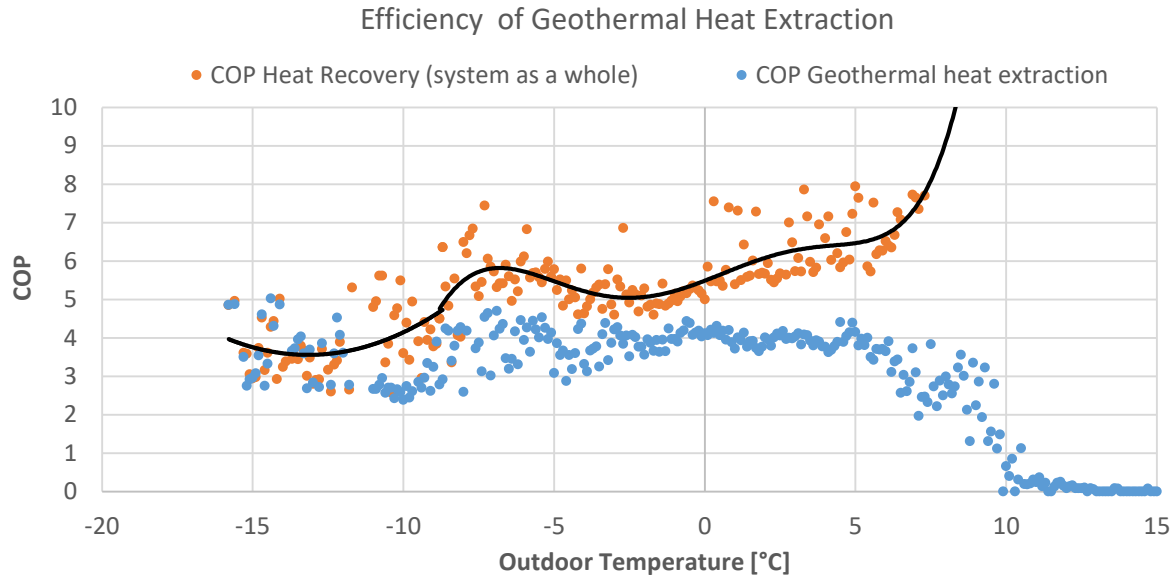

Figure 5.9 Comparison between COP heat recovery of the system as a whole and COP of the geothermal function.

The average COP heat recovery takes also into account moments when the boreholes are active for relatively high outdoor temperatures (e.g. +5°C). This means that the closer the two trends depicted in Figure 5.9, the more heat is extracted from the boreholes (as a percentage of the total heating demand). For temperatures close to -7.5°C, the two efficiencies start overlapping demonstrating that the geothermal heat extraction starts supplying an important part of the heating demand.

The average heating demand increases linearly with a decrease in the outdoor temperature, this means that the graphs shown in this chapter can be related to the demand. However, the peak loads' distribution is related to the activities (hours of the day) and these cannot be visualized if the values are averaged on the ambient temperature.

For this reason, the effectiveness of the system was also studied in relation to the Heat Recovery Ratio (Eq. 3.15), which is representative of the thermodynamic cycle and, therefore, the heat supplied by the refrigeration unit. Figure 5.10 shows the two aforementioned COPs averaged on the Heat Recovery Ratio (HRR), the values have been filtered in order to exclude values for outdoor temperatures lower than 13°C. Additionally, Figure 5.11 displays the control parameters affecting the COP.

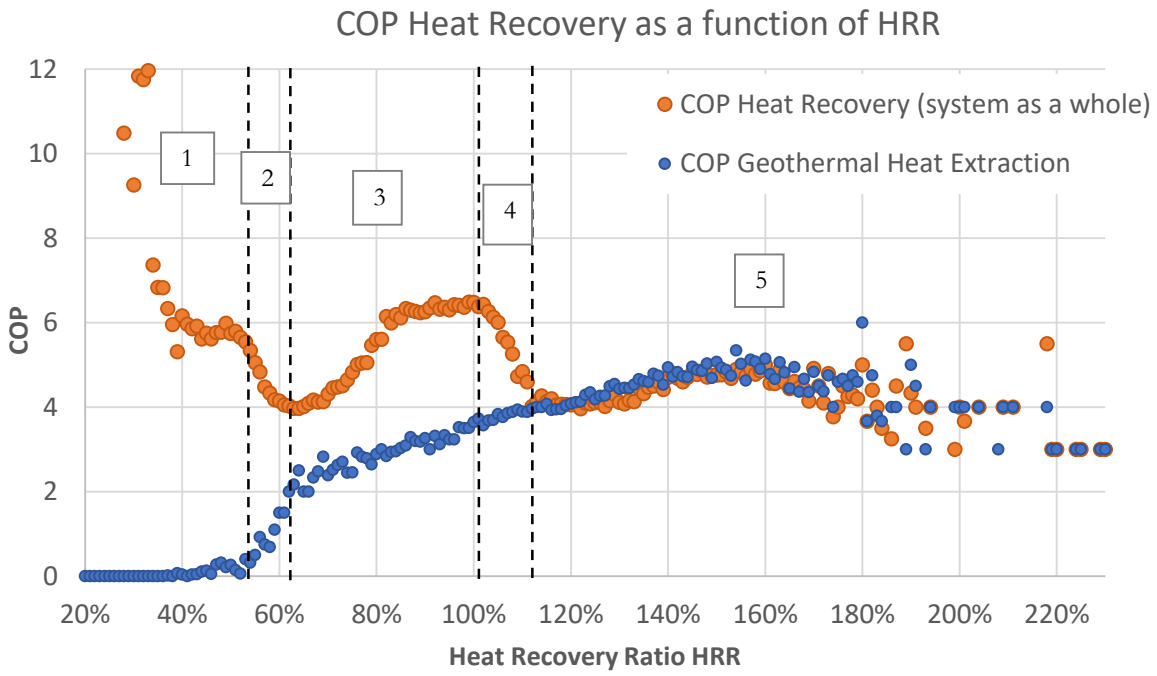

Figure 5.10 COP heat recovery and COP of geothermal heat extraction as a function of the Heat Recovery Ratio.

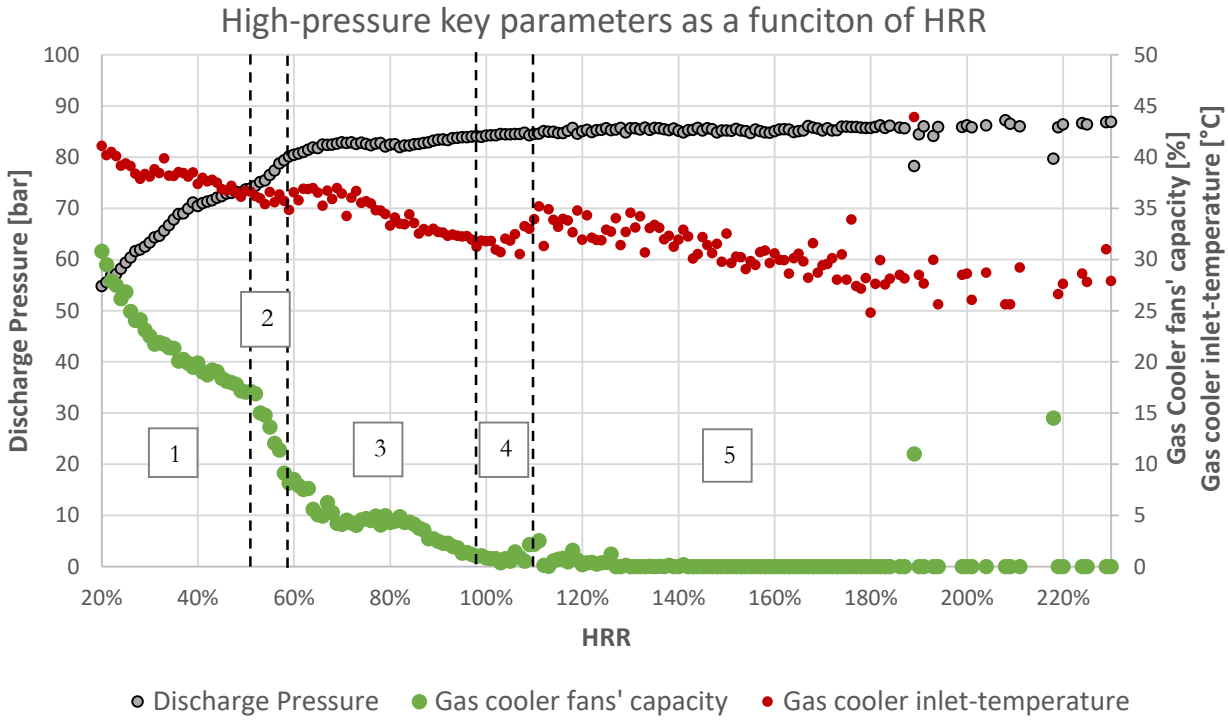

Figure 5.11 Key parameters of the high-pressure side as a function of the Heat Recovery Ratio.

In the first section of the graph, for a HRR between 20 and 52%, the system is operating a subcritical cycle. The COP relatively high because the heating demand is satisfied almost completely by the waste heat of the floating condensing mode. The second section starts when the system switches to transcritical operation until it reaches a reasonable value for the discharge pressure.

Between 60 and 100% (section 3) the system increases the pressure slowly but steadily reaching the design pressure (roughly 85 bar). In this area, the COP is expected to slightly improve (due to the optimization of

the pressure level) but it is not supposed to improve as much as it does. One of the reasons for such a peak is the simultaneous lowering of the return temperature coming from the space heating system (red points in Figure 5.11).

Region 4 is where the system starts extracting heat from the ground (geothermal extraction at its minimum). The losses of performance in this area are due to an increase of the return temperature at the gas cooler inlet. When the geothermal activation is needed, the parallel compressors capacity, connected to the load evaporator, jump from zero to its minimum value. The latter was found to be too high (in this installation) to ensure efficient heat recovery operations. In other words, when the heating demand needs a few kilowatts more the parallel compressors are activated at the minimum but this greatly exceeds the few kilowatts needed. The excess of available heat is also visible from the small jump of the gas cooler fans capacity in region 4.

In the last area, region 5, is where the geothermal integration works slightly above the minimum and the gas cooler is not by-passed. Indeed, part of the heat is constantly rejected from the gas cooler. With a COP varying between 4.5 and 5, the parallel compressors work in region 5 for almost 245 hours per year, satisfying only the peaks of heating demand. The high HRR reached in region 5 is characterized by an improvement of the COP. This is definitely related to the decrease of the gas cooler inlet-temperature. This decrease is also visible in Figure 4.16 and it is due to the preheating of outdoor air during specific activities of the supermarket in the early morning.

Finally, from Figure 5.10 it can be seen that the geothermal function is also working for low values of HRR. One can speculate that this happen when the thermodynamic cycle moves quickly from a high to low values of HRR and vice versa (e.g. low average heating demand and sudden high peaks). In these cases, the parallel compressors quickly reach the hourly start-and-stops limit, forcing the boreholes to operate even when the heating demand is low.

5.2.1. Technical considerations

The very first technical limitation when dealing with heat recovery in CO2 transcritical refrigeration units is due to the heat recovery control strategy. All the best theoretical strategies deal with controlling the pressure according to the heat supplied. In practice, there isn't any device on the market which can implement such a strategy. The most modern controllers work with temperature sensors and, then, translate such an output in an equivalent heat request.

Regarding the gas cooler, its potential capacity regulation is also very hard to implement in real installations. First of all, a rapid change in the temperature inside the gas cooler (if by-passed) causes a rapid pressure drop in the high pressure branch which needs to be compensated. This effect can be diminished utilizing a gas cooler with two separate internal circuits, so that it is possible to by-pass only one of them. Secondly, when the gas cooler is by-passed, a lot of refrigerant accumulated inside moves into the liquid receiver. If this was not taken into account during the design phase (receiver volume), some liquid can arrive at the compressors' suction point. A third technical limitation lays in the difficulty of achieving a partial increase of the expansion valve inlet-temperature simply regulating the gas cooler fans power. This is due to the fact that the gas cooler is designed for the "worst" conditions achieved in summer. In other words, when the refrigerant mass flow is significantly higher than the winter conditions. For this reason, the gas cooler is usually over-dimensioned for the winter operations, making it difficult to control.

Taking into account all these technical constrains in the gas cooler regulation, the control strategy B, described in section 5.1, facilitates the control of the system. In other words, utilizing such a control strategy is possible to shift the issues of regulating the gas cooler's capacity to the regulation of the parallel compressors' capacity. This is technically more feasible. The necessary small extra-energy cost was quantitatively evaluated for the case study and it is presented in the next chapter 5.3.4.

5.3. Modelling – Heat Recovery mode

A model to simulate the performance of the heat recovery from the refrigeration system was created to evaluate potential benefits of an optimal pressure control and to compare the two control strategies described in the previous section.

Furthermore, without a boreholes' field the supermarket would have needed external sources to supply heat (e.g. district heating). For this reason, the avoided heat supplied from secondary sources was calculated and presented at the end this chapter. In the last part of this thesis work, the model presented in this section was combined with the one built for the summer operations (chapter 6) in order to perform the techno-economic assessment of the geothermal integration.

5.3.1. Inputs

The field measurements were analysed through a mathematical model in order to calculate the exchanged thermal and electrical powers. In this way, it was possible to calculate the COPs and to explain the obtained trends. Then, such a mathematical model, which is described in the methodology, has been further simplified in order to test several control strategies and evaluate savings for different scenarios.

This simplified model follows the formulas presented in the methodology, with the difference that the inputs are not field measurements but functions. The outputs are the COP heat recovery and the additional necessary heat from secondary sources. These are expressed as a function of the outdoor temperature which is then treated using the BIN-hours method to calculate the total annual savings.

The inputs expressed as functions of the ambient temperature are given in The three different control strategies evaluated are the ones already described in chapter 5.1. The first is the one adopted by the Danfoss system, referred as *"Current control"*. The others are the theoretical control strategies referred as "*Gas cooler capacity regulation*" and "G*eothermal capacity regulation*".

First the simplified model with the current control is compared to the filed measurements in order to validated the model and assessing the error. Then, the effect of the pressure control is assessed comparing the current control strategy with the one named "G*eothermal capacity regulation"*. Finally, the two theoretical control strategies are compared in order to highlight their differences.

Table 5-1. As it can be noticed, the suction conditions are assumed to be constant, in fact, their fluctuation was found to be very limited during examined period.

The three different control strategies evaluated are the ones already described in chapter 5.1. The first is the one adopted by the Danfoss system, referred as *"Current control"*. The others are the theoretical control strategies referred as "*Gas cooler capacity regulation*" and "G*eothermal capacity regulation*".

First the simplified model with the current control is compared to the filed measurements in order to validated the model and assessing the error. Then, the effect of the pressure control is assessed comparing the current control strategy with the one named "G*eothermal capacity regulation"*. Finally, the two theoretical control strategies are compared in order to highlight their differences.

Table 5-1 Modelling inputs for heat recovery mode.

Demands	
Freezers cooling demand	y = 0.1227* Tamb +22.271
Cabinets cooling demand	IF Tamb <= 10; y= 52 [kW] IF Tamb >= 10; y = 1.7293*T.Amb. + 34.707 [kW]
Tap water demand	y= 21 [kW]
Space heating demand	y = -1.7973*T.Amb. + 45.882 [kW]
High-pressure branch	
Gas cooler inlet-temperature	y=33[°C] or averages from field data**
High-pressure expansion valve inlet-temperature	y=10 [°C]
Gas cooler outlet-temperature	IF T.Amb. < 6 y=10 [°C]; IF T.Amb. >= 6 y= 4 + T.Amb. [°C]
Heat recovery forward temperature	y= -0.0021*T.Amb^3 - 0.0185* T.Amb^2 - 0.1673*T.Amb + 43.533 [°C]
Discharge pressure	Control as described in paragraph 5.1
Low-pressure branch	
Evaporation temperature freezers	y= -32 [°C]
Evaporation temperature cabinets	y= -4 [°C]
Evaporation temperature load evaporator	y= 0.2 [°C]
Freezers useful superheat	y= 13.5 [°C]
Cabinets useful superheat	y= 7.5 [°C]
Load evaporator internal superheat	y= 3.5 [°C]
MT compressors suction temperature	y= 0.3802* T.amb + 14.196 [°C]
Parallel compressors suction temperature	y= 0.5056* T.amb + 18.157 [°C]
LT compressors suction temperature	y= -4 [°C]
Receiver pressure	y= 40 [bar]

*Tamb = Outdoor Temperature [°C]

** For comparing the model output and the calculated COP, the input values for the gas cooler inlet-temperature were taken as averages of the field data.

5.3.2. Model validation

To begin with, it was necessary to validate the model built according the current control strategy in order to use it as a matter of comparison. First, an approach using a fixed value for the gas cooler inlet-temperature (assumed to be the same as the outlet-temperature from the second desuperheater) was used. The obtained COP heat recovery is shown in Figure 5.12. The decrease in the performance is due to the activation of the boreholes.

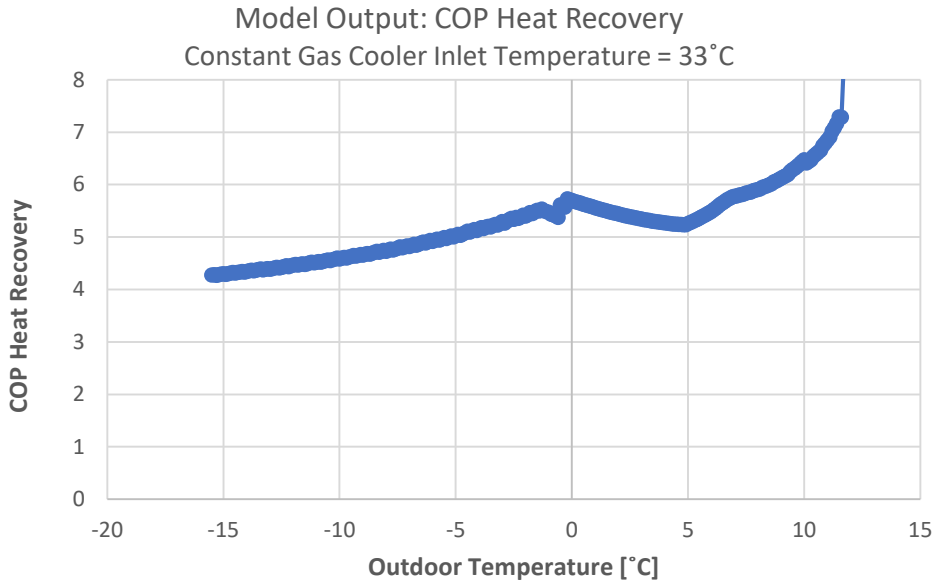

Figure 5.12 Model Output: COP heat recovery calculated with fixed gas cooler inlet-temperature.

As shown in Figure 5.7, the COP heat recovery is strongly affected by the gas cooler inlet temperature. Therefore, the model accuracy was assessed using as input for the gas cooler inlet-temperature values from field data averaged on the outdoor temperature. Figure 5.13 shows the graphical comparison.

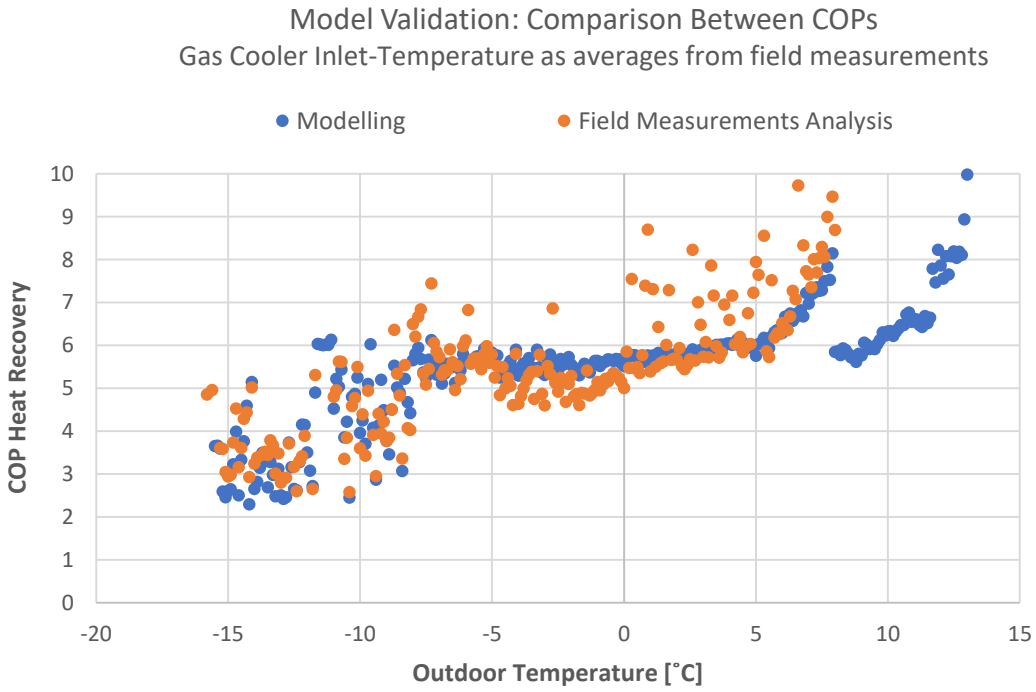

Figure 5.13 Comparison between COP from field data analysis and modelling.

It is worth to notice the mismatch of the model for outdoor temperatures ranging from 8 to 13˚C. This is due to the fact that the model was built to satisfy always both space heating and tap water demands. In the real system there is a drop in the tap water production for these values of the outdoor temperature. In other words, the real system does not increase the pressure to deliver tap water, which is considered a B product from the heat recovery, while the built model does it since that tap water demand would need to be satisfied by electric resistances and the field measurements analysis does not take this into account. This effect can also be seen in Figure 5.14 where discharge pressures are compared.

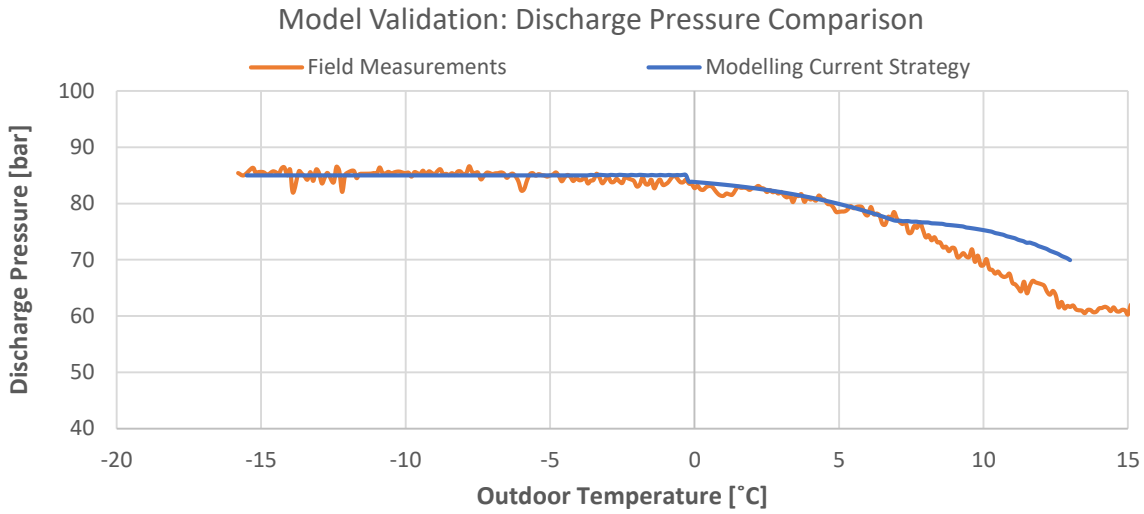

Figure 5.14 Comparison between discharge pressure from field data analysis and modelling.

The ultimate validation consists of comparing the estimated compressors power consumption and the one measured from the power meters. This comparison is shown in Figure 5.15. It must be noticed that both approaches have been tested: using averaged values from field measurements for the gas cooler inlet temperature or using a fixed value of 33˚C.

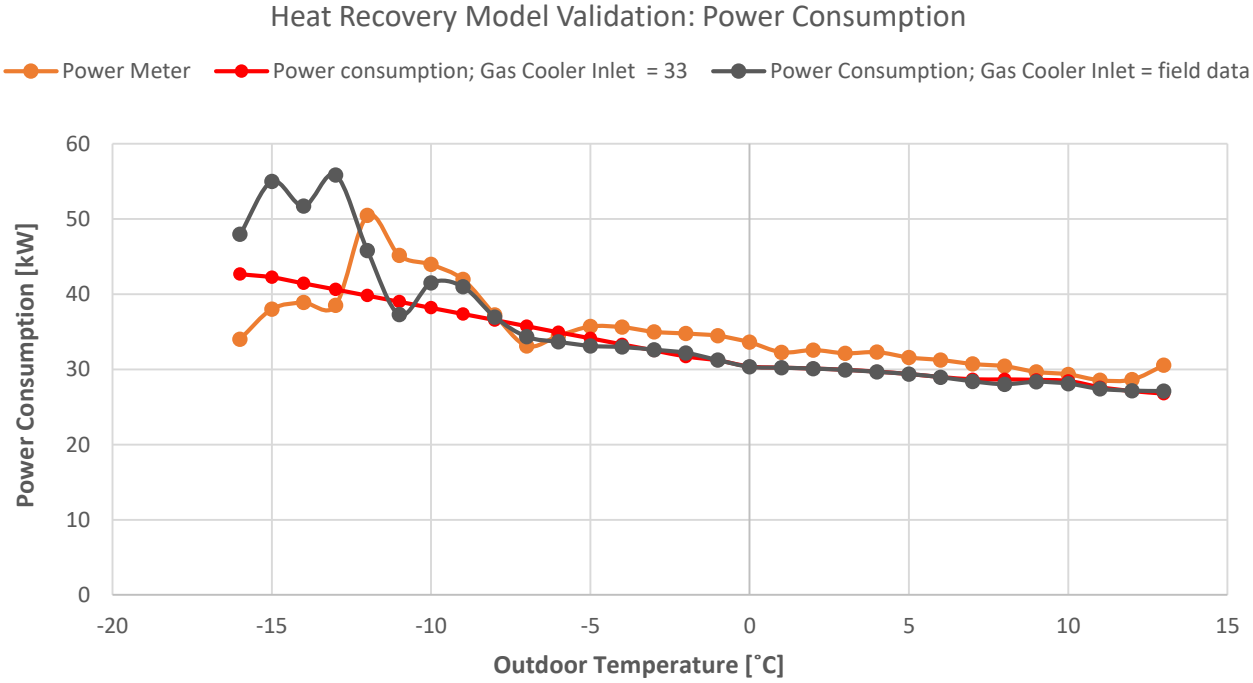

Figure 5.15 Comparison between power consumption from field data analysis and modelling.

The calculated error on the annual energy consumption was estimated to be 8% when using 33°C as fixed value for the gas cooler inlet temperature, while 7% when using field data averaged on the ambient temperature.

5.3.3. Effect of optimal pressure control

A second model was built in order to evaluate the differences between the best theoretical discharge pressure control which is used in both "*Geothermal capacity regulation*" and *"Gas cooler capacity regulation"* described in section 5.1 and the control really implemented. In this second scenario, the pressure is controlled following the scheme depicted in Figure 5.2. The graphical comparison between the two pressures is shown in Figure 5.16.

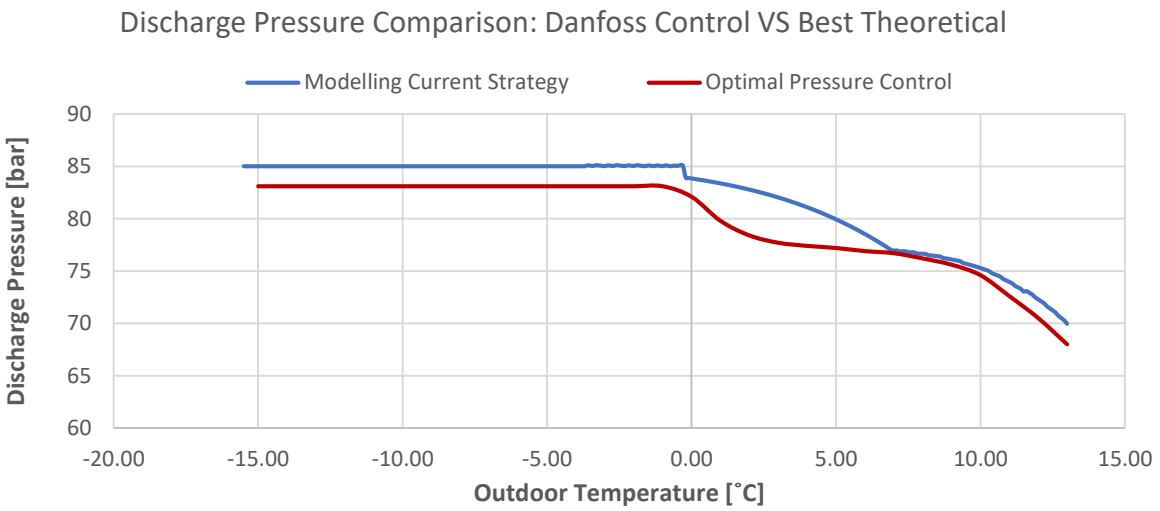

Figure 5.16 Comparison of discharge pressure between current control and optimal theoretical control.

The obtained COP is displayed in Figure 5.17 together with the one obtained by modelling the *"Geothermal capacity control"* strategy. This strategy was chosen as a comparison since the current control does not by-pass the gas cooler. The two curves match pretty well when the geothermal heat extraction is activated, in fact, the biggest improvements are obtained while the pressure is going from the minimum transcritical pressure to the optimal value (in this case, 83.1 bar).

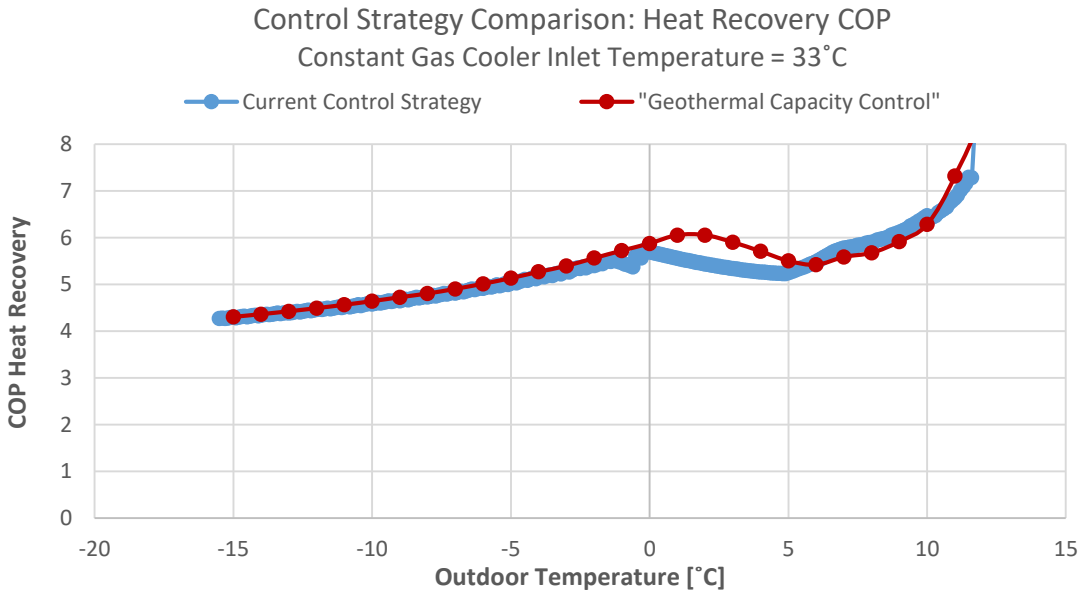

Figure 5.17 Comparison of COP heat recovery between "Current control" and "Geothermal capacity control".

Knowing the heat recovery demand and the BIN hours from the field data, it is possible to estimate the improvements both in terms of energy savings and seasonal performance. The energy savings due to this improved strategy, for the Stockholm climate, are estimated to be 2965 kWh/year, while the average COP over the heating season increases of 6% going from 5.8 to 6.1. The practical meaning of this improvement is what would be the maximum theoretical benefit if the set points of the controller displayed in Figure 5.2 would be perfectly fine-tuned.

5.3.4. Effect of gas cooler by-pass

Finally, the third comparison aims at identifying the differences between the two theoretical control strategies described in section 5.1.1 and 5.1.2. The difference lays in the fact that the strategy "*Geothermal capacity control*" does not by-pass the gas cooler when necessary while the "G*as cooler capacity control*" does. From a thermodynamic perspective, the performance of the cycle is exactly the same. The only difference is that the *"Geothermal capacity control"* spends some extra-energy for the gas cooler fans and geothermal pumps. However, this control strategy has some important technical benefits as already discussed in section 5.1.2. The graphical comparison between the two heat recovery COPs is shown in Figure 5.18. The influence on the COP is almost negligible, in fact, average COP over the heating period goes from 6.1 to 6. The same is true for the extra energy spent which is roughly 864 kWh/year.

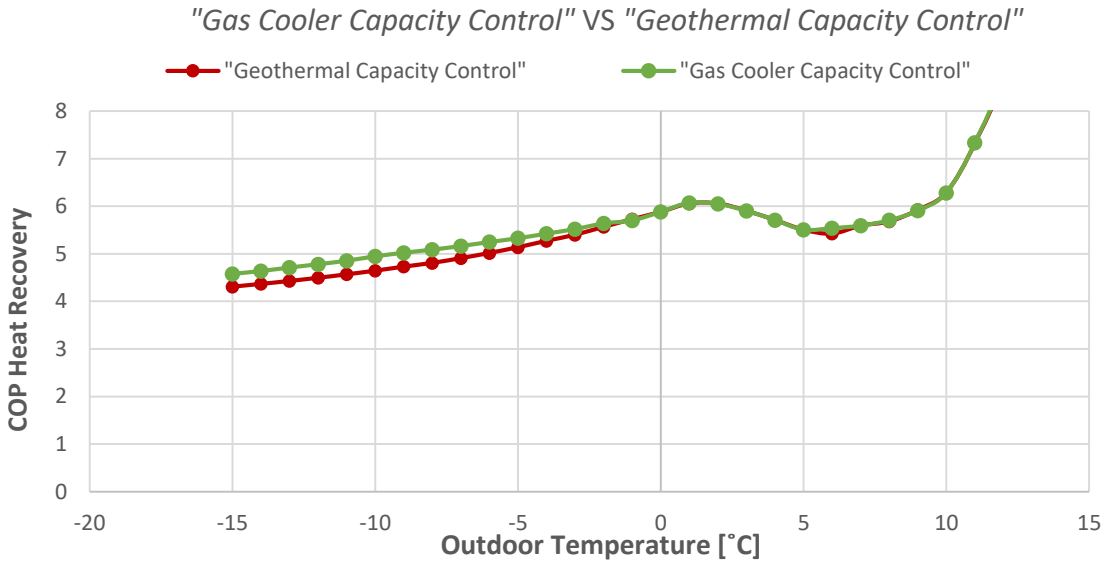

Figure 5.18 Comparison of COP heat recovery between "Geothermal capacity control" and "Gas cooler capacity control".

5.3.5. Saved heat from external sources

In case that the system was not integrated with the geothermal boreholes, additional heat from external sources ($\dot{Q}_{external}$) would have been necessary. Since in this installation the gas cooler was never by-passed during the examined period, $\dot{Q}_{external}$ was evaluated calculating the differences between the maximum potential thermal power that could be recovered and the heating demand. The methodology consisted of firstly calculating the maximum mass flow ($\dot{m}_{max}$) of refrigerant that could be circulated in the high-pressure branch at the maximum discharge pressure. This was estimated assuming that the temperature at the high-pressure expansion valve was equal to the gas cooler inlet-temperature (gas cooler by-passed), therefore, assuming the maximum quality at the exit of the high-pressure expansion valve(χ_{max}).

$$\dot{m}_{max} = \dot{m}_{liq} * (1 + \chi_{max}) \quad (5.2)$$

In Eq. 5.2, $\dot{m}_{liq}$ represents the amount of liquid refrigerant necessary for satisfying the cooling loads. Then, the maximum potential heat recovered $\left(\dot{Q}_{hr_{max}}\right)$ is calculated considering that all the heat available between compressors discharge and the inlet of the high-pressure expansion valve can be recovered. Finally, the necessary heat from external sources is calculated as shown in Eq. 5.3.

$$\dot{Q}_{external} = \dot{Q}_{hr} - \dot{Q}_{hr_{max}} \tag{5.3}$$

For the given demand in the studied supermarket, the refrigeration system needs a very small amount of extra heat to satisfy the demands in the coldest days. The annual necessary extra energy is estimated to be 759 kWh/year (utilizing Stockholm's BIN hours). The latter value can be seen as thermal energy savings since it should be provided by an external source.

5.4. Discussion of the Results

Field measurements show that the COP heat recovery of the refrigeration system reaches a minimum of 3 and goes up to 50 for mitigated outdoor temperatures. The average COP for the whole heating season is 7.5. Indeed, for outdoor temperatures higher than 7.5˚C, heat is delivered almost for free being recovered from the waste heat rejected by cabinets and freezers.

Additionally, field measurements show the strong correlation between heat recovery performance and the return temperature from the space heating system. When the outdoor temperature is lower than -8 ˚C, the space heating return increases. This drives the gas cooler inlet-temperature up. Indeed, it goes from roughly 33˚C to roughly 40˚C for the lowest outdoor temperatures.

Looking at the real pressure control of the refrigeration system, it was found that it is very close to the optimal regulation advised by theoretical studies (Sawalha, 2012). The difference between best theoretical regulation and the implemented one lays in the proper settings of the space heating controller. The optimization of those settings was out of the boundaries of this study, however, the performance improvements on a seasonal perspective are found to be very little.

An alternative theoretical control strategy was identified and compared to the best strategy described in previous studies (Karampour et al., 2018). Heat could be extracted from the ground while the gas cooler is not by-passed. The results suggest that the variation in the average COP over the heating season is almost negligible. However, there are important technical advantages, since controlling challenges are shifted from regulating the heat recovered controlling the gas cooler outlet-temperature to regulating the heat recovered controlling the MT compressors' capacity which is technically easier. Moreover, this alternative control strategy has the co-benefit of cooling the ground, therefore, improving the subcooling performance. This is discussed in chapter 8.5.

Finally, the amount of heat that needs to be provided by the geothermal integration in winter was found to be very limited on an annual basis. For this reason, the savings due to the geothermal integration, during winter, are almost negligible. Indeed, the boreholes are mainly used to satisfy the peaks of heating demand. Therefore, their contribution is not relevant from an annual energy use perspective. However, from a design perspective they are very important since without a geothermal integration, a way of providing extra heating capacity should be installed (e.g. electric boilers back-up; district heating connection).

6. Subcooling

Figure 6.1 highlights the effect of the geothermal sub-cooling. The difference between the high-pressure expansion valve inlet-temperature and the gas cooler outlet-temperature is the clear effect of the geothermal subcooling.

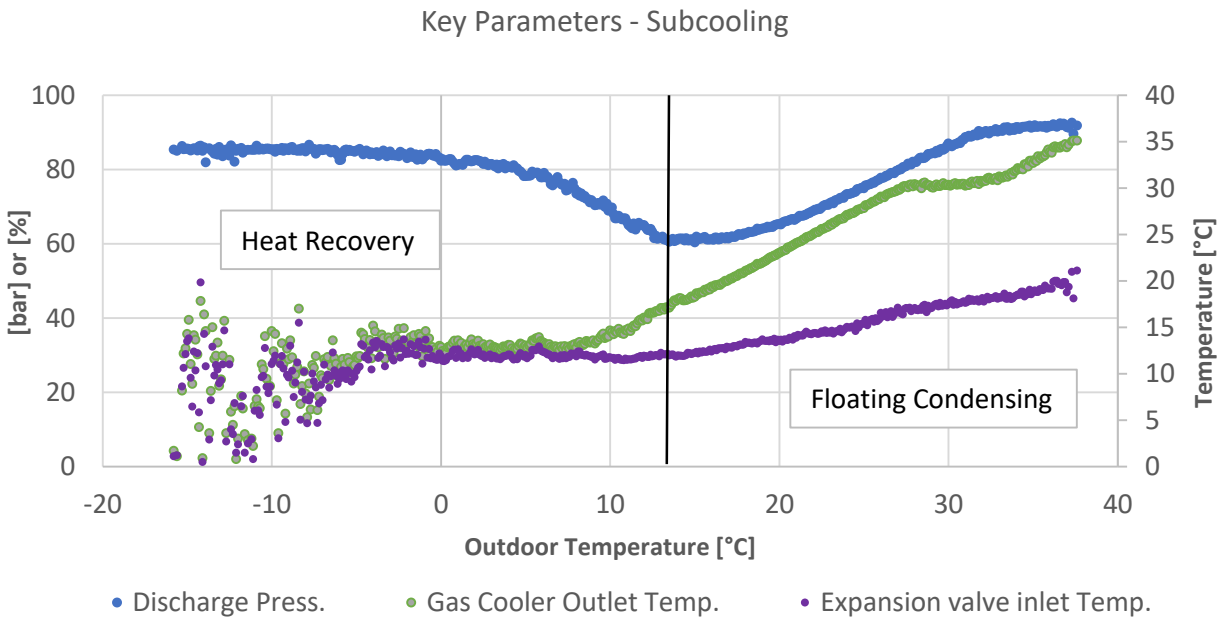

Figure 6.1 Subcooling key parameters plotted as a function of the outdoor temperature. Discharge Pressure (primary axis); Gas Cooler fans' capacity (primary axis) and high-pressure expansion valve inlet temperature (secondary axis).

During winter operations, the geothermal subcooling is not utilized except for mitigate outdoor temperature (T. Amb. ≥ 10°C). While in summer, this function is fully utilized. Generally, the subcooling potential is limited by the boreholes mean fluid temperature. During the warmest period, a temporary overheating of the cold source, due to the amount of heat dumped into the ground, limits the subcooling potential. This is why the high-pressure expansion valve inlet-temperature raises with the increase of the outdoor temperature. It must be said that in this installation, this effect is very limited due to an over-dimensioning of the geothermal field.

Figure 6.2 shows the thermal power injected (blue line) and extracted (red line) from the ground as a function of the operational hours. The area delimited between the x-axis and the plotted function represents the total heat injected (roughly 73 MWh) or extracted (roughly 18.3 MWh), in kWh. In this installation, the design power of the heat exchanger used for the geothermal subcooling was 100 kW, however, for 95% of the time the subcooling power does not exceed 45 kW.

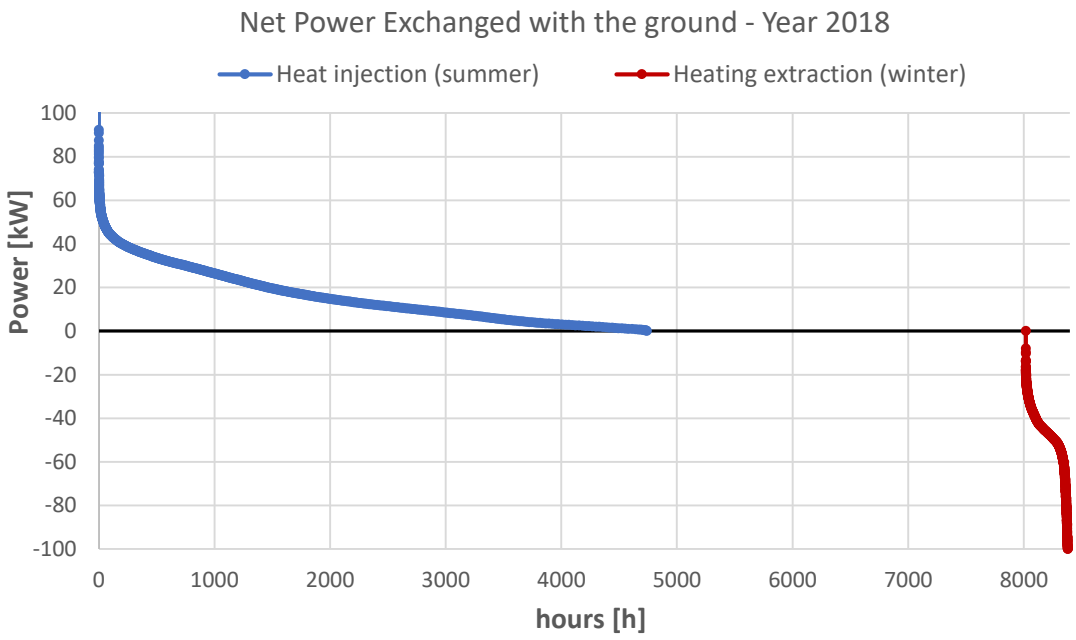

Figure 6.2 Net thermal power exchanged with the ground - Year 2018.

Looking at Figure 6.2, it is clear that the ground is strongly unbalanced. For this reason, in this system, the economic benefits of the geothermal integration are almost totally connected to the subcooling effect. Moreover, it must be said that for almost 3500 hours per year the ground is not utilized and that for roughly 1000 hours the power injected is lower than 5 kW. The low usage rate of the boreholes is typical in these installations and is one of the most important factors when evaluating the economic benefits as will be discussed in chapter 8.

6.1. Evaluation of the savings

As well known, subcooling the refrigerant, before the high-pressure expansion valve, leads to savings of compressors' power. Figure 6.3 shows the system's branch connected to the geothermal subcooler. The savings were calculated estimating the extra refrigerant mass flow that would have been needed if the temperature at the internal heat exchange inlet (6' in Figure 6.3) had been equal to the one at the gas cooler outlet (point 5 in Figure 6.3).

Since the priority of a refrigeration system is to satisfy the cooling demand, this can be considered fixed regardless the conditions at the high-pressure expansion valve inlet. Knowing the thermodynamic conditions at the inlet and outlet of the evaporators, the necessary mass flow of liquid refrigerant can be calculated.

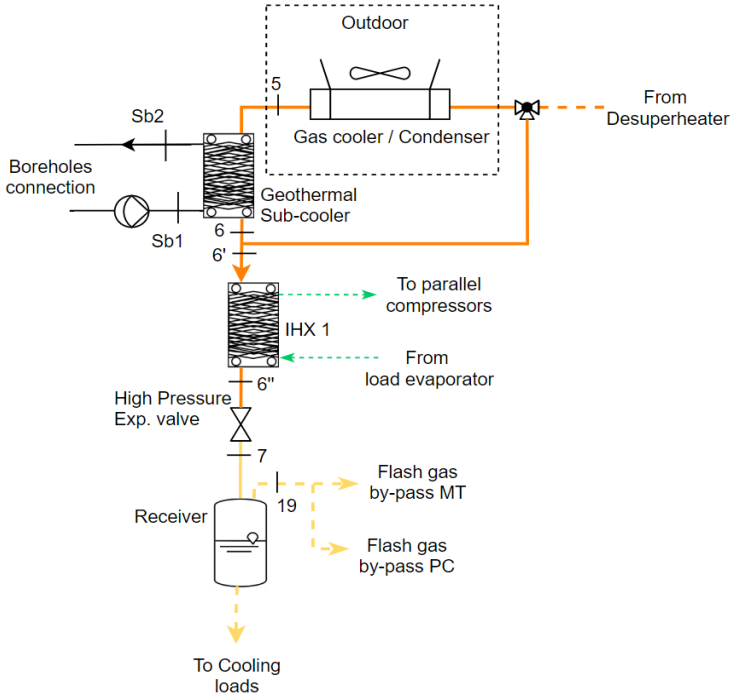

Figure 6.3 Connection with geothermal boreholes for subcooling function.

The extra power consumption is due to the extra amount of flash gas that would have been generated for the same amount of liquid refrigerant. The relationship between the total amount of mass flow and the necessary liquid refrigerant is given by Eq. 6.1, here reported with numbers referring to Figure 6.3.

$$\dot{m}_{liq} = \dot{m}_{gas} * \left(1 - \chi_7(h_{6''}\,;\, P_{receiver})\right) \tag{6.1}$$

The heat injected (blue) into the ground and the power savings (green) are shown in Figure 6.4 (values averaged on the outdoor temperature). The trends in Figure 6.4 are strictly connected to the key parameters displayed in Figure 6.1. As expected, the trend of the savings becomes very steep after that the gas cooler outlet-temperature overcome the critical temperature.

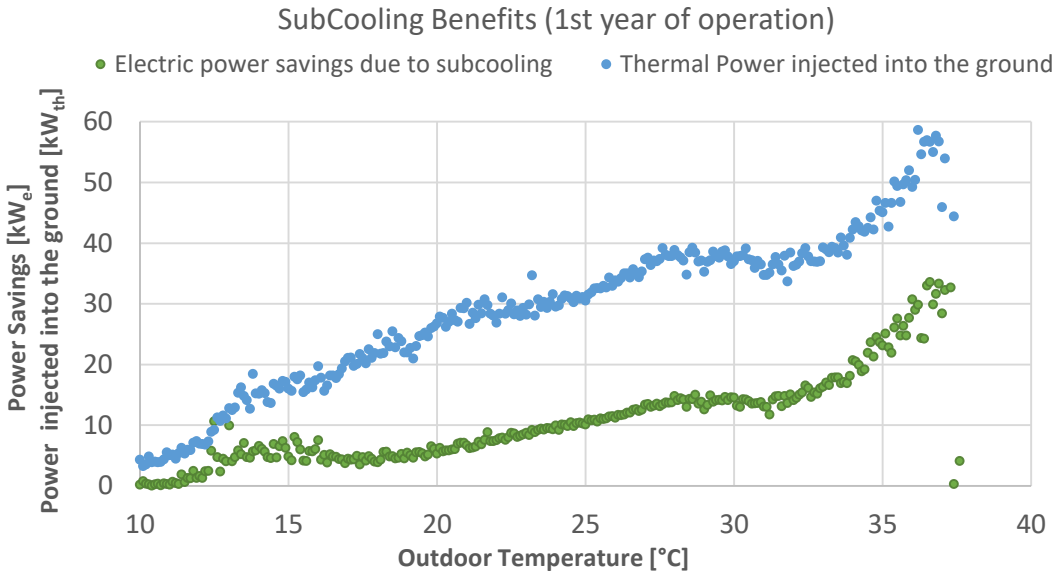

Figure 6.4 Subcooling savings as a function of the outdoor temperature.

The majority of the savings are due to the reduced power consumption of the parallel compressors. However, for relatively low ambient temperatures, the savings are obtained on the MT compressor's power. This is due to the fact that, for these temperatures the flash vapour barely reaches the minimum mass flow elaborated by the parallel compressors. When the climate is warmer, the air-conditioning is active for more hours and being connected to the parallel compressors, it enables the flash gas to be by-passed on the parallel compressors' suction line.

It is worth to mention that the power consumption of the pumps used to recirculate the secondary fluid in the boreholes was taken into account when calculating the savings depicted in Figure 6.4. The power absorbed by the pumps was assumed to be 5% of the heat injected into the ground (Karampour et al., 2018)

The energy saved during the first year of operation is given in Table 6-1, highlighting its share of the total energy consumed by the installation.

Table 6-1 Energy savings due to subcooling.

Month	Total Electricity Consumption [MWh]	Total Electricity Savings (due to subcooling) [MWh]	Savings as percentage of total electricity consumption [%]
Jan.	25.92	0.00	0%
Feb.	21.68	0.09	0%
Mar.	23.66	0.72	3%
Apr.	23.65	1.89	8%
May	23.36	2.37	10%
Jun.	20.07	2.40	12%
Jul.	35.98	7.51	21%
Aug.	28.97	4.30	15%
Sep.	23.24	3.23	14%
Oct.	23.06	2.02	9%
Nov.	21.06	0.00	0%
Dec.	22.63	0.02	0%
TOT	**293.28**	**24.55**	**8.4%**

6.1.1.Sub-cooling Efficiency

Knowing the power injected into the ground and the relative savings, it is possible to calculate the ratio between energy saved and subcooling capacity. Figure 6.5 displays such a ratio as a function of the outdoor temperature. As expected, the power savings per kW of sub-cooling capacity rears up for outdoor temperatures higher than 29°C. This corresponds to the point where the gas cooler outlet-temperature overcome the critical temperature. In that region, the enthalpy variation per each degree of subcooling is much higher than in the liquid zone.

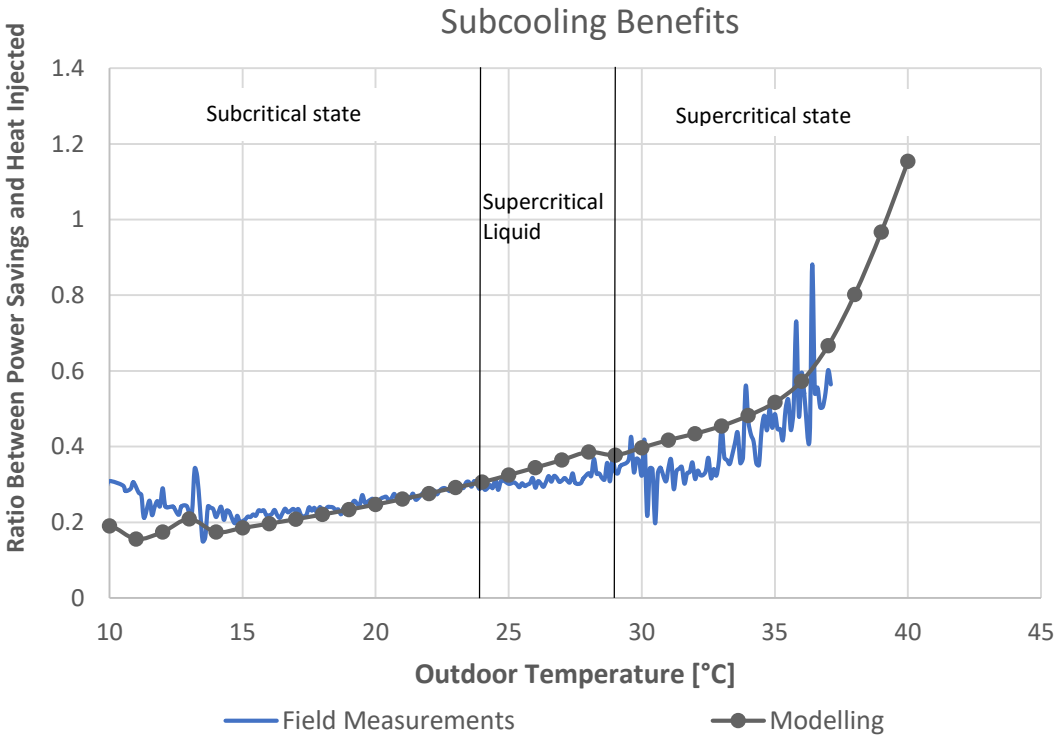

Figure 6.5 Ratio between subcooling savings and heat injected into the ground.

The curves presented in Figure 6.5 can be interpreted as a subcooling efficiency. If one assumes an electricity price of 1 SEK/kWh, the value displayed on the y-axis would be the monetary value of each kWh of cold used for subcooling the refrigerant at a certain outdoor temperature. This curve could also be used to evaluate mechanical subcooling. However, this is out of the boundaries of this analysis.

6.2. Modelling - Subcooling

The aim of this modelling section was to evaluate the reduction of savings resulting from a reduction of subcooling capacity. The model described in this paragraph does not take into account the integration with the geothermal boreholes. Such an integration is studied in chapter 8 utilizing the combination of the model used for evaluating the heat recovery period and the one described in this chapter.

Also in this case, the simulation is based on inputs and outputs expressed as a function of the outdoor temperature. The outputs are then treated using the BIN hours method. The inputs for the subcooling modelling are displayed in Table 6-2.

Table 6-2 Modelling inputs for subcooling period.

Demands	
Freezers Cooling Demand	y = =0.1227* T.Amb. +22.271
Cabinets Cooling Demand	IF T.Amb. <=10; y= 52 [kW] IF T.Amb. > 10; y = 1.7293*T.Amb. + 34.707 [kW]
Tap Water Demand	y= 21.5 [kW]
Space heating Demand	y = 0 [kW]
Air Conditioning Demand	y= 0.2034*(T.Amb.)^2 -7.3557* T.Amb. +82.554 [kW]
High-pressure branch	
Gas Cooler Inlet Temperature	y= Outlet from Tap Water desuperheater [°C]
Expansion valve inlet-temperature	IF T.Amb. < 10; y = 10 [°C] IF T.Amb. >= 10; y= 0.3363*T.Amb.+7.1985 [°C]
Gas Cooler Outlet temperature	IF T.Amb. >30 y= 2 + T.Amb. [°C]; IF T.Amb. <= 30 y= 4+ T.Amb. [°C]
Discharge Pressure	IF T.Amb. < 2 Tcond = 7 + T.Amb. [°C]; IF 24 <= T.Amb.<=31 y= 2*T.Amb. +26 [bar] IF T.Amb. > 31 y= 88 [bar]
Low-pressure branch	
Evaporation temperature Freezers	y= -30 [°C]
Evaporation temperature Cabinets	y= -5 [°C]
Evaporation temperature load evaporator	y= 0.2 [°C]
Freezers internal superheat	y= 14 [K]
Cabinets internal superheat	y= 7.5 [K]
MT compressors suction Temperature	y= -0.871* T.amb + 25.75 [°C]
Parallel compressors suction Temperature	y= -0.284* T.amb + 17 [°C]
LT compressors suction Temperature	y= -4 [°C]
Receiver Pressure	y= 40 [bar]

*Tamb = Outdoor Temperature [°C]

**Tcond = Condensation Temperature [°C]

It is worth to notice that the given function for the high-pressure expansion valve inlet temperature was used only to compare the models results with the field measurements analysis. When this model was implemented for the techno-economic analysis, in chapter 8, the high-pressure expansion valve inlet temperature was obtained through an iterative process.

In order to calculate the reduced savings Eq. 3.4 and Eq.3.8 were used. These equations are reported below with subscript referring to Figure 6.3

$$\dot{Q}_{sub} = \dot{m}_{liq}(1 + \chi_7) * (h_5 - h_6) \tag{3.4}$$

$$\chi_7 = \frac{h_{6,,} - h_{liq}}{\Delta h_{vap,rec}} \tag{3.8}$$

In Eq. 3.4 $\dot{m}_{liq}$ is the liquid mass flow of refrigerant necessary for cabinets and freezers and $\dot{Q}_{sub}$ is the power injected into the ground through the subcooling heat exchanger.

As already mentioned, this model simulates which would have been the savings if the maximum power injected into the ground was limited to a certain value. In Figure 6.6 the resulting reduced savings curves are given for different values of the maximum subcooling capacity.

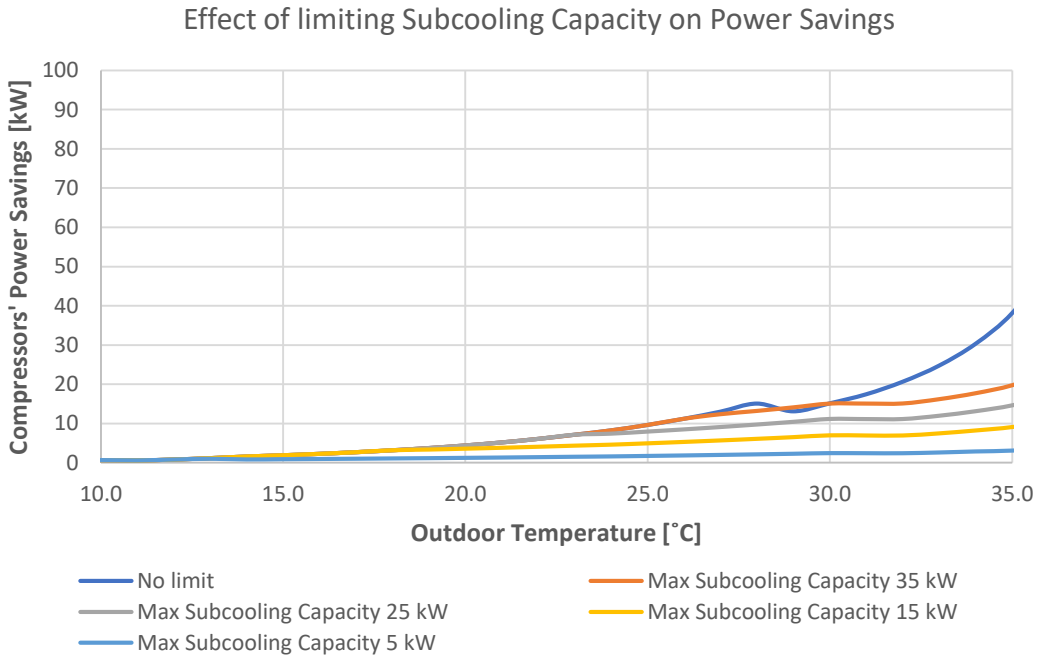

Figure 6.6 Effect of limited subcooling capacity on power savings.

The fluid mean temperature in the boreholes is affected by the amount of heat injected/extracted. This, in turn, affects the maximum subcooling capacity. However, it is important to notice that Figure 6.6 does not take into account the effects of the boreholes' response to different loads.

In other words, the results presented in this paragraph do not take into account what is the system that is providing the subcooling. Indeed, the curves given in Figure 6.6 represent only the reaction of the refrigeration system to a certain subcooling capacity. However, the techno-economic analysis discussed in chapter 8 takes also into account the boreholes' response.

Figure 6.7 displays the power injected into the ground as a function of the amount of hours for which each of the power's value occurs (same as Figure 6.2). The horizontal lines in Figure 6.7 represent the values at which the maximum subcooling capacity was limited to generate the curves shown in Figure 6.6.

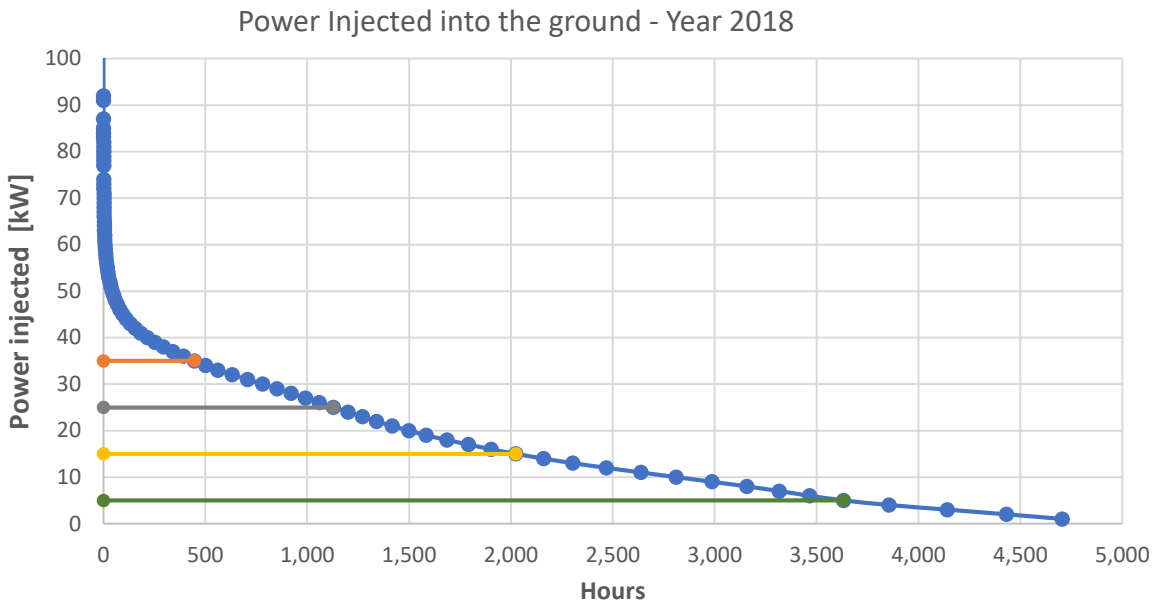

Figure 6.7 Power injected into the ground as a function of the operational hours.

The output from the model are the curves shown in Figure 6.6. For each value of the outdoor temperature a certain power saving and power injected into the ground is given. Therefore, knowing the amount of operational hours for each value of the outdoor temperature, the annual energy savings can be calculated from the curves shown in Figure 6.6. The result is displayed in Figure 6.8.

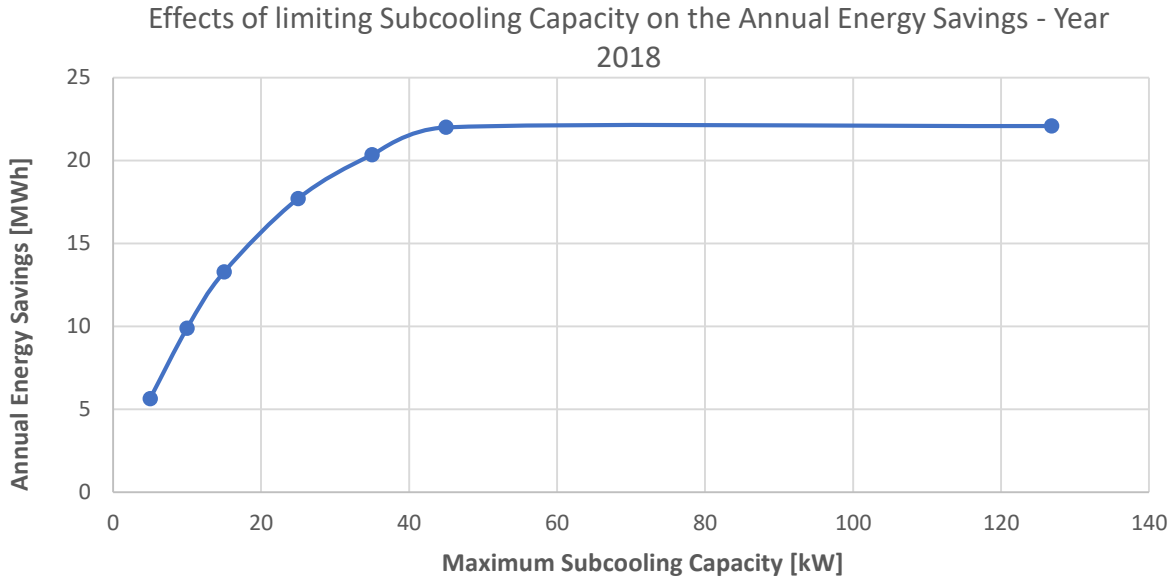

Figure 6.8 Annual energy savings as a function of the maximum subcooling capacity.

The total energy consumption estimated through this simplified model is 277 MWh/year and the savings due to subcooling are 22 MWh/year corresponding to 8% of the total energy consumption. The modelling results are 6-8% lower than the one obtained from the field measurements analysis (Table 6-1), demonstrating the reliability of the simplified model.

It is worth to mention that the results shown until this point are based on field measurements recorded during the year 2018. That year was particularly warm compared to the typical weather in that Climate zone (same as Stockholm). The difference between the Stockholm BIN hours and the field data can be seen in graph displayed in Figure 6.9. To have more general results, the Stockholm BIN hours were utilized in the techno-economic evaluation.

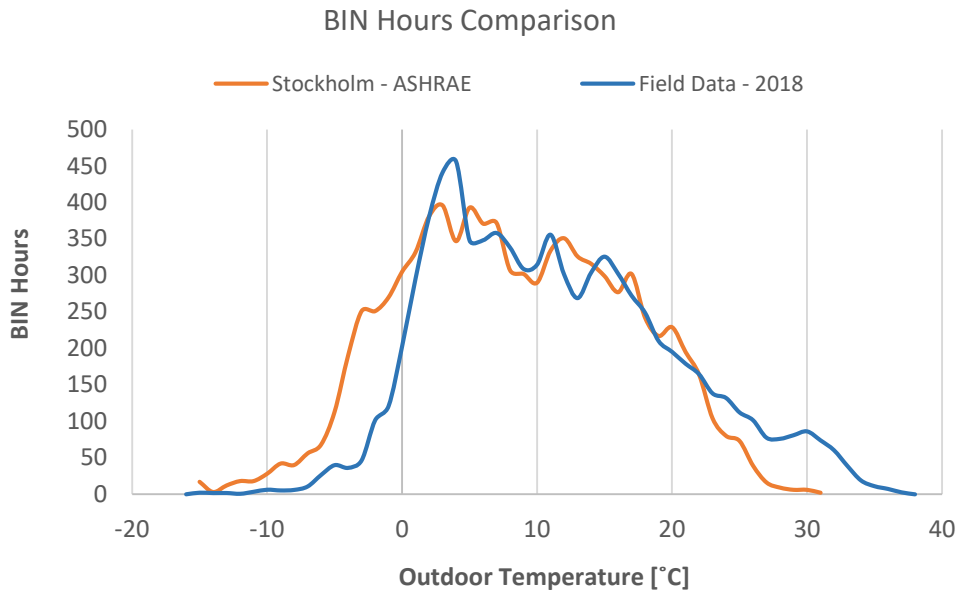

Figure 6.9 Comparison between BIN hours and filed measurements.

6.3. Discussion of the results

To begin with, the system shows a heavily unbalanced ground, a lot of heat is injected during summer (roughly 73 MWh/year) but very little is extracted in winter (roughly 18.3 MWh/year). Going forward, field data shows that the system achieves up to 15˚C of subcooling during the warmest period of the year. Thanks to that, the annual energy savings due to the geothermal subcooling are estimated to be 8.4% of the total power consumption.

A model was built in order to perform the techno-economic assessment of the geothermal integration, presented in chapter 8. The comparison between the simplified model and field measurements shows an error of roughly 6-8%. Moreover, the subcooling design capacity was found to be over-estimated for the real needs of the installation, a design capacity of 45 kW would have been enough to guarantee 95% of the energy savings.

Finally, it is worth to notice that the field data were recorded in 2018, which was a particularly warm year in Sweden. For this reasons, the calculated energy savings, for that year, are thought to be overestimated compared to the average annual savings that one can expect.

7. Free-Space-cooling

Due to the lack of proper measurement points, it was not possible to evaluate the free cooling gains from the geothermal integration. However, when examining the borehole return temperature, it seems very improbable that any free space cooling was obtained during the examined period. Figure 7.1 shows borehole's outlet temperature averaged on an hourly basis. As it can be seen, during spring-summer, the temperature is always higher than 10°C, considering the modern space cooling systems, it seems not possible to provide space cooling at this temperature level. Experts in this field confirmed it is usually very difficult to obtain free space cooling from the geothermal connection.

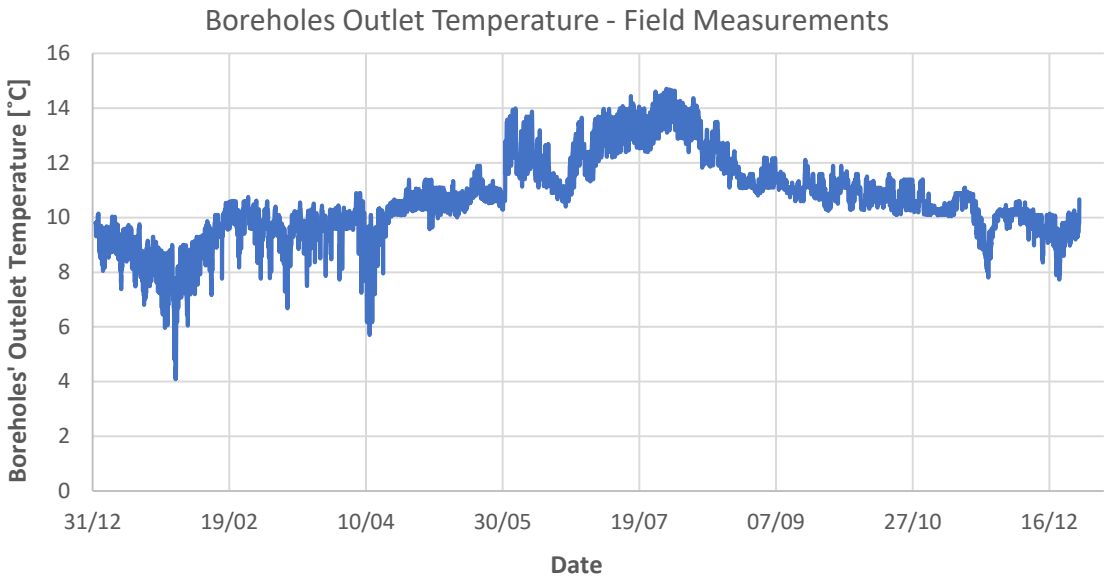

Figure 7.1 Field Measurements: boreholes outlet temperature..

One of the reasons for the high outlet temperature could be the contemporary functioning of the subcooling heat exchanger. Indeed, the heat injected into the ground from that heat exchanger has a relatively high-temperature. It might be that the system could have provided free-space-cooling in case that the subcooler was not working. This brings-up the question; which of these two options should be prioritized subcooling or free-space-cooling?

This question can be answered looking at the curves displayed in Figure 6.5. The inverse of the COP of an Air Conditioning (AC), supplying space cooling to the building, can be compared with the values shown on the vertical axis of that graph. For example, assuming a COP of 3 for a common AC device, the inverse would be 0.33. When this value is higher than the ratio between the expected power savings and subcooling capacity (Figure 6.5) it is more profitable to utilize the geothermal integration for free-space-cooling rather than subcooling.

Due to time constrains, the free-space-cooling potential was not further investigated and was left for the future work. Furthermore, the free-space-cooling benefit was not considered in the techno-economic assessment since it was not observed in the studied supermarket.

8. Techno-economic assessment of the geothermal integration

The aim of this chapter is to identify which are the parameters, in terms of demand profile and climate zone, that most affect the economics of a geothermal integration. Combining the models described in chapter 5.3 and 6.2, it was possible to relate the power savings due to a geothermal integration (summer and winter) to an hourly profile of the ground load (heat injection and extraction). The latter profile represents the input for a borehole simulation software called Earth Energy Designer (EED). Through the software it is possible to identify the optimal borehole field size and configuration for a given load. Knowing the relationship between the load on the ground and the savings, a specific field size can be linked to its expected savings. Finally, assuming a reasonable lifetime of the installation and a discount rate, the annual savings can be expressed as a present value.

When evaluating the potential economic benefits of the boreholes integration, one needs to take into account the difference in OPEX and CAPEX between having or not a geothermal storage. This difference can be referred as ΔNPV and if it is negative, the geothermal storage is the best option. The conceptual representation of the ΔNPV is shown in Figure 8.1 Due to time constrains it was not possible to evaluate the investment cost for the alternatives. Indeed, this strongly depends on the location and on the providers of the other technologies or energy vectors. This is further discussed in the last paragraph of this chapter.

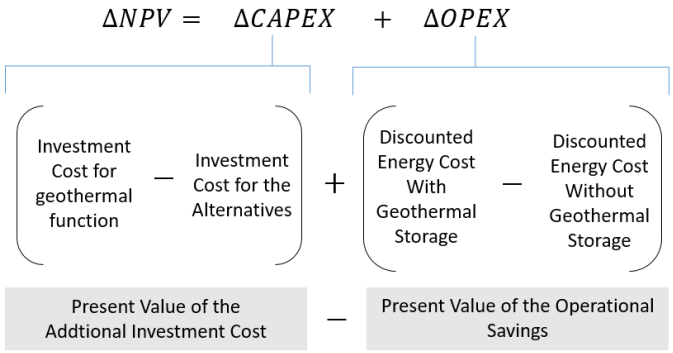

Figure 8.1 Methodology for the techno-economic assessment, Net Present Value of geothermal storage

Regarding the methodology, the load on the ground affects not only the size and configuration but also the outlet-temperature from the boreholes. The latter is directly related to the inlet temperature of the high-pressure expansion valve which, in turn, affects the heat injected into the ground. This correlation must be solved through an iterative process. In this work such a calculation was performed iterating between the geothermal simulation software EED and the refrigeration system model based on a VBA code. The iterative process is shown in Figure 8.2.

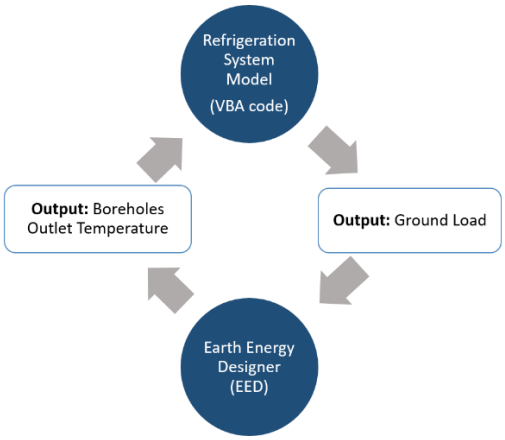

Figure 8.2 Methodology for the techno-economic assessment, iteration between software.

8.1. Boreholes Field Inputs

As depicted in Figure 6.9, the year 2018 was particularly warm. Therefore, the modelling outputs were multiplied for the Stockholm BIN hours rather than the value measured on the field. The inputs used for EED can be classified as inputs depending on the geographical location, inputs depending on the borehole heat exchanger and inputs depending on the heating and cooling loads. The latter were obtained as output from the refrigeration system model. The other main inputs are summarized in Table 8-1.

The ground properties were retrieved from Sveriges Geologiska Undersökning (SGU), the data for the borehole heat exchanger were not available for the studied supermarket, therefore, they were obtained from previous studies (Mateu-royo et al., 2018) and consultation with experts in this field. The heat carrier fluid is the same used in the case study and the thermodynamic properties were taken from (Melinder, 2010). The simulation period was set to 15 years and the minimum mean fluid temperatures was set to -6°C, while several maximum mean fluid temperatures were tested as explained in the next paragraph.

Table 8-1 Inputs for geothermal simulation software (EED).

Location Dependent (Swedish Geographical Survey, 2019)		
Thermal conductivity	3.4	W/mK
Volumetric heat capacity	2.4	MJ/m3K
Ground Surface Temperature	6.6	degC
Geothermal heat flux	0.04	W/m2
Borehole Heat Exchanger		
Pipes type	PE DN32 SDR-17	
Diameter	110	mm
Shank spacing	70	mm
Volume Flow rate per borehole	0.5	l/s
Heat Carrier Fluid		
Methanol – Water	29%	Mass fraction
Thermal conductivity	0.433	W/mK
Specific heat capacity	3917	J/kgK
Density	955.5	Kg/m3
Viscosity	0.002161	Kg/ms
Freezing point	-25.9	degC

8.2. Borehole Field Optimization

For the studied supermarket, due to the geographical location and heating demands, most of the economic benefits of the boreholes are connected to the subcooling function. For this reason, the subcooling capacity was utilized as optimization parameter to find the optimal total length of the geothermal field. Therefore, first it was necessary to identify different optimal sizes of the geothermal field for different subcooling capacities. Then, it was possible to choose a certain size of the geothermal storage considering the investment cost (due to the storage size) and the expected savings (mainly due to the subcooling function).

The design of the optimal size, for a given maximum subcooling capacity, starts calculating the maximum ground load (ground heat extraction and injection). The heat extraction is maximised by never by-passing

the gas cooler (Control strategy *"Geothermal capacity regulation"*). While, the heat injection is maximised when the inlet-temperature at the high-pressure expansion valve is at its minimum (10°C). Figure 8.3 shows the output of this first step. The heat injection corresponds to the subcooling capacity while, the heat extraction represents the heat utilized in heat pump mode. For the sake of clarity, the curve named *"Heat Extraction GC by-pass",* in Figure 8.3*,* represents the heat that would be extracted applying the control strategy "*Gas Cooler capacity regulation*" explained in chapter 5.1.

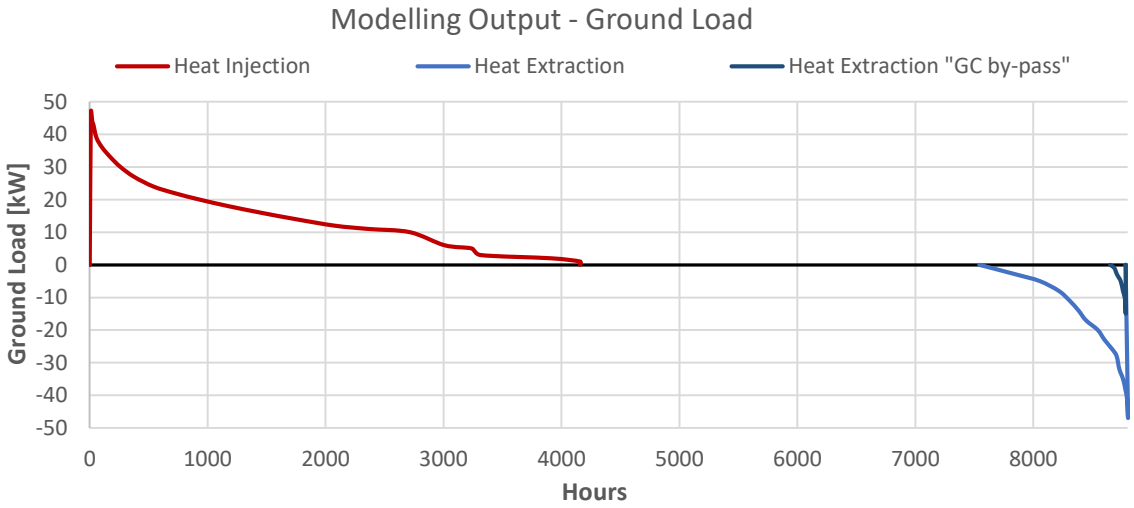

Figure 8.3 Modelling Output: Example of load on the ground.

Once obtained the ground load, it was possible to limit the subcooling power and the necessary borehole length, applying a power coverage factor (in this case, only maximum subcooling capacity). It must be said that two of the main parameters required by the EED software, apart from the ground heat loads, are the maximum and minimum mean fluid temperatures. Indeed, for this application, these need to be changed together with the maximum heat injection.

Therefore, a maximum mean fluid temperature was selected, calculating the maximum inlet-temperature at the high-pressure expansion valve in the worst conditions (for a given subcooling design capacity). In this case, an outdoor temperature of 30°C was utilized as design condition. After that, it was possible to choose the maximum mean fluid temperature to be used as a constrain.

For the next step, one needed to assume a certain profile of the mean fluid temperature as a function of the outdoor temperature. This was, then, translated into a yearly load profile on an hourly basis using the refrigeration model and the BIN hours method. Then, the iteration shown in Figure 8.2 was carried out until the results and assumptions converge. Figure 8.4 shows the optimized high-pressure expansion valve inlet-temperature for different subcooling capacities and relative maximum mean fluid temperature constrain.

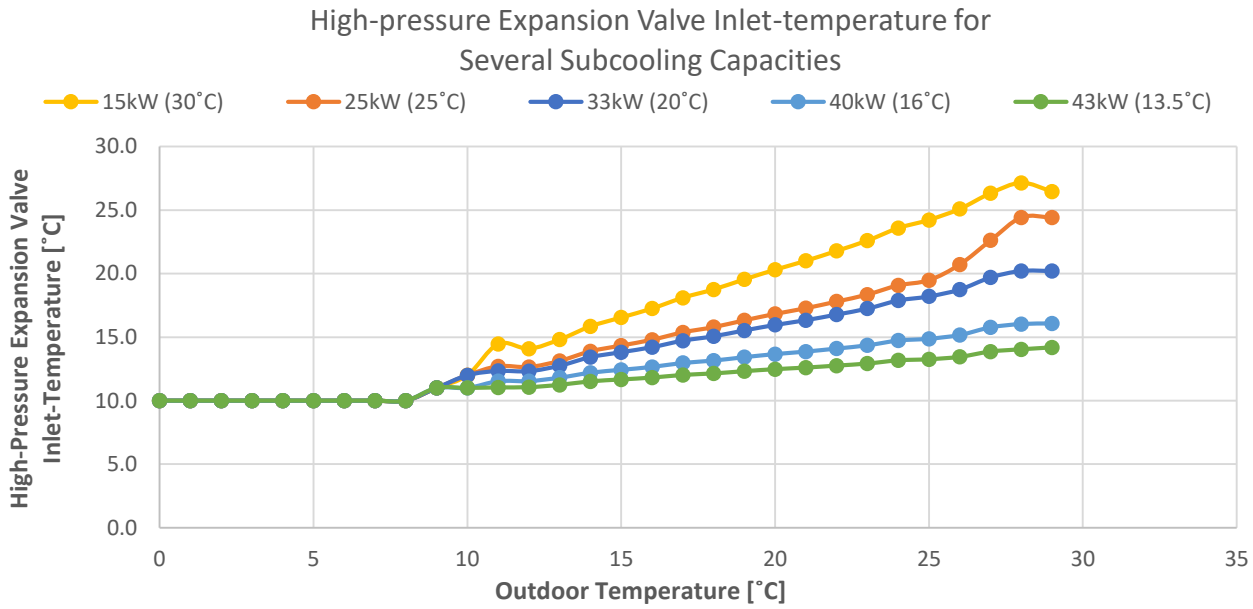

Figure 8.4 Modelling output: high-pressure expansion valve inlet-temperature for several subcooling capacities.

Once solved the iteration mentioned above, it was known the relation between the storage size and expected annual energy savings. The different solutions with the respective savings are shown in Table 8-2. It is worth to notice how negligible is the amount of the extra heat that would be necessary from secondary sources.

Table 8-2 Modelling output: optimized geothermal field size for several subcooling capacities.

Design Subcooling Capacity [kW]	Max Mean Fluid Temperature [˚C]	Number of Boreholes	Spacing [m]	Depth [m]	Subcooling Savings [MWh/year]	Heat Saved from Secondary Sources [MWh/year]
43	13.5	11	11	207	12.0	0.76
40	16	10	11	211	11.5	0.76
33	20	4	10	193	10.2	0.76
25	25	3	5	160	9.1	0.76
15	30	1		188	7.2	0.76

The two types of energy savings need to be transformed into economic value to be summed. For doing this, the electricity price was assumed to be 1 SEK/kWh and 0.8 SEK/kWh was chosen as price for external heat supply (Karampour et al., 2018). Figure 8.5 shows the variation of the Annual Energy Savings (AES) as a function of the maximum design capacity.

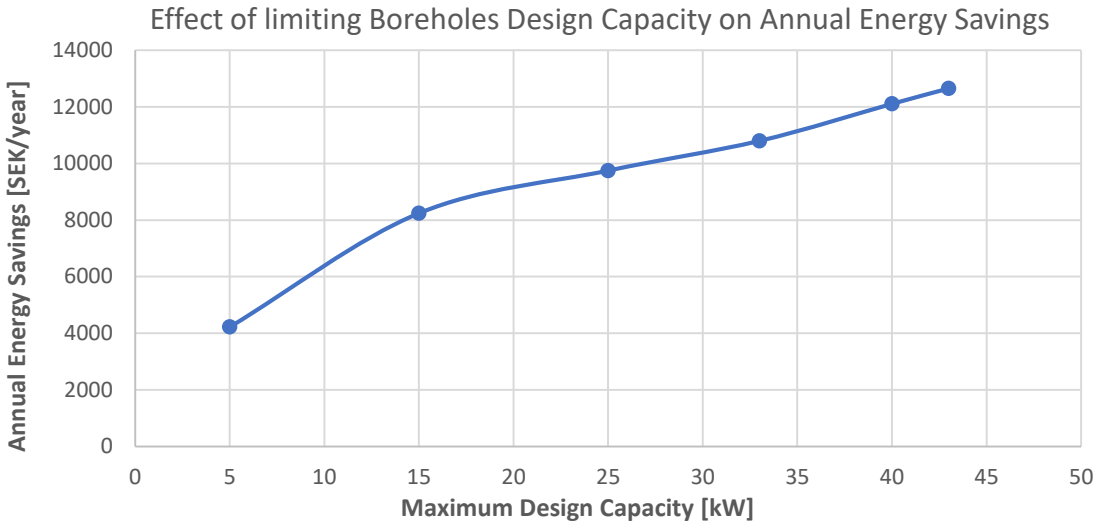

Figure 8.5 Modelling Output: Annual Energy Savings as a function of the design capacity.

8.3. Present Value of the Operational Savings

Once having identified the optimal size of the geothermal field, as well as, the related yearly savings an economic analysis was carried out. The yearly savings were transformed into a present value, using the concept of Equivalent Annual Savings (EAS). When an annuity is constant and no investment is done, the NPV can be expressed as in Eq. 8.1. This formula was used to identify which would have been the present value of the operational savings. The latter represents the present value of 15 years of annual energy savings.

$$Present\ Value\ of\ Operational\ Savings = EAS * \frac{1-(1+r)^{-n}}{r} \tag{8.1}$$

In Eq. 8.1 n represents the expected life time of the installation in years, while r is the discount rate. The latter consists of the cost of borrowing capital and it is strictly dependent on the market (food retail), on the country (Sweden) and on the company (Supermarket chain). The life time of the installation (n) was assumed to be 15 years, while the discount rate (r) was assumed to be 7.4% (ICA Gruppen, 2018).

For each of the solutions presented in Table 8-2 a corresponding present value of the operational savings was estimated using the related annual savings and Eq. 2.1. The overall result is shown in Figure 8.6. Each of the solutions brings a label indicating the design subcooling capacity and the maximum mean fluid temperature constrain.

The more the subcooling capacity is reduced, the more beneficial the investment is. This is due to the fact that the "*boreholes' capacity factor*" increases at reduced designed capacities. On the other hand, decreasing the maximum mean fluid temperature enables the system to work at higher subcooling capacities for more hours, but the cost for the additional required length is higher than the additional EAS.

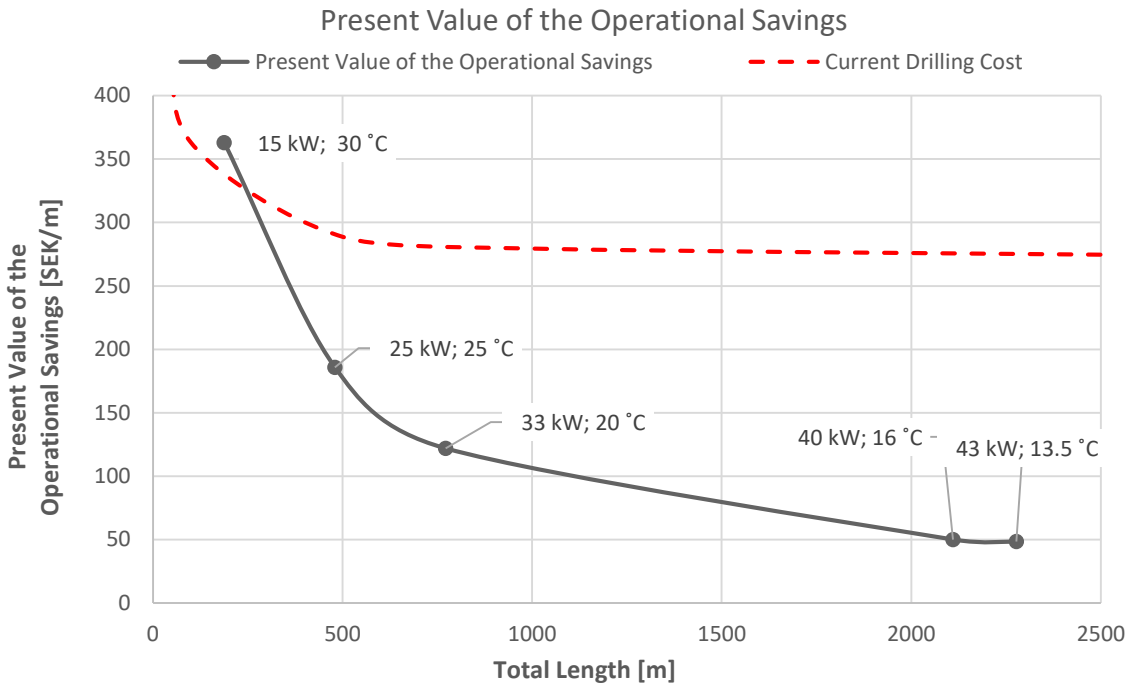

Figure 8.6 Results of the techno-economic assessment: present value of the operational savings for the case study

The cost per meter was chosen as an indicator since, this is the only parameter for determining the investment cost known from literature (Mazzotti et al., 2018) and (Karampour et al., 2018). The average cost per meter in Sweden is roughly 270 SEK/m (Mazzotti et al., 2018) and (Karampour et al., 2018) to this an additional fixed cost of 9300 SEK must be added. The latter is the cost for establishing a medium-size drilling site (Mazzotti et al., 2018).

From Figure 8.6, it is clear that, for the current installation, the only operational savings do not pay back the boreholes' investment cost. One of the reasons, is the ground unbalance. The system is injecting way more heat during summer than what it is extracting during winter. This drives the geothermal field size up. Indeed, this is one of the reasons why the solution with a smaller geothermal storage, are more profitable. The ground balance for some of the tested solutions is shown in Figure 8.7.

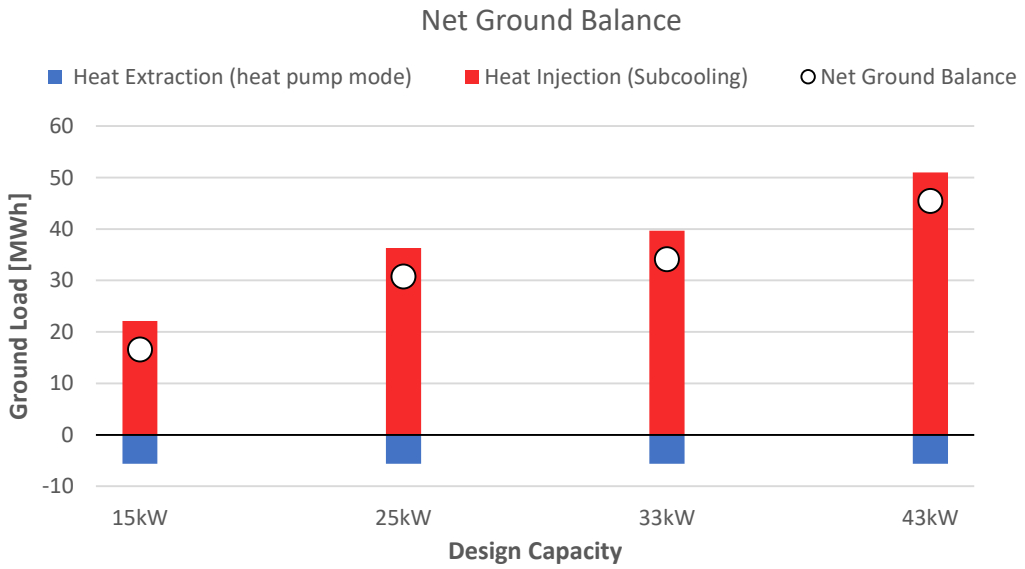

Figure 8.7 Model Output: Ground Balance for different sizes of the geothermal storage.

8.4. Sensitivity Analysis

To scope of this sensitivity analysis, was to identify which parameter affect the results the most. For a matter of time constrains some simplification needed to be done. The minimum mean fluid temperature was not and the evaporation temperature for the load evaporator were not optimized for the following cases. This is relevant for all the cases were a considerable amount of heat is extracted from the ground. The case study presented in the previous paragraph is used as reference case. The first parameter to be varied was the climate zone, therefore, the BIN hours. The solution for three different climates is presented in Figure 8.8.

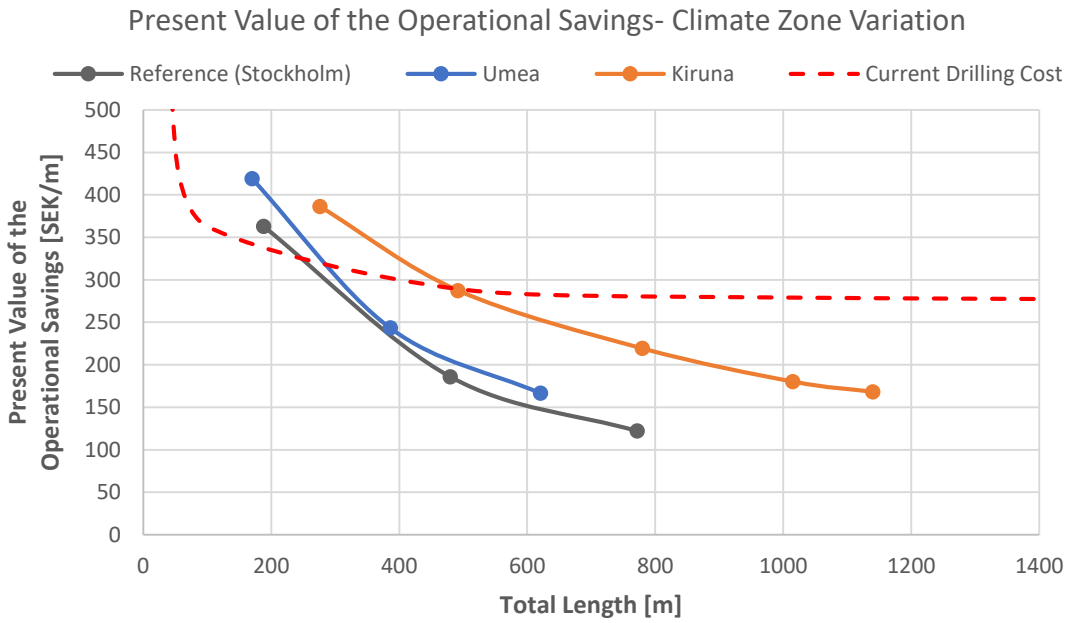

Figure 8.8 1st Sensitivity analysis: present value of the operational savings varying the climate zone

The sensitivity analysis does not take into account that the heating demand as a function of the outdoor temperature could be different for another climate zone. In other words, the study simulates what would be the result if the same building (e.g. same insulation, materials etc…) was virtually moved to another area.

The result shows that the geothermal integration becomes economically feasible for the Umea climate zone. This is due to the fact that this is the scenario with the most balanced ground. In this cases, it is worth to mention that the total energy consumption for the two cases was increased considering that the heat would be extracted at a different evaporation temperature than the built model. Moreover, since the minimum fluid temperature constrain was not optimized, the curve for the Kiruna case is thought to slightly underestimate the present value of the operational savings.

The second sensitivity analysis was performed varying the cooling capacity. This was done, to study the influence of integrating a geothermal storage with a supermarket of a different size. In doing so, the same ration between cooling and heating loads (HRR) was maintained. Two other systems that were tested, were characterized by a higher and a smaller cooling demand (respectively displayed in Figure 8.9 and Figure 8.10).

For the "bigger" system the tap water demand was kept the same as in the reference scenario (constant, 21.5 kW) and the space heating demand was set in order to obtain the same heat recovery ratio (HRR). The cooling loads were taken from (Karampour et al., 2018).

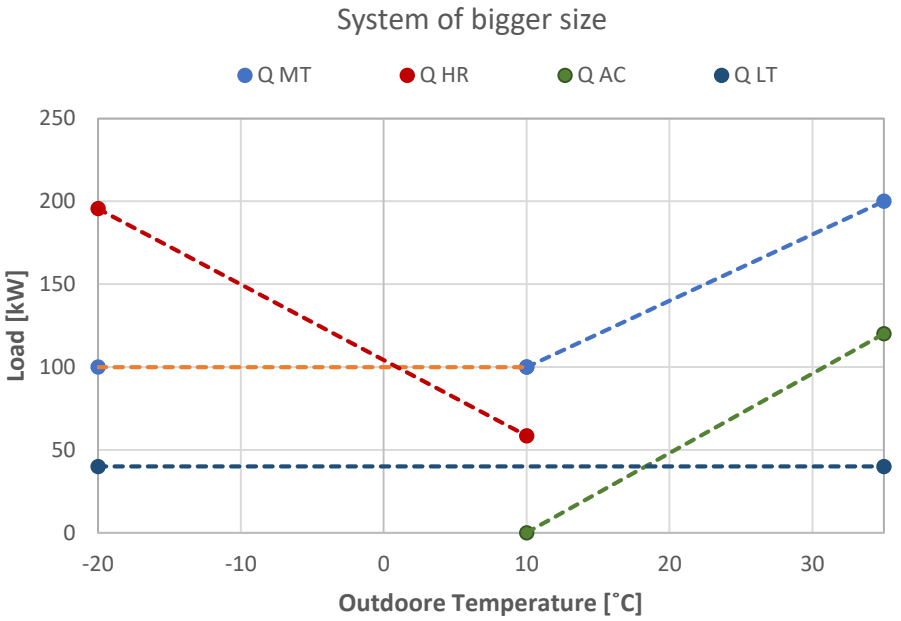

Figure 8.9 2nd Sensitivity analysis: Demands profile for a system of a bigger size.

For the scenario simulating a smaller supermarket, the heat recovery ratio was kept the same (heating demand calculated accordingly) while the cooling demands were taken from a real system studied in another project. This system was equipped only with one heat exchanger for heat recovery and the tap water demand was almost negligible. Moreover, air condition was not provided by the refrigeration system.

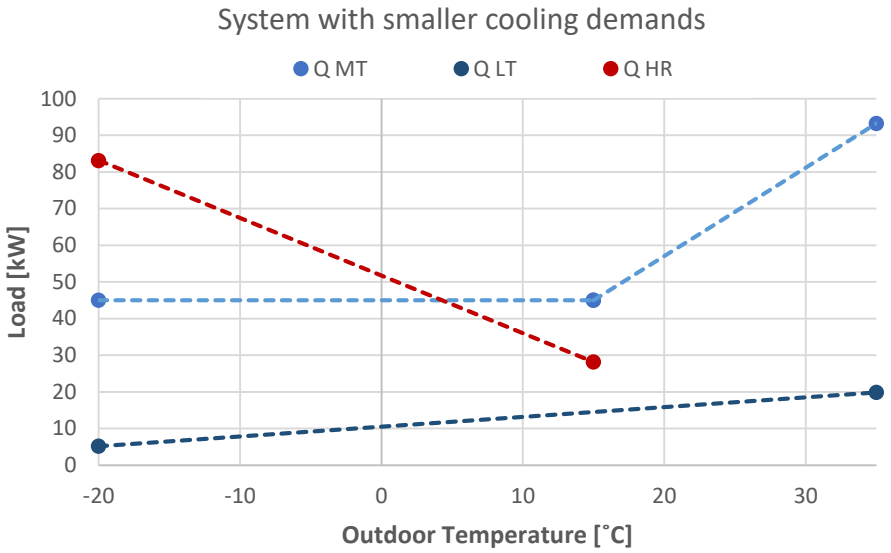

Figure 8.10 2nd Sensitivity analysis: Demands profile for a system of a smaller size.

The resulting curves with the variation of the present value of the operational savings are shown in Figure 8.11.

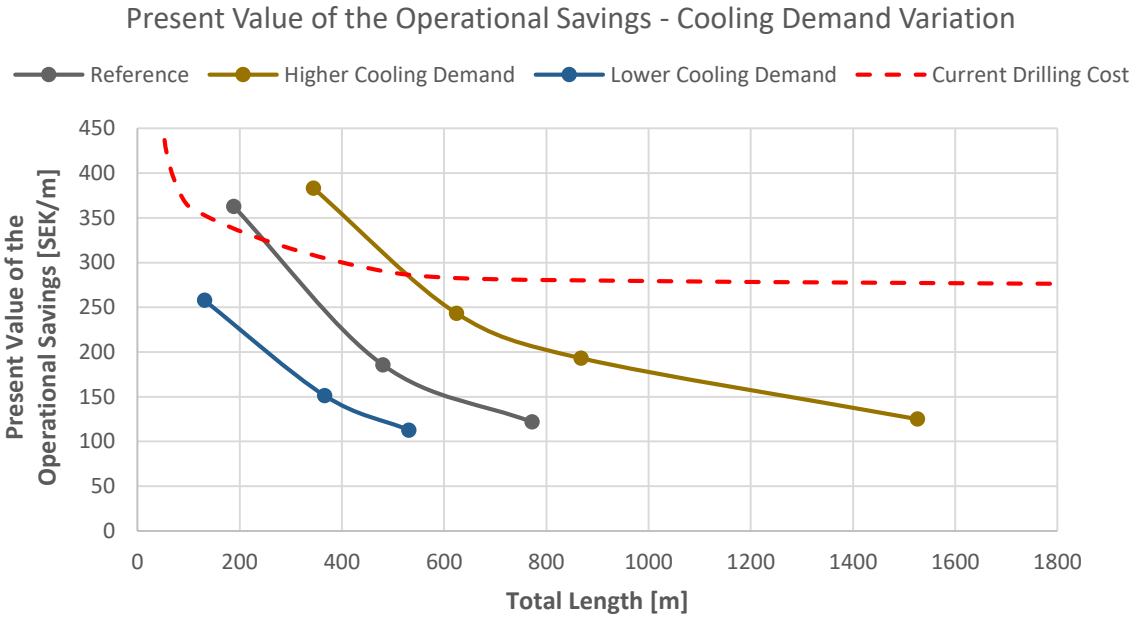

Figure 8.11 2nd Sensitivity analysis: present value of the operational savings varying the supermarket's size.

As it can be noticed, the economics of the geothermal integration seems to be poorly affected by a capacity variation. Obviously, a bigger system presents a slightly better result since is able to better cushion the fixed cost for setting up a drilling site.

Finally, the third tested parameter was the Heat Recovery Ratio (HRR). To new scenarios were simulated keeping the same cooling demands but modifying the space heating demand. The two HRR curves obtained are shown in Figure 8.12, together with the reference case.

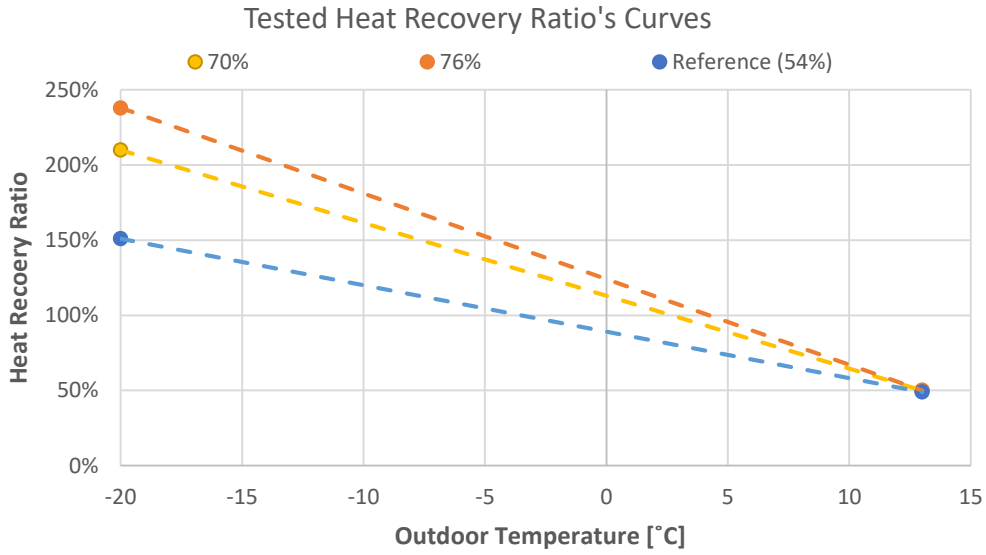

Figure 8.12 3rd Sensitivity analysis: Heat Recovery Ratios of the tested scenarios.

The percentage values which are used to name the curves in Figure 8.12, represent the average annual HRR for each curve considering Stockholm's BIN hours. It is worth to mention that the HRR for outdoor temperatures higher than 13˚C is technically not zero since part of the heat is always recovered for tap water production. However, in order to not consider the weight of the heat provided as waste heat when the

system is controlled in floating condensing mode, the HRR was imposed to 0 in order to have comparable averages.

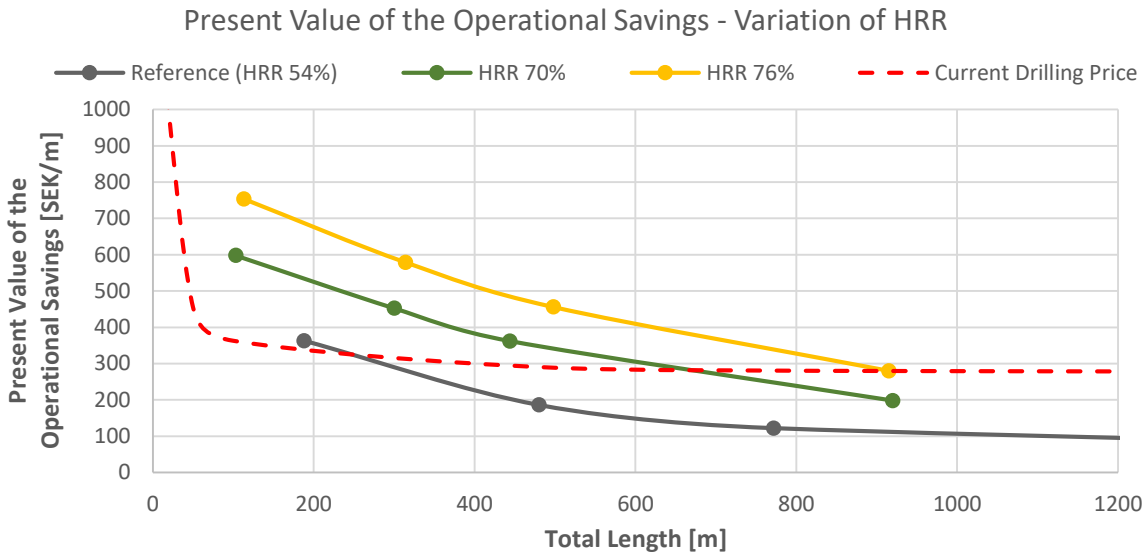

Figure 8.13 3rd Sensitivity analysis: present value of the operational savings varying the HRR's size.

The results clearly show that, for the considered boreholes investment cost, the geothermal connection start being financially feasible for an average HRR of 70%.

8.5. Effect of the Heat Recovery Control Strategy

In the scenario "HRR 70%" the gas cooler was assumed to be by-passed when possible (control strategy "*Gas cooler capacity regulation*"). As already mentioned, one of the difference between the two control strategies, presented in section 5.1.2, lays in the potential benefit of extracting more heat from the ground. However, the modelling result shows that the additional pumping cost compensates the benefits of extracting more heat, in this case. The comparison between the two control strategies, for this scenario, is displayed in Figure 8.14.

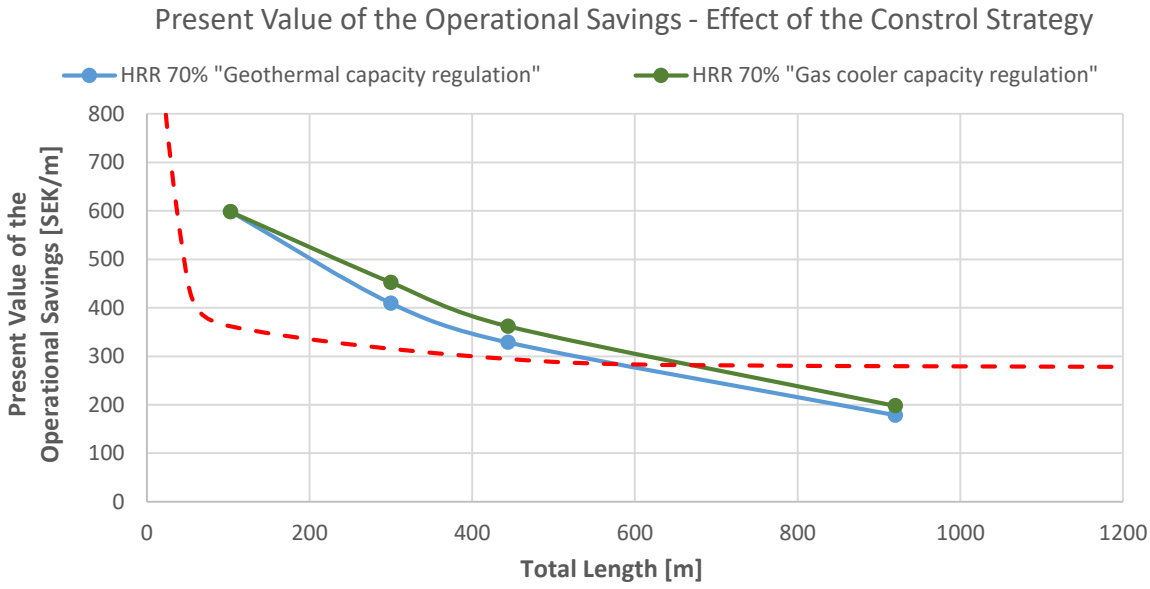

Figure 8.14 3rd Sensitivity analysis: effect of the heat recovery control strategy.

8.6. Discussion of the results

In this last part of the study, a methodology was developed to evaluate the variation of the economic benefits and the size of the geothermal field. The peak design capacity and the temperature constrain used for the maximum mean fluid temperature in the boreholes were found to be the most important design parameters which affects the optimal geothermal storage size.

For this case study, the techno-economic assessment shows that the operational savings obtained by the geothermal integration do not justify the storage investment cost. This is due to the ground unbalance and the small amount of operational hours of the geothermal field.

However, during the design phase, a system that satisfied the heating demand must be foreseen. If a system is equipped with boreholes, in theory it should not need any additional heating capacity. Therefore, the additional cost of the alternatives must be considered when evaluating the economic benefit of the geothermal storage (as shown in Figure 8.1). When taking into account the main alternatives, the heat coming from district heating is a good example. Therefore, the relative connection fee could be one of the cost for the alternatives that can be considered.

Moreover, when a refrigeration system is integrated with geothermal boreholes, the compressors taking care of the flash gas (parallel or MT) can be smaller. This is due to the fact that less flash gas is generated at the design conditions. The price difference between a system with higher compressors 'capacity and a smaller system integrated with boreholes, is a potential cost differential that can be summed to the cost of the alternatives.

Table 8-3 shows a minimum extra-price that could be paid for an alternative system solution (e.g. system with higher compressors 'capacity connected to a district heating network). In case the cost of the alternative solution was less expensive than these values, the geothermal integration would not represent a favourable option.

Table 8-3 Results of the techno-economic analysis

Design Subcooling Capacity [kW]	Number of Boreholes	Spacing [m]	Depth [m]	Boreholes Investment Cost [SEK]	Present Value of the Operational Savings [SEK]	Minimum Cost for the Alternatives [SEK]
43	11	11	207	624'100	112'400	511'700
40	10	11	211	579'000	107'600	471'400
33	4	10	193	217'700	95'900	121'800
25	3	5	160	138'900	91'000	47'900
15	1		188	60'000	70'000	-10'000

A sensitivity analysis was performed to evaluate in which case, in terms of location and size, a supermarket should consider a geothermal integration. Within the limitations of this work, the outcome demonstrates that a variation of the cooling capacity of a system (for the same HRR) does not greatly affects the profitability of implementing a geothermal storage. In the same way, also the climate zone does not strongly affect the economics of this solution. The third parameter analysed was the heat recovery ratio (HRR). The outcome demonstrate that this is the parameter affecting the economic benefits the most. In the Stockholm's climate, financial profits are visible starting from a seasonal average HRR of approximately 70%. An example of a system with a high HRR is a supermarket embedded in a shopping mall which is providing heat to the whole building. The high profitability of this scenario was already mentioned by (Karampour et al., 2018).

Finally, the effect of the alternative heat recovery control strategy described in chapter 5.1 was assessed. The results demonstrate that the extra-energy spent for the auxiliaries is almost totally compensated by the gains of cooling the ground. It must be mentioned that the control strategies were modelled considering that one of the two strategies would have been implemented for the whole simulated period (15 years). There could be an optimal value where the ground is cooled down only for a certain amount of time. Additionally, other scenarios could be investigated and a more accurate assumption on the pump power could be done. However, despite the last considerations, from an annual energy consumption perspective the difference between the two strategies is negligible for the considered climates.

9. Conclusion

To begin with, the field measurements analysis showed that the size of the geothermal storage was over-dimensioned for the application. This was also true for other components such as gas cooler, parallel compressors and load evaporators. Despite this, the system performance in the period going from July 2018 to July 2019 was found to be comparable to the state-of-the-art CO2 refrigeration system (Karampour and Sawalha, 2018).

An important aspect is that this system does not have any additional heat source for space heating. Therefore, the heat supplied by the refrigeration system is representative of the space heating demand to the building. For this reason, the demand profile is a good piece of information to be used for other studies.

Looking at the performance, the average COP heat recovery ranges from 3 to 8 for outdoor temperatures lower than 7.5°C. For warmer periods, the COP heat recovery goes up to 50 thanks to the heat wasted from the refrigeration cycle. Overall, the average value over the whole winter period was 7.5.

During the analysed period, the geothermal heat pump was operated only for 245 hours during the analysed year. Indeed, it was used mainly for satisfying the peaks of heating demand. This happened mainly in the morning during the first opening hours of the supermarket.

Despite the small amount of operational hours, it was possible to determine that the geothermal heat pump function does not lead to a steep decrease in the heat recovery performance, if properly designed. Indeed, an important mistake that can lead to a loss of performance is the scarce capacity regulation of the parallel compressors. The minimum mass flow that can be elaborated by the parallel compressors determines the minimum heating capacity of the geothermal heat pump. Since this function is mainly used to cover the peaks, a high value for the minimum capacity leads to an on-off functioning, thus to a dramatic drop in performance.

During this study, the best theoretical heat recovery control function was compared with the one really implemented. Such a comparison led to the development of a modified control strategy. According to the theory, only after that the gas cooler has been by-passed, the geothermal function should be activated. However, the modelling performed shows that, from a thermodynamic perspective, there is no-difference if the geothermal heat extraction is activated before increasing the gas cooler-outlet temperature. The only difference lays in the extra-energy spent for the gas cooler fans and for pumping the secondary fluid in the boreholes. It must be said that even if from an energy perspective there is a little difference, this alternative control strategy has important technical co-benefits. The main advantage is to shift from controlling the heat recovery through the gas cooler capacity's regulation to controlling through the parallel compressors capacity regulation.

Regarding the spring-summer performance, the energy savings due to subcooling were estimated to be 8.6% of the total power consumption. These were the main operational savings related to the geothermal integration. Indeed, a negligible amount of energy is saved during winter. This is due to the fact that the refrigeration system can satisfy roughly 95% of the heating demand without using the ground. Regarding Free-space-cooling, it was not deeply investigated for the lack of time and data. However, for the given outlet temperature from the boreholes, it seems unlikely that a supermarket could obtain a considerable amount of free-space-cooling. Part of the suggested future work deals with a deeper analysis of the free-space-cooling potential.

Generally, for the Stockholm's climate, the energy savings due to subcooling were estimated to be in the order of 5-10% of the total power consumption. For the given costs (Swedish market), loads (average size) and boundaries of the system (Swedish climate), the operational savings are found to not pay back the necessary investment for the boreholes.

Indeed, the profitability of a geothermal storage strongly depends on the cost of the alternatives. This represents the additional CAPEX that would be needed if a storage was not included in the design. Generally, there should be a supplementary CAPEX for the summer operations and an additional cost for

the winter operations. These are connected, respectively, to the subcooling function and to the heat pump function. Some examples are: a lower compressor 'cost thanks to the subcooling and a lower or null district heating connection fee.

In terms of designing best practices, there are two possible ways. The first is to design the geothermal storage to make the supermarket energy independent. This means, to design in a way that the geothermal heat pump function will totally satisfy the peaks of heating demand. The second option is to design, trying to optimize the subcooling or heat pump function (depending on the climate and demands).

The first option is favourable when the alternatives are relatively expensive and the CAPEX savings from these can cover 90-70% of the boreholes investment cost. The second option is favourable for systems where the alternatives are relatively cheap. In that case, the operational savings can pay back 45-90% of the investment cost.

Regardless the design approach, the integration of a CO2 refrigeration system is particularly profitable for supermarkets which are satisfying a high heating demand, compared to the cooling load. This means refrigeration systems operating with a ratio between heating and cooling loads higher than an average supermarket. For instance, a supermarket providing heat to the neighbouring facilities could greatly benefit from a geothermal storage.

Indeed, the main parameter influencing the economics of this type of solution is the seasonal average Heat Recovery Ratio (HRR). This is why the most promising suggested future work is to investigate the potential of selling the heat recovered from a CO2 refrigeration system integrated with boreholes to a district heating network.

It is worth to mention that every system is unique, in fact, the numerical results presented in this work are system specific. Nevertheless, the concepts and best practices presented are generally valid.

10. Future Work

Due to time constrain several interesting aspects were not investigated. Therefore, they are left for future work. These are listed below.

Selling heat to district heating networks

Since the most favourable solutions are the ones with high HRR, an interesting idea is to use to boreholes to increase the heating capacity and inject heat into the district heating network. The heat produced in this way could be competitive with the overall efficiency of the district heating network.

Free-space-cooling

One of the main aspects that was not deeply studied in this work is the free-space-cooling potential. Boreholes could ideally provide space cooling to a building. Unfortunately, for the current system layout and operational strategies, free-space-cooling, seems not possible. However, the feasibility of some innovative solutions should be assessed. One of this could be to split the geothermal field, using only part of it for space heating and free-space-cooling. This could lead to a better match of the temperature levels needed for this applications.

Heat Recovery Control Strategies

In chapter 5.1 the practical challenges of implementing a gas cooler by-pass are mentioned. A field measurements analysis of a system controlling the heat recovery, through gas cooler capacity's regulation, should be performed. Then, the heat recovery performance should be compared to the one of the case presented in this work. Such a comparison would give a better understanding of the technical benefits of regulating the heating capacity only extracting heat from the ground and without by-passing the gas cooler.

Alternative cooling loads

During winter the ground is cooled down to provide more heat to the building. In case boreholes were installed only to satisfy the peaks of heating demand, an alternative solution could be used. Indeed, a cheaper option is to utilized the gas cooler as a load evaporator after that it has been by-passed. The load evaporator would be used as an air-to-CO2 heat pump. This system solution and relative control strategy is described by (Heerup, 2019). Another potential idea, would be to use a heat exchanger installed in parallel with the gas cooler.

Sources

Berglöf, K., 2018. The ClimaCheck method To Measure – Analyze and optimize refrigeration processes .

Danfoss, 2019. Capacity controller for transcritical CO2 booster control, AK-PC782A.

Danfoss, n.d. Controller for appliance control, AK-CC 550A.

Gullo, P., Hafner, A., Banasiak, K., 2018. Transcritical R744 refrigeration systems for supermarket applications: Current status and future perspectives. Int. J. Refrig. 93, 269–310. https://doi.org/10.1016/j.ijrefrig.2018.07.001

Heerup, C., 2019. Operation Costs for Heat Recovery from Supermarkets to District Heating Grids. https://doi.org/10.18462/iir.icr.2019.

ICA Gruppen, 2018. Annual Report.

Karampour, M., Sawalha, S., 2018. State-of-the-art integrated CO2 refrigeration system for supermarkets: A comparative analysis. Int. J. Refrig. 86, 239–257. https://doi.org/10.1016/J.IJREFRIG.2017.11.006

Karampour, M., Sawalha, S., 2016. Energy Efficiency Evaluation of Integrated CO2 Trans-critical System in Supermarkets: A Field Measurements and Modelling Analysis 1, 1–15. https://doi.org/10.6182/jlis.2016.14(1).001

Karampour, M., Sawalha, S., 2014. Investigation of using internal heat exchangers in CO<inf>2</inf> trans-critical booster system. 11th IIR Gustav Lorentzen Conf. Nat. Refrig. Nat. Refrig. Environ. Prot. GL 2014 1–8.

Karampour, M., Sawalha, S., Arias, J., 2016. Eco-friendly Supermarkets - an Overview.

Karampour, M., Sawalha, S., Mateu-Royo, C., Rogstam, J., 2018. Geothermal storage integration into supermarket's CO2 refrigeration system 1–9. https://doi.org/10.22488/okstate.18.000029

Kauko, H., Kvalsvi, K.H., Hafner, A., 2016. How to build a new eco-friendly supermarket.

Mainar Toledo, D., Garcìa Peraire, M., 2016. How to refurbish a supermarket.

Mateu-royo, C., Karampour, M., Sawalha, S., 2018. Integration of Geothermal Storage in Co 2 Refrigeration.

Mazzotti, W., Lazzarotto, A., Acuña, J., Björn, P., 2018. Deep Boreholes for Ground-Source Heat Pump, effsys Expand.

Melinder, Å., 2010. IIR -- Properties of Secondary Working Fluids for Indirect Systems (Secondary Refrigerants or Coolants, Heat Transfer Fluids). International Institute of Refrigeration (IIR).

Monzó, P., 2018. Modelling and monitoring thermal response of the ground in borehole fields. KTH Ind. Eng. Manag. Stock. Sweden, PhD Thesis. Royal Institute of Technology.

Rogstam, J., Abdi, A., Sawalha, S., 2013. Carbon dioxide in ice rink refrigeration.

Royo, C.M., 2017. Field Measurements and Modelling Analysis of CO2 Refrigeration Systems with Integrated Geothermal Storage.

Sawalha, S., 2012. Investigation of heat recovery in CO2 trans-critical solution for supermarket. Int. J. Refrig. 46, 1–12. https://doi.org/10.1016/j.ijrefrig.2012.10.020

Sawalha, S., 2008. Carbon Dioxide in Supermarket Refrigeration.

Shecco, 2018. Green & Global Natural Refrigerant around the world. Accel. Adv. HVAC&R Nat.

Shecco, 2016. F-GAS REGULATION SHAKING UP THE HVAC&R INDUSTRY.

Swedish Geographical Survey, 2019. No Title [WWW Document]. URL https://apps.sgu.se/kartvisare/kartvisare-brunnar.html

Thanasoulas, S., 2018. Evaluation of CO2 Ice rink heat recovery system performance.